Assessment of Sequentially vs. Fully Coupled Dynamic Analysis of Offshore Wind Turbines

Rick Damiani and Fabian Wendt
National Renewable Energy Laboratory

Zachary Finucane and Laura Hulliger
Keystone Engineering

Satish Chilka and Dan Dolan
Moffatt and Nichol

Produced under direction of the Bureau of Safety and Environmental Enforcement by the National Renewable Energy Laboratory (NREL) under Work for Others Agreement number E15PS00085.

NREL is a national laboratory of the U.S. Department of Energy
Office of Energy Efficiency & Renewable Energy
Operated by the Alliance for Sustainable Energy, LLC

This report is available at no cost from the National Renewable Energy Laboratory (NREL) at www.nrel.gov/publications.

Strategic Partnership Project Report
NREL/TP-5000-68618
February 2018

Contract No. DE-AC36-08GO28308

NREL
NATIONAL RENEWABLE ENERGY LABORATORY

Assessment of Sequentially vs. Fully Coupled Dynamic Analysis of Offshore Wind Turbines

Rick Damiani and Fabian Wendt
National Renewable Energy Laboratory

Zachary Finucane and Laura Hulliger
Keystone Engineering

Satish Chilka and Dan Dolan
Moffatt and Nichol

Suggested Citation
Damiani, Rick, Fabian Wendt, Zachary Finucane, Laura Hulliger, Satish Chilka, and Dan Dolan. 2018. *Assessment of Sequentially vs. Fully Coupled Dynamic Analysis of Offshore Wind Turbines*. Golden, CO: National Renewable Energy Laboratory. NREL/TP-5000-68618.

NREL is a national laboratory of the U.S. Department of Energy
Office of Energy Efficiency & Renewable Energy
Operated by the Alliance for Sustainable Energy, LLC

This report is available at no cost from the National Renewable Energy Laboratory (NREL) at www.nrel.gov/publications.

National Renewable Energy Laboratory
15013 Denver West Parkway
Golden, CO 80401
303-275-3000 • www.nrel.gov

Strategic Partnership Project Report
NREL/TP-5000-68618
February 2018

Contract No. DE-AC36-08GO28308

NOTICE

Cover Photos by Dennis Schroeder: (left to right) NREL 26173, NREL 18302, NREL 19758, NREL 29642, NREL 19795.

NREL prints on paper that contains recycled content.

List of Acronyms/Nomenclature

ASE	aero-servo-elastic
AHSE	aero-hydro-servo-elastic
COD	co-directional (per International Electrotechnical Commission 61044-3 [4])
DLC	design load case
ECM	extreme current model (per IEC 61044-3 [4])
ESS	extreme sea state (per IEC 61044-3 [4])
EWLR	extreme water level reference (per IEC 61044-3 [4])
EWM	extreme wind model (per IEC 61044-3 [4])
FC	fully coupled
Hmax	maximum wave height
Hs	significant wave height
IEC	International Electrotechnical Commission
Keystone	Keystone Engineering
metocean	meteorological ocean
MIS	misaligned (per IEC 61044-3 [4])
MSL	mean sea level
MW	megawatt
NCM	normal current model (per IEC 61044-3 [4])
NOAA	National Oceanic and Atmospheric Administration
NREL	National Renewable Energy Laboratory
NSS	normal sea state (per IEC 61044-3 [4])
NTM	normal turbulence model (per IEC 61044-3 [4])
NWLR	normal water level reference (per IEC 61044-3 [4])
OD	outer diameter
OEM	original equipment manufacturer
RNA	rotor nacelle assembly
SC	sequentially coupled
t	wall thickness
Tp	peak spectral period
ULS	ultimate limit state
z	z coordinate
1P	rotor frequency
3P	blade-passing frequency

Executive Summary

A loads analysis on fixed-bottom offshore wind turbines was conducted focusing on the differences in ultimate limit state load predictions between the so-called fully coupled (FC) and sequentially coupled (SC) modeling approaches. The FC approach is deemed more accurate and rigorous, as it simultaneously accounts for aerodynamics, structural dynamics, control dynamics, and hydrodynamics. In the SC method, which is widely used by the offshore wind industry, the turbine original equipment manufacturer and substructure designer work independently on their respective subsystems, exchanging only loads and stiffness properties at the interface between the substructure and tower. As such, this method does not require sharing design specifics and thus better protects proprietary information and more clearly defines the liability bounds for all parties involved in the offshore wind turbine design.

The loads analysis was conducted through aero-hydro-servo-elastic simulations of 5-megawatt offshore wind turbines on a monopile and jacket substructure, which are the most common substructures and expected to be sited in different water depths and to have significantly different dynamic behaviors. Two sites along the Eastern U.S. seaboard were selected corresponding to two offshore wind energy lease areas that could host a monopile-based and a jacket-based offshore wind turbine, respectively, and for which the authors could gather meteorological ocean data. We simulated power production (operational) and parked (extreme event) load cases on publicly available models of turbine and substructures, and extracted loads on several subcomponents.

When considering the maximum load values across all operational cases (A001-A008) for each method, the rotor nacelle assembly and tower loads were found to be within 3% and 6% for the jacket and monopile configuration, respectively. When considering the maximum load values across all parked cases (B001-B008), the rotor nacelle assembly and tower loads were within 13% and 7% for the jacket and monopile configuration, respectively, and the SC results yielded lower loads than the FC results. For the substructure loads across all power-production cases, results showed differences of up to 60% for the jacket members. Specifically, with the SC approach predicting higher loads, the monopile maximum loads were in close agreement (6%–11%), and with no clear trend regarding the conservatism of any particular method. Across all of the parked cases (B001–B008), one jacket member load channel was ~50% higher using the SC approach, whereas several other member loads were decreased by up to 39% when compared to the FC approach; the monopile loads were predicted to be 11% less with the SC method.

Our findings yielded some significant differences that require further investigation to address any remaining concern regarding the practicability of the sequentially coupled analysis method for the design of offshore wind systems. Some of these differences can have important implications on the design of the support structures—with the potential effect of either overdesigned or underdesigned components—and should be further investigated. A comparative study that relates the observed differences in ultimate load predictions between SC and FC to the commonly utilized safety factors is also recommended by the authors. At this point, no clear statement can be made to determine whether the FC or SC approach is generally preferred or more conservative.

Table of Contents

List of Figures

List of Tables

1 Background

Offshore wind turbines are mounted on support structures that include a tower, substructure, and the foundation to the seabed. To date, more than 2,000 offshore wind turbines have been installed worldwide, mostly in the North Sea and Baltic Sea in Europe, but the first U.S. offshore wind project began operation in 2016 (the Block Island Wind Farm off the coast of Rhode Island). Most of these operating wind turbines are mounted on foundations that are rigidly fixed to the seabed in shallow water (0–50 m depth) using monopile, jacket, or gravity-based substructures. However, new technology is being developed that will allow floating wind turbines to operate in deeper water up to 1,000 m. Figure 1 shows a range of the most common types of substructures and concepts currently being considered.

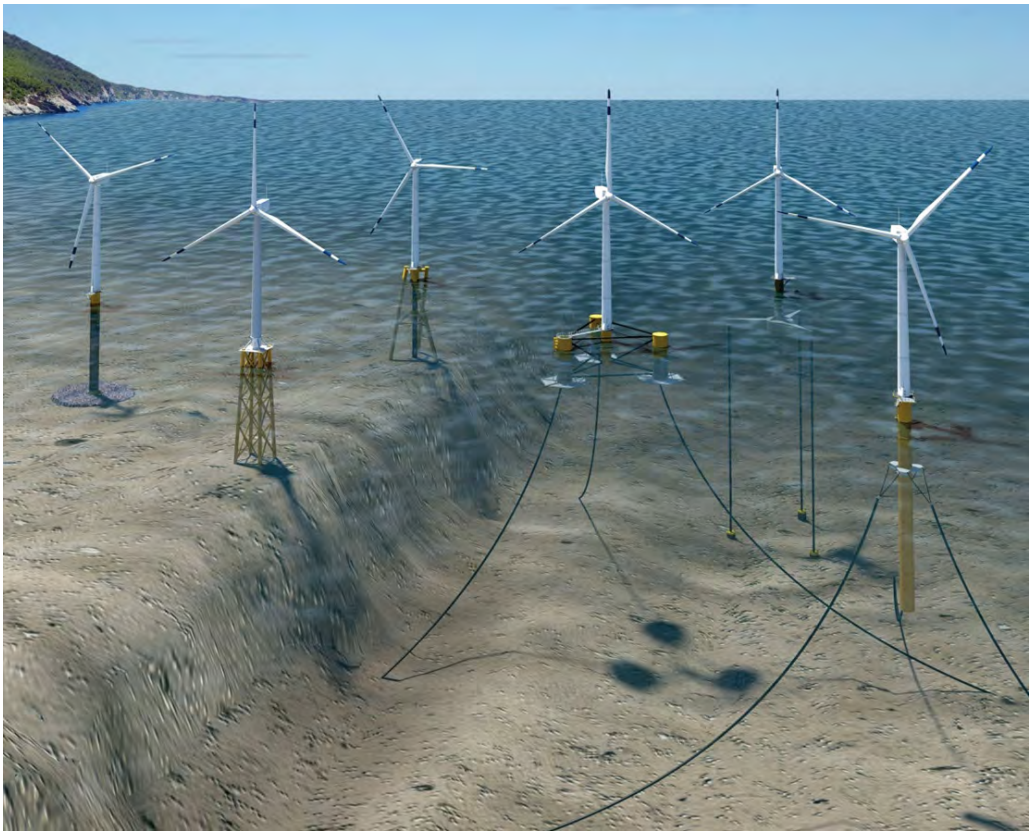

Figure 1. Offshore wind turbine substructure designs for varying water depths. ***Illustration by Josh Bauer, NREL***

The most common substructures are the monopile and multimember lattice, or "jacket." Seventy-five percent of all offshore wind installations use monopiles (see Figure 2), which can be considered the baseline for offshore wind. Based on the authors market assessment of offshore wind projects that are under construction or have announced design details, monopiles will remain the dominant substructure type, but jackets will increase from a 10% share to a 16% share in the next few years.

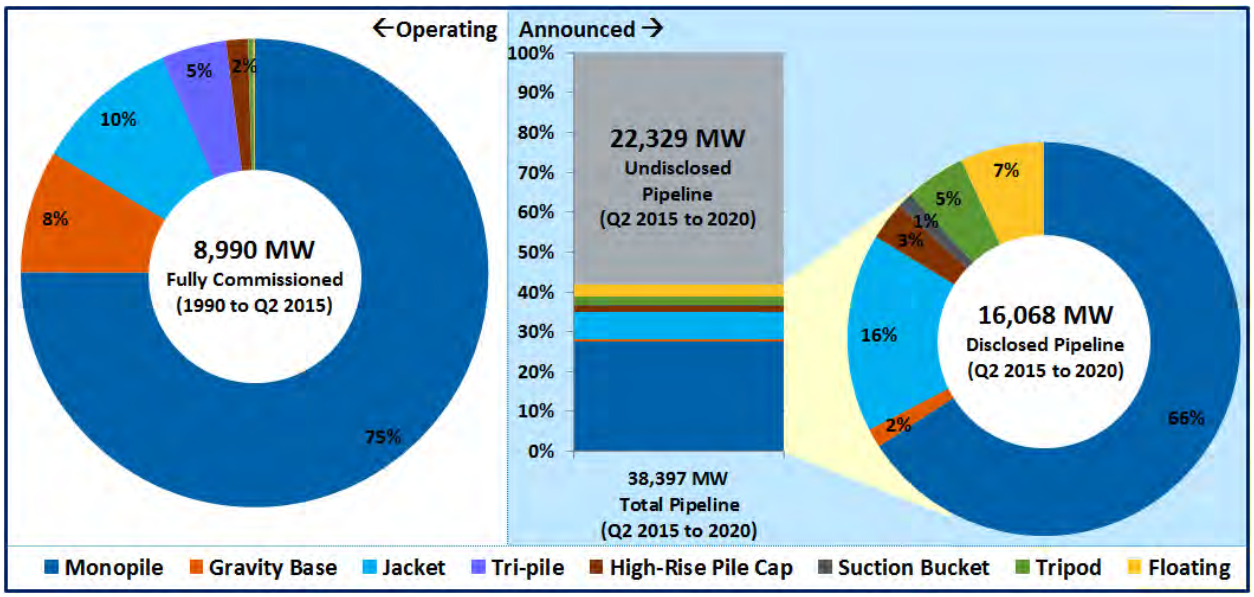

Figure 2. Global offshore wind substructure market share (Smith, Stehly, and Musial, 2015)

Offshore wind turbine substructures are subjected to a variety of loading during both normal operation and extreme events (e.g., faults and winter and tropical storms). These loads include those that occur directly on the substructure, such as wave, current, and wind loads, and those that are transferred from the turbine and support tower. The load calculation for offshore wind turbine systems is particularly challenging because of the rotor variable speed and turbulent inflow, the aeroelastic interaction of the blades and wind field, the coupling between the rotor nacelle assembly (RNA) and support structure, and the potential for significant dynamic amplification of these loads if the resulting frequencies are similar to any of the natural vibration frequencies of the RNA and support structure. The latter issue must be addressed carefully as the potential for a resonant or near-resonant response of the OWT will lead to significantly greater loads. These amplified loads can result in large displacements during operation, thereby causing premature shutdown, overload of structural components, and accelerated accumulation of fatigue damage.

The analysis of offshore wind turbines is conducted using design tools that have been validated under actual operating conditions to allow for the full design and type certification under International Electrotechnical Commission (IEC) standards and classification society guidelines. For offshore wind turbines, the analysis method must consider the aerodynamic/hydrodynamic loads and responses of the entire system (e.g., the turbine, tower, substructure, and foundation) coupled to the turbine control system dynamics. A fully coupled (FC) (turbine and support structure) modeling approach is more rigorous and allows for a thorough system optimization; however, intellectual property concerns can sometimes preclude this approach. In fact, turbine control system algorithms and turbine properties are not available within the public domain and often are not even made available to offshore substructure designers who work directly for the turbine manufacturers. As a result, engineering firms and contractors are prevented from directly performing an integrated, coupled analysis of the complete system.

In many cases, two separate analyses using different software tools and an information exchange may be necessary to design an offshore wind system. In the sequentially coupled (SC) approach, the turbine and substructure designers will independently determine a reduced set of dynamic properties of their subsystems, which is exchanged and included in their independent subsystem models. The turbine manufacturer then simulates the wind-induced response at the tower support flange (base loads), considering the reduced model of the substructure and the hydrodynamic loads provided by the substructure designer. In turn, the substructure designer uses these tower base loads as inputs for the analysis of the substructure and its foundation (by adding aerodynamic and hydrodynamic loads to the substructure below the tower).

However, concerns exist that an SC analysis could potentially reduce the quality and accuracy of the design process when compared to the fully coupled one. The industry, including turbine manufacturers, design firms, and regulatory agencies, seek a better understanding of the impact of uncertainties introduced by a SC versus FC design approach.

Although the ability to conduct design optimization is limited to some degree with a sequentially coupled analysis method, the central questions are whether this approach can be adequate for design purposes, or if a significant amount of design-related uncertainty is introduced. In fact, it could be hypothesized that because of a possible lack of convergence and/or less-than-ideal transfer of dynamic properties among different models, some structural modes that are important for the design might not get captured by the SC process.

In response to these questions, the National Renewable Energy Laboratory (NREL) and its partners proposed and were awarded a contract for research under the Bureau of Safety and Environmental Enforcement's (BSEE's) Solicitation Number E15PS00085. This report summarizes the work done under that solicitation, and which focused on the differences in ultimate load prediction between the fully coupled and sequentially coupled modeling approach. The analysis was conducted through aero-hydro-servo-elastic simulations of offshore wind turbines on a monopile and jacket substructure; these two are the most common substructures and are expected to be sited in different water depths and to have significantly different dynamic behaviors.

The research team consisted of NREL and two subcontractors: Keystone Engineering (Keystone), and Moffatt & Nichol; the team encompasses the most experienced modeling and engineering capabilities in the U.S. offshore wind industry today.

The main objective of the study was to illustrate the differences between the two approaches to design and analyze offshore wind turbines, and to provide guidelines for improved and expedited convergence. The results from this study underline the need for a more in-depth investigation of the differences noted between the two modeling approaches: although predictions tend to closely agree among the two approaches, for most load channels, some larger differences indicate that the sequentially coupled approach can be less conservative under certain circumstances and load cases than the FC approach, especially for substructure loads. "Conservative" is defined as one approach producing larger loads than the other.

This report is organized as follows. Section 2 offers details on the actual analysis procedure used. Section 3 describes the geographical and meteorological ocean (metocean) parameters of the

sites selected for the study including data such as: directional joint probability of wind speed, wave height, wave periods, water depth, and soil characteristics. The sites were selected in light of current and proposed developments along the East Coast of the United States. The turbine parameters are also shown in the same section. In Section 4, an overview of the support structures is provided. Section 5.4 discusses the main assumptions in the simulations and the load cases and conditions analyzed; the initial verification among all employed models is given in Section 6. Key results are discussed in Section 7. Conclusions with recommended future steps are given in Section 8.

2 Definition of the Analysis Methods

As mentioned previously, the goal of the study was to compare two methodologies used in current practice for offshore wind turbine design. A commonly used, sequentially coupled approach is compared to the more rigorous FC approach, which entails computing simultaneous aerodynamics, hydrodynamics, structural dynamics, and control system effects. Section 2.1 and Section 2.2 discuss the details of the two methods used in this study. Because some of the challenges in implementing these approaches relate to communication among the various parties, NREL assumed the role of the turbine original equipment manufacturer (OEM), and NREL's subcontractors focused on their respective substructure analyses (Keystone on the jacket, and Moffatt &Nichol on the monopile configuration). The goal was to compare the ultimate limit states (ULS) loads resulting from a semicoupled analysis against the ULSs derived from an FC approach, as this can help assess potential issues with the load predictions from the SC approach. NREL performed the FC analysis and acted as the turbine operator for the SC approach. Two driving load cases were selected (see Section 5.4 to learn more about the power production and extreme event load case).

NREL used FAST v8, an aero-hydro-servo-elastic computer-aided-design tool widely used in both the research community and industry (NREL 2016). NREL modified FAST v8's modules SubDyn (substructure structural dynamics) and ElastoDyn (turbine structural dynamics) to include pile stiffness effects and allow for the introduction of superelement matrices at the tower-substructure interface.

Keystone and Moffatt & Nichol utilized SACS (Bentley Systems) and EDP (Extended Design Program by Digital Structures Inc.), two offshore structural analysis and design tools that have been proven in the oil and gas industry to model the substructure and hydrodynamic loads in the SC approach.

Just like in a real-world case, this project was conducted with physical separation between turbine and substructure designers, giving rise to the challenges associated with the SC modeling approach (e.g., different modeling tools and data exchange protocols). Therefore, the various models built in FAST v8 and in the subcontractors' software had to be cross-verified to guarantee matching of fundamental structural and hydrodynamic characteristics. NREL provided the substructure geometric and structural definition above the mudline (together with FAST v8's SubDyn/HydroDyn input files) and the turbine tower and RNA structural and inertial properties. Pile head stiffness matrices were supplied by Keystone and Moffatt & Nichol as input to NREL's FC simulations to achieve a realistic representation of the pile/soil interaction, similar to the one that is modeled in SACS and EDP.

To narrow down the potential sources of disagreement that come from using different modeling software packages included with the FC and SC approach, the simulations performed in both methods used the same wave surface profile, wind inflow, and linearized soil stiffness.

The turbine-specific loads (e.g., tower base and blade root moments) were calculated by NREL's FAST simulations. FAST v8 was run with a simplified substructure matrix representation and externally generated substructure loads for the SC approach, and with a complete SubDyn substructure model and internally generated hydrodynamic loads in the FC approach. The

substructure member loads were computed by Keystone and Moffatt & Nichol for the SC approach, and by NREL for the FC approach.

2.1 Sequentially Coupled Analysis

The SC analysis method is still the most common design method used in the offshore wind industry for fixed-bottom systems, such as jackets and monopiles. The aerodynamic and hydrodynamic loads are calculated separately by the turbine OEM and the foundation designer, respectively. Loads and dynamic stiffness data computed at the tower-bottom flange (the interface) are transferred between the two parties. This method allows for maximum control of each party's responsibility and of the respective intellectual properties, with no exchange of the details of the turbine and substructure designs. A clear separation of design responsibilities is inherent to the SC approach.

A superelement representation of the substructure and foundation (i.e., 6-by-6 stiffness, mass, and damping matrices) is created by the foundation designers (Keystone and Moffat & Nichol in this study) and included in the aero-servo-elastic (ASE) simulations (e.g., FAST v8 in this study) run by the turbine OEM (NREL in this study) to account for the response of the structure below the tower. The loading effects on the turbine and tower as a result of the hydrodynamic forcing on the substructure are provided by the foundation designers as an equivalent load vector (three forces and three moments) time history at the tower-bottom flange. The superelement and associated equivalent hydrodynamic forcing at the tower base is a simplified method in the ASE simulations to account for the compliance, damping, and excitation of the substructure during loads analysis simulations of the wind turbine.

To calculate this time history, the foundation designers run finite-element dynamic simulations of the substructure and calculate the distributed wave loads, which are then reduced to the tower base using the same reduction bias that was used to generate the superelement. Note that wind loads are not included in this step.

The last step of this method requires one more exchange of time-variant loads. The coupled tower-base loads as calculated by the ASE simulations are then transferred back to the foundation designers, who, in turn, perform new load calculations, thereby subjecting the substructure to the original hydrodynamic forcing as well as the newly received loads at the tower-bottom flange.

In summary, the steps followed for the SC approach performed in this study include the following:

A. Keystone and Moffatt & Nichol (substructure designers) run hydrodynamic simulations on their respective substructure and linearized foundation. No representation of the turbine is considered in these simulations (only the substructure/hydrodynamics are modeled here)

B. Keystone and Moffat & Nichol provide NREL (representing the OEM) with the equivalent loads (three forces and three moments) at the tower base in an ASCII, time-series format

C. Keystone and Moffatt & Nichol provide NREL with the tower-based loads and equivalent stiffness, mass, and damping matrices (K, M, and C [6-by-6] matrices) for a superelement, referenced at the tower base, which represents the properties of the substructure and foundation

D. NREL runs a variety of FAST v8 simulations that include flexible RNA and tower, aerodynamic loads, and a superelement representation of the substructure (K, M, C matrices). Equivalent loads at the tower base are injected into the simulations based on the data from Keystone and Moffatt & Nichol to simulate the effects of the substructure hydrodynamic loading on the remainder of the offshore wind turbine

E. NREL passes the resulting tower-base loads from the FAST simulation outputs to Keystone and Moffatt & Nichol

F. Keystone and Moffatt & Nichol run new simulations with their models of the substructure and foundation adding the loads at the tower base provided by NREL, which represent aerodynamic and inertia loads originating from the turbine

G. NREL postprocesses FAST results for loads in the main components of the RNA and tower, using the simulation data from step D

H. Keystone and Moffatt & Nichol postprocess their respective simulation results for loads and deflections in the substructure components.

This process is illustrated in Figure 3.

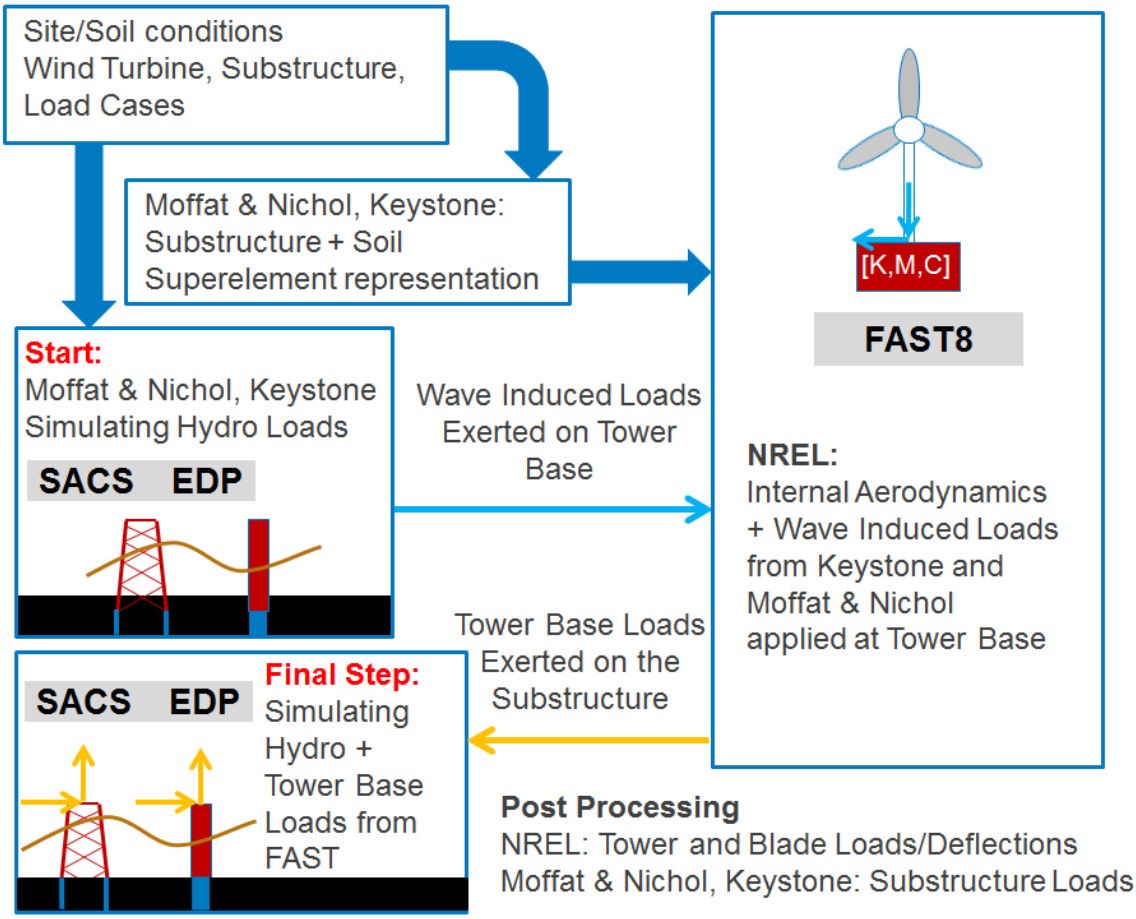

Figure 3. Schematics of the SC analysis method used in this study (Damiani et al. 2017)

For an actual design application, Keystone and Moffatt & Nichol would assess their substructure design and potentially make adjustments to the wall thickness and geometry of the substructure. Once these adjustments are completed, the SC analysis process will start over with step A. This process is repeated until the substructure design and the corresponding loads converge on a suitable solution. Because of resource and time constraints associated with this project, only one iteration from step A–H was completed.

2.2 Fully Coupled Analysis

The FC analysis method requires the use of an aero-hydro-servo-elastic (AHSE) computer-aided-engineering tool capable of simultaneously simulating aerodynamics, hydrodynamics, structural dynamics, and control system effects on an offshore wind turbine. FAST v8 is one such tool that was created by NREL and is publicly available. In this study, we modeled the substructures (monopile and jacket) via FAST v8's SubDyn module.

The FC analysis only requires one entity (NREL in this study) to perform the AHSE simulations on the complete model of the offshore wind turbine, including the RNA, tower, substructure, and foundation. The foundation is modeled by characteristic linear stiffness properties at the mudline as calculated by the substructure designers (Keystone and Moffatt & Nichol in this study). The

FC method is expected to yield more realistic load predictions, but also requires detailed design specifics on the substructure and turbine to be exchanged by the various parties.

In summary, the steps followed for the FC approach as performed in this study are:

A. Keystone and Moffatt & Nichol provide NREL with the stiffness properties at the mudline ([6-by-6] stiffness matrix and apparent fixity pile properties)

B. Keystone and Moffatt & Nichol provide NREL with the wave elevation time series to calculate the hydrodynamic loads

C. NREL runs FAST simulations of the wind/wave design load cases (DLCs) considered, for the entire system: the RNA, tower, substructure, and foundation, including aerodynamics, hydrodynamics, structural dynamics and control system dynamics

D. NREL passes the resulting loads for the major components of the substructures to Keystone and Moffatt & Nichol for postprocessing and comparison to the results from the SC approach

E. NREL postprocesses loads for the major components of the turbine and RNA.

This process is illustrated by Figure 4.

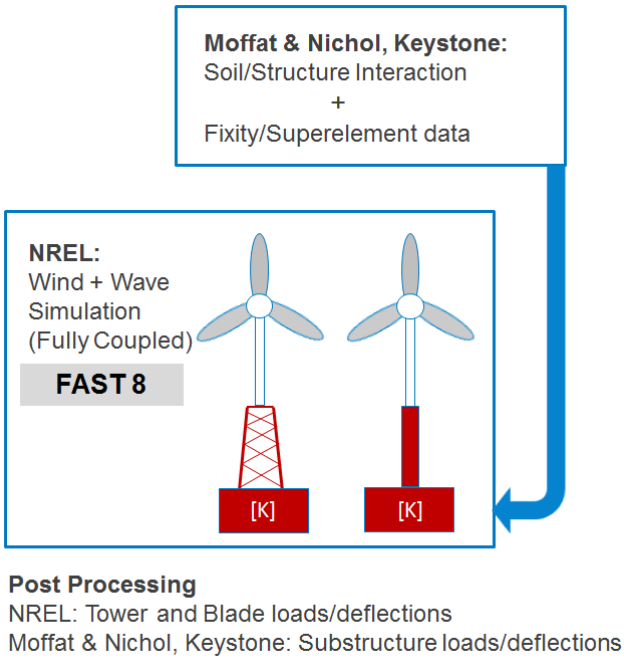

Figure 4. Schematics of the FC analysis method (Damiani et al. 2017)

Note that FAST v8 was run with the same hydrodynamic and aerodynamic seeds as in the SC method to avoid artifacts in the comparison of the two methods. All of the loads were extracted by NREL for the major components of both the turbine and substructure and compared to the SC method results.

3 Select Environmental and Turbine Parameters

3.1 Environmental Conditions

As mentioned earlier, two different offshore wind turbine configurations were selected: a monopile (suited for shallow waters [depths < 30 m]) and a lattice substructure, or jacket, (located in deeper waters [depths >50 m]). Two suitable geographical sites were thus selected along the Eastern U.S. seaboard, where offshore wind development is currently taking place and wind energy areas have been leased. NREL proposed and BSEE approved the following two sites shown in Table 1.

Table 1. Selected Analysis Sites

Site No.	Location	Substructure Type	Actual Depth/Modeled Depth
1	Frying Pan Shoals, North Carolina	Monopile	23.5 m/20 m
2	Long Island, New York	Multimember (Jacket)	40.8 m/50 m

3.1.1 Frying Pan Shoals Site (Buoy 41013)

The selected site for the monopile study is located within the proposed North Carolina offshore wind Call Area (Wilmington East) as announced by the Bureau of Ocean Energy Management (BOEM) on August 11, 2014. The water depth and wave characteristics (shown in Figure 7) correspond to the location of National Oceanic and Atmospheric Administration (NOAA) Buoy 41013 (shown in Figure 5).

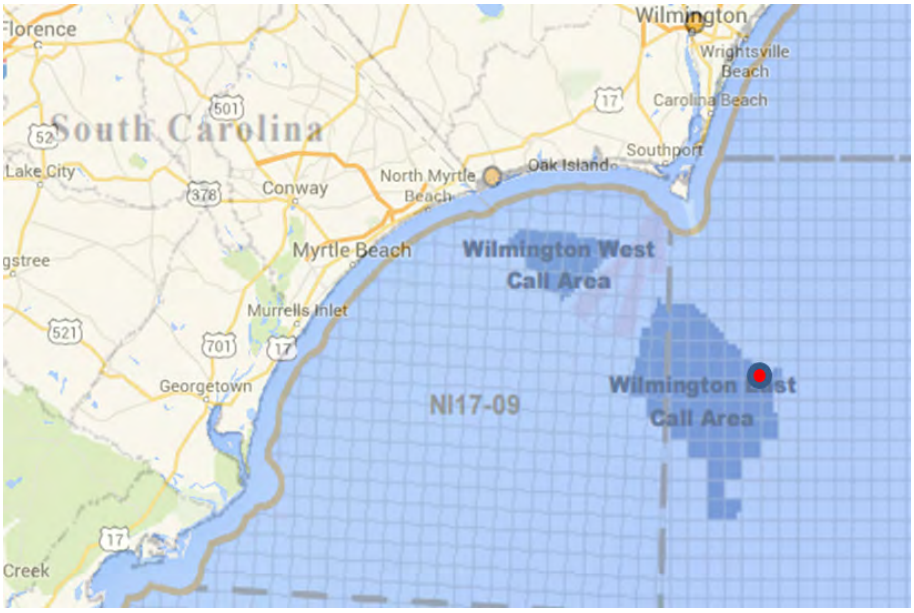

Figure 5. Location of NOAA Buoy 41013 within Wilmington East's Call Area (indicated by the red dot) (BOEM 2014)

3.1.2 Long Island Site (Buoy 44025)

The selected site for the multimember configuration is located within the New York lease area OCS-A 0512 announced by BOEM on March 15, 2017. The water depth and wave

characteristics (shown in Figure 8) correspond to the location of NOAA Buoy 44025 (shown in Figure 6).

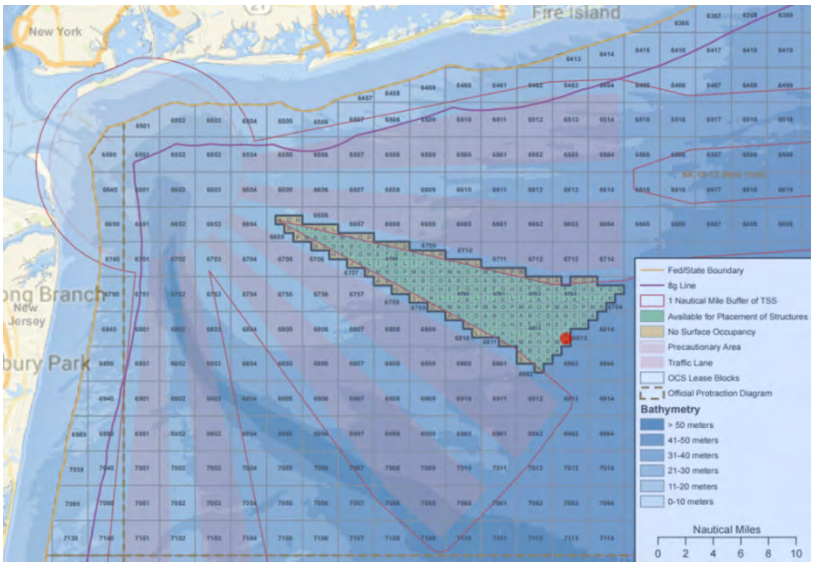

Figure 6. Location of NOAA Buoy 44025 within New York's offshore wind energy area (indicated by the red dot) (BOEM 2016)

3.1.3 Overview of Metocean Conditions

Because both locations discussed in Section 3.1.1. and 3.1.2 coincide with NOAA buoys, detailed information regarding the wave and wind conditions is available in the public domain. Table 2 gives water depth and 50-yr significant and maximum wave heights for both sites. This information is based on the analysis presented in Damiani, Dykes, and Scott (2016). Figure 7 shows the wave height as a function of hub-height (90 m above the mean sea level [MSL]) wind speeds at the North Carolina site, and Figure 8 provides the same information for the Long Island site. To correlate wave height and wave period with hub-height wind speed, the NOAA buoy wind speed data were extrapolated to hub height (90 m) using a vertical wind shear exponent of 0.1, which is oftentimes used for offshore locations. The wave height and wave period data shown in Figure 7 and Figure 8 are based on binned measurement data from 1991 to 2000 for Long Island and from 2003 to 2011 for Frying Pan Shoals.

Ocean currents were analyzed following the IEC standard (International Electrotechnical Commission 2008) guidance for the normal current model and extreme current model (more in Section 5.4), with both wind-driven near-surface currents and subsurface currents. The former were aligned with the assumed wind directions, whereas the latter were assumed to be aligned with the wave propagation directions.

Table 2. 50-yr Extreme Metocean Conditions at the Two Sites Seleced for This Study

		50-yr 1-hr Wave		
Site Name	**NOAA BUOY #**	**Hs [m]**	**Tp_Hmax [s]**	**Hmax(*) [m]**
Frying Pan Shoals	41013	10.8	13.3	18.3
Long Island	44025	9.5	12.5	17.6

(*) Hmax was limited to the breaking wave height

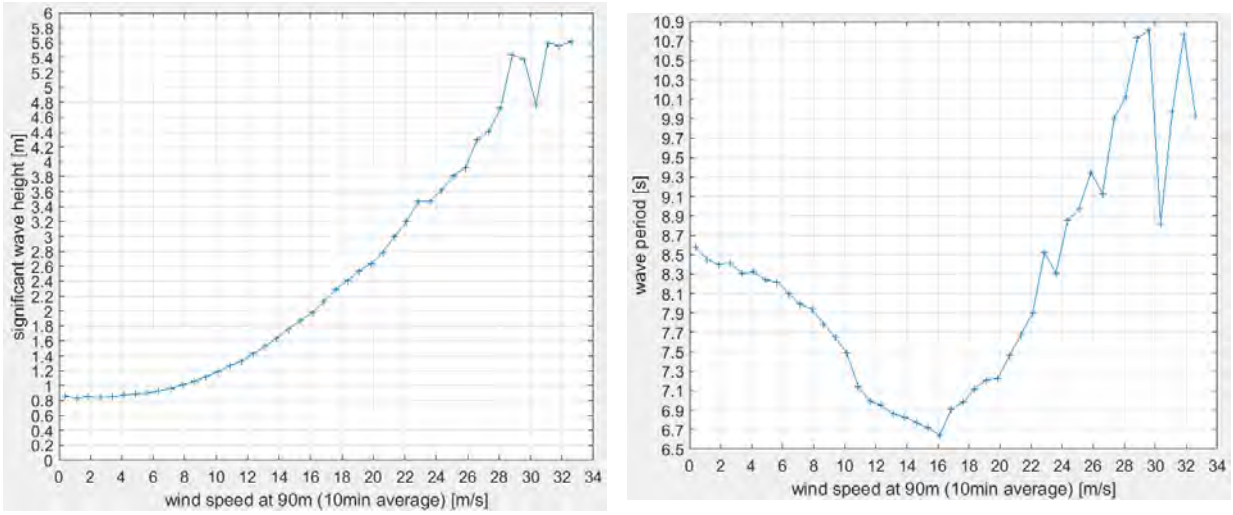

Figure 7. Significant wave height (left-hand side) and peak spectral period (right-hand side) as a function of wind speed at hub height for the Frying Pan Shoals site

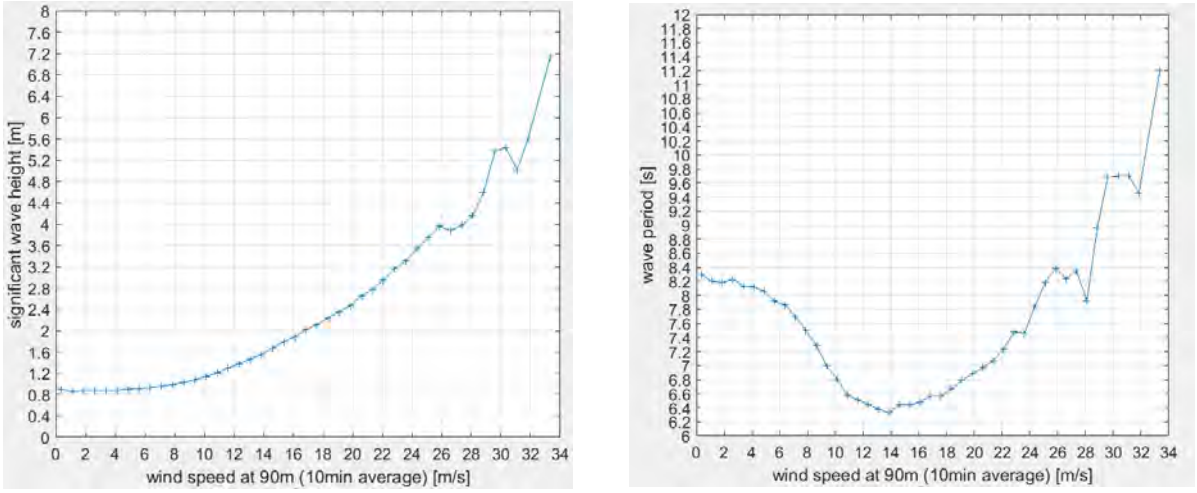

Figure 8. Significant wave height (left-hand side) and peak spectral period (right-hand side) as a function of wind speed at hub height for the Long Island wind energy area site

3.1.4 Characterization of Soil Conditions

Unfortunately, soil stratigraphic information was not publicly available for the two sites of interest; therefore, an approximate soil profile was used for both sites. This soil profile is

representative of sand layers, with the least dense top layer (dynamically "softest" stiffness) being the largest contributor to the dynamic response of the system. The simplified stratigraphy profile is given in Table 3.

Moffatt & Nichol and Keystone calculated equivalent stiffness matrices at the pile heads (mudline) to be used both in their respective simulations as well as by NREL. The subcontractors further provided stiffness, mass, and damping matrices of the equivalent superelements (substructure plus foundation effects) at the tower-base flange.

Table 3. Soil Stratigraphy Profile Assumed for This Study

Depth [m]	Specific Weight [kN/m^3]	Friction Angle [deg]
0–5	10	33
5–14	10	35
14–55.5	10	38.5

3.2 Wind Turbine Configuration

The NREL 5-megawatt (MW) (Jonkman et al. 2009) turbine was utilized for this study. The turbine key parameters are shown in Table 4. Note that the hub height was maintained constant throughout the study, therefore different towers were utilized for the monopile and jacket substructures to account for different tower interface heights associated with the two substructures. In Table 4, the acceptable range of first eigenfrequencies is shown. That frequency band was used by the subcontractors as an aid in the design of the piling. The lower bound was calculated as 1.1 times the upper limit 1P (rotor passing) frequency and the upper bound as 0.9 times the lower limit of the 3P (blade passing) frequency.

Table 4. Turbine Key Parameters

Parameter	Value
Rating	5 MW
IEC Class	I-B
Rotor Configuration	Upwind, three blades
Control	Variable speed, collective pitch
Drivetrain	High-speed, multistage gearbox
Rotor/Hub Diameter	126 m, 3 m
Hub Height	90 m
Cut-In, Rated, Cut-Out Wind Speeds	3, 11.4, 25 m/s
Cut-In, Rated, Cut-Out Rotor Speeds	6.9, 12.1 rpm
Rated Tip Speed	80 m/s
Overhang, Shaft Tilt, Precone	5 m, 5°, 2.5°
Rotor Mass	110,000 kg
Nacelle Mass	240,000 kg
Acceptable System First Eigenfrequency Range	(0.22; 0.31 Hz) Soft stiff

4 Support Structure Definition

Two substructure designs were selected based on the availability of their design specifics as public domain data:

- The Offshore Code Comparison Collaboration (OC3) monopile design (Jonkman and Musial 2010) was chosen as a good representation of the expected monopile response in shallow waters (<40 m water depths).
- The Offshore Code Comparison Collaboration, Continued with Correlation (OC4) jacket design (Popko et al. 2012) was chosen as a representative model of a multipile, multimember, lattice structure in transitional waters (40–60 m water depths).

4.1 Overview of the Monopile Configuration

The OC3 monopile configuration is made up of a constant cross section (outer diameter of 6 m with a wall thickness of 0.060 m), which assumes a 36-m embedment length. The tower base connects at an elevation of 10 m above MSL.

The monopile extends from the tower base down to the mudline, which is at 20 m below MSL. Construction steel with a Young's modulus of 210×10^9 Pa, shear modulus of 80.8×10^9 Pa, and an effective density of 8,500 kg/m^3 was assumed as the main structural material. The value of 8,500 kg/m^3 is meant to be an increase above steel's typical value of 7,850 kg/m^3 to account for the secondary mass of paint, bolts, welds, and flanges not directly included in the engineering models used in this study.

The tower-base diameter (6 m) and thickness (0.027 m) linearly taper to a top diameter of 3.87 m and a thickness of 0.019 m at a height of 87.6 m above MSL; the effective mechanical steel properties of the tower used in the Dutch Offshore Wind Energy Convertor (DOWEC) study, as given in Table 9 of (Kooijman et al. 2003), were assumed. The resulting distributed support structure properties are given in Table 5. A detailed description of the OC3 monopile can be found at (Jokman and Musial 2010). Note that the OC3 transition piece was modeled as an integral part of the monopile, with no special arrangements or provisions for its analysis.

A structural damping ratio of 1% of critical was assumed.

Table 5. Distributed Properties for the Monopile and Tower Used In This Study for the Frying Pan Shoals Site

Z MSL [m]	TMassDen [kg/m]	TwFAStiff [Nm^2]	TwSSStif [Nm^2]	TwGJStif [Nm^2]	TwEAStif [N]	TwFAIner [kg m]	TwSSIner [kg m]	TwFAcgOf [m]	TwSScgOf [m]
-56	9,517.14	1.04E+12	1.04E+12	7.98E+11	2.35E+11	41,979.2	41,979.2	0	0
-20	9,517.14	1.04E+12	1.04E+12	7.98E+11	2.35E+11	41,979.2	41,979.2	0	0
10	9,517.14	1.04E+12	1.04E+12	7.98E+11	2.35E+11	41,979.2	41,979.2	0	0
10	4,306.51	4.74E+11	4.74E+11	3.65E+11	1.06E+11	19,205.6	19,205.6	0	0
17.76	4,030.44	4.13E+11	4.13E+11	3.18E+11	9.96E+10	16,720	16,720	0	0
25.52	3,763.45	3.58E+11	3.58E+11	2.75E+11	9.30E+10	14,483.4	14,483.4	0	0
33.28	3,505.52	3.08E+11	3.08E+11	2.37E+11	8.66E+10	12,478.7	12,478.7	0	0
41.04	3,256.66	2.64E+11	2.64E+11	2.03E+11	8.05E+10	10,689.2	10,689.2	0	0
48.8	3,016.86	2.25E+11	2.25E+11	1.73E+11	7.45E+10	9,098.9	9,098.9	0	0
56.56	2,786.13	1.90E+11	1.90E+11	1.46E+11	6.88E+10	7,692.7	7,692.7	0	0
64.32	2,564.46	1.59E+11	1.59E+11	1.23E+11	6.34E+10	6,455.7	6,455.7	0	0
72.08	2,351.87	1.33E+11	1.33E+11	1.02E+11	5.81E+10	5,373.9	5,373.9	0	0
79.84	2,148.34	1.10E+11	1.10E+11	8.43E+10	5.31E+10	4,433.6	4,433.6	0	0
87.6	1,953.87	8.95E+10	8.95E+10	6.89E+10	4.83E+10	3,622.1	3,622.1	0	0

The geometry of the embedded portion of the monopile is given in Table 6. The pile was sized based on extreme loads calculated from maximum operational and parked load cases assuming the metocean conditions discussed earlier. Moffatt & Nichol verified the capacity of the pile under maximum wave, current, and thrust from the turbine.

Table 6. Embedded Pile Geometry

Depth Below Mudline [m]	Outer Diameter [m]	t [m]
0–36	6	0.06

Finally, a summary of the undistributed properties of the support structure is shown in Table 7.

Table 7. Undistributed Properties for the Support Structure (Monopile Configuration)

Parameter	Value
Tower-Top Height Above MSL	87.6 m
Tower-Base Height Above MSL	10 m
Overall Mass	522,617 kg
Center of Gravity Location (with respect to mudline along tower centerline)	37.172 m
Structural Damping Ratio (All Modes)	1%

4.2 Overview of the Jacket Configuration

A drawing of the OC4 jacket (traditional four-legged jacket with cross braces) is shown in Figure 9, which also highlights the monolithic transition piece (TP) used. The TP is a complex subcomponent of the support structure, which would require a dedicated study for its design and analysis, especially with regard to fatigue. Because the primary focus of this study relies on ULS analysis, the OC4 simplified model of the TP was deemed sufficient to highlight differences in the employed calculation methods. In future studies, the TP geometry should be defined with care and then a fatigue limit state analysis could be carried out by following the approaches indicated in this study (see also Section 2).

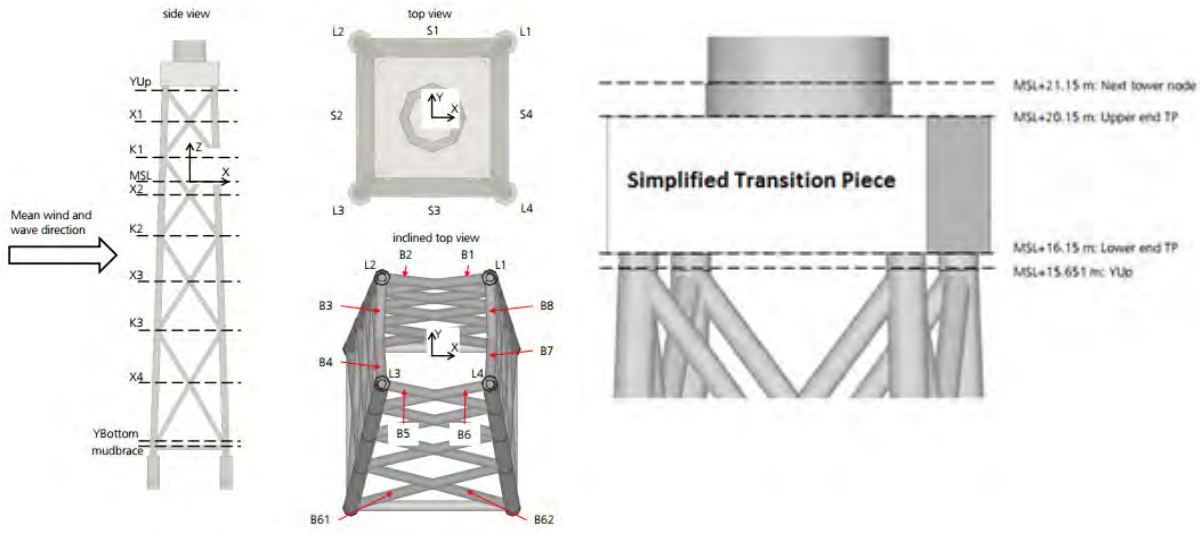

Figure 9. Overall schematic of the jacket and transition piece for the multimember substructure used in this study

A detailed description of the OC4 jacket can be found in (Vorprahl 2013). The tower-distributed mass and stiffness properties are given in Table 8. The tower for this configuration has a base diameter of 5.6 m with a wall thickness of 0.032 m, whereas the outer diameter at the top is 4 m and the wall thickness is 0.03 m.

Table 8. Distributed Properties for the Tower on Top of the Jacket

Z MSL [m]	TMassDen [kg/m]	TwFAStiff [Nm^2]	TwSSStif [Nm^2]
20.15	4,900.473	4.56E+11	4.56E+11
21.85	4,900.473	4.44E+11	4.44E+11
25.25	4,200.272	4.17E+11	4.17E+11
28.65	4,057.18	3.91E+11	3.91E+11
32.05	3,915.575	3.67E+11	3.67E+11
35.45	3,770.476	3.42E+11	3.42E+11
38.85	3,626.859	3.19E+11	3.19E+11
42.25	3,477.86	2.97E+11	2.97E+11
45.65	3,291.027	2.72E+11	2.72E+11
49.05	3,102.113	2.48E+11	2.48E+11
52.45	3,123.485	2.26E+11	2.26E+11
55.85	2,969.644	2.07E+11	2.07E+11
59.25	2,639.437	1.91E+11	1.91E+11
62.65	2,517.769	1.76E+11	1.76E+11
66.05	2,398.659	1.62E+11	1.62E+11
69.45	2,282.134	1.49E+11	1.49E+11
72.85	2,173.814	1.37E+11	1.37E+11
76.25	2,344.182	1.42E+11	1.42E+11
79.65	2,687.067	1.57E+11	1.57E+11
83.05	2,971.055	1.69E+11	1.69E+11
86.45	3,260.985	1.60E+11	1.60E+11
88.15	3,260.985	1.55E+11	1.55E+11

The geometry of the piles is given in Table 9. The piles were sized based on extreme loads calculated from maximum operational and parked load cases assuming the metocean conditions discussed earlier. Similar to what was done for the monopile by Moffatt & Nichol, Keystone verified the capacity of the pile under maximum wave, current, and thrust from the turbine.

Table 9. Embedded Pile Geometry

Depth Below Mudline [m]	OD [m]	t [m]
0–55.5	2.082	0.06

5 Modeling Assumptions and Design Load Cases

5.1 Hydrodynamics

Because of the limited resources for this study, all models were analyzed in a "clean" condition (no marine growth). Additionally, no "constrained" waves and no stretching were considered in this study. Wave stretching models provide a more realistic representation of the near-surface wave kinematics than linear wave theory (Airy 1841). However, different wave stretching schemes exist in the literature, and important differences exist in the various software implementations, which can give rise to significantly different structural responses (Rodenbusch and Forristall 1986). To minimize the effects related to potential differences in the utilized hydrodynamics models, only linear wave (Airy) theory was considered. Constrained waves, which are large, deterministic waves embedded in a typical stochastic wave time-history profile were not included in this study for two reasons. First and foremost, constrained waves are thought to be the most important for relatively static structures (such as oil and gas fixed-bottom platforms) and less important for highly dynamic response machines, such as wind turbines, in which stochasticity is crucial. Second, the method suggested in (International Electrotechnical Commission 2008) is computationally inefficient and requires extensive preprocessing time (Rainey and Camp 2007), which was not available for this study. New and more efficient methods have recently been proposed in the literature. Future research could include this effect in this type of investigation.

5.2 Coordinate Systems, Load Channels, and Substructure Nodes of Interest

Global and local coordinate systems were established at the beginning of the analysis and agreed upon by all team members (see Figure 10a).

For loads on the tower and monopile, the global coordinate system, wherein the x-axis is aligned with the nominal wind direction, the z-axis points upward, and the y-axis is determined by the right-hand rule. For the jacket members, a local coordinate system is also employed (see Figure 10b), with the z-axis along the member axis, the x-axis in the horizontal plane, and the y-axis is determined by the right-hand rule.

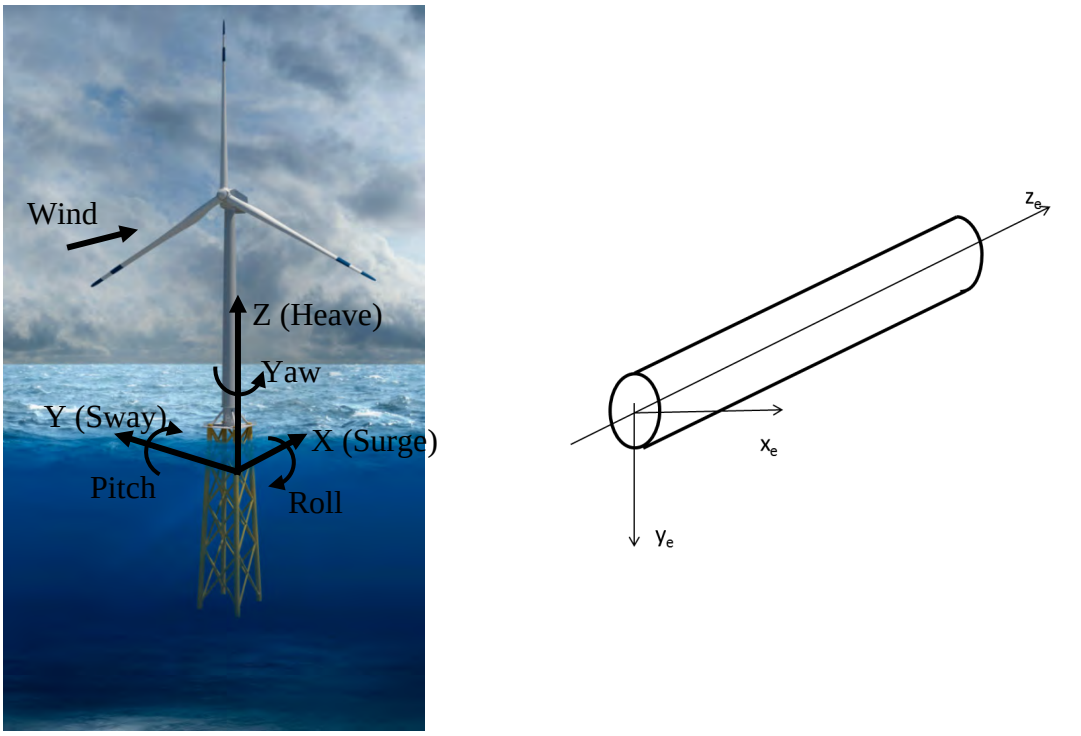

Figure 10. Global coordinate system (a) and local coordinate system for a typical structural member (b)

For blade loads, the coordinate system has the z-axis along the blade axis, the y-axis along the chord, and the x-axis is determined by the right-hand rule (see Figure 11a). The low-speed shaft coordinate system has the x-axis aligned with the shaft axis, the z-axis pointing upward, and the y-axis is determined by the right-hand rule (see Figure 11b).

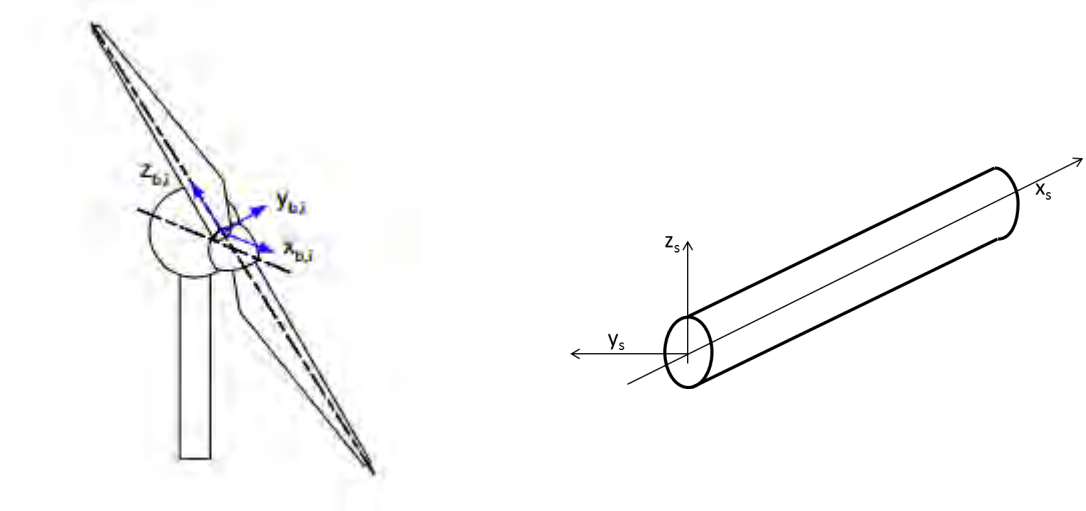

Figure 11. Blade (a) and shaft (b) local coordinate systems

5.2.1 Load Channels

For the comparison between fully coupled and sequentially coupled approaches, we considered two sets of load channels, one for the RNA and tower, and one for the substructure.

The RNA and tower loads included blade root loads, low-speed-shaft loads, tower-top (denoted as yaw-bearing) loads, and tower-bottom loads (see also Table 10). For the blade root loads, we calculated shears (Fx, Fy) and bending moments (Mx, My) per the blade coordinate system. For completeness, we also included the axial force (Fz) and torsion (Mz), although they do not account for dynamic extensional effects and the torsional degree of freedom of the blades. These latter loads are, for typical rotor sizes and stiffness, relatively small and not driving the design. Nonetheless, future rotor blades (longer and more slender) might present significant torsional and axial loads, and this aspect should be revisited.

Shaft loads included bending moments (My, Mz; i.e., pitch and roll bending moments) per the coordinate system in Figure 11b. Yaw-bearing and tower-base loads included three forces (Fx, Fy, Fz) and three moments (Mx, My, Mz) per the global coordinate system.

Table 10. RNA and Tower Load Symbols Used in This Report

Component	Load	Symbols Used in the Graphs	Units Used in Graphs and Tables (Unless Otherwise Noted)
Blade Root	Fx–Fz, Mx–Mz	BladeRootFx, BladeRootFy, BladeRootFz, BladeRootMx, BladeRootMy, BladeRootMz	kN, kNm
Shaft	My, Mz	LSSMy, LSSMz	kNm
Yaw Bearing (Tower Top)	Fx–Fz, Mx–Mz	YawBearingFx, YawBearingFy, YawBearingFz, YawBearingMx, YawBearingMy, YawBearingMz	kN, kNm
Tower Base	Fx–Fz, Mx–Mz	TowerBaseFx, TowerBaseFy, TowerBaseFz, TowerBaseMx, TowerBaseMy, TowerBaseMz	kN, kNm

For the monopile, we compared the loads at the stations located at 0 m MSL (Mx, My), -10 m MSL (Mx, My), and the mudline (Fx, Fy, Fz, Mx, My, Mz) per the global coordinate system.

Table 11. Monopile Load Symbols and Units Used in This Report

Component	Load	Symbols Used in the Graphs	Units Used in Graphs and Tables (Unless Otherwise Noted)
Loads at 0 m MSL	Mx–My	MSL_Mx, MSL_My	MNm
Loads at -10m MSL	My, Mz	Mx_10m_depth, My_10m_depth	MNm
Loads at Mudline (-20 m MSL)	Fx–Fz, Mx–Mz	Fx_mudline, Fy_mudline, Fz_mudline, Mx_mudline, My_mudline, Mz_mudline	MN, MNm

Figure 12 and Table 12 show the selected nodes of the jacket where certain load components (per the member coordinate system) were extracted and compared between the two methods. K1L1 and K1L2 represent upper leg nodes (upwind and downwind, respectively), wherein axial forces were extracted for leg members 23 and 19; K4L2 and K4L1 represent lower leg nodes, wherein axial forces and bending moments were extracted for brace members 37, 41, 45, and 47; RL2 and RL1 represent pile head locations at the mudline (upwind and downwind, respectively), wherein all six components of internal loads were calculated.

Table 12. Nodes and Members Analyzed for the Jacket, Including Load Components Considered in This Report

Node	Member	Load	Symbols Used in the Graphs	Units Used in Graphs and Tables (Unless Otherwise Noted)
K1L2	23	Fz	K1L2	kN
K1L1	19	Fz	K1L1	kN
K4L2	41	Mx, My, Fz	K4L2_YZ	kNm, kN
K4L2	47	Mx, My, Fz	K4L2_XZ	kNm, kN
K4L1	37	Mx, My, Fz	K4L1_YZ	kNm, kN
K4L1	45	Mx, My, Fz	K4L1_XZ	kNm, kN
K5L2	33	Fz	K5L2	kN
RL2	111	Fx--Fz, Mx--Mz	RL2	kN, kNm
RL1	109	Fx--Fz, Mx--Mz	RL1	kN, kNm

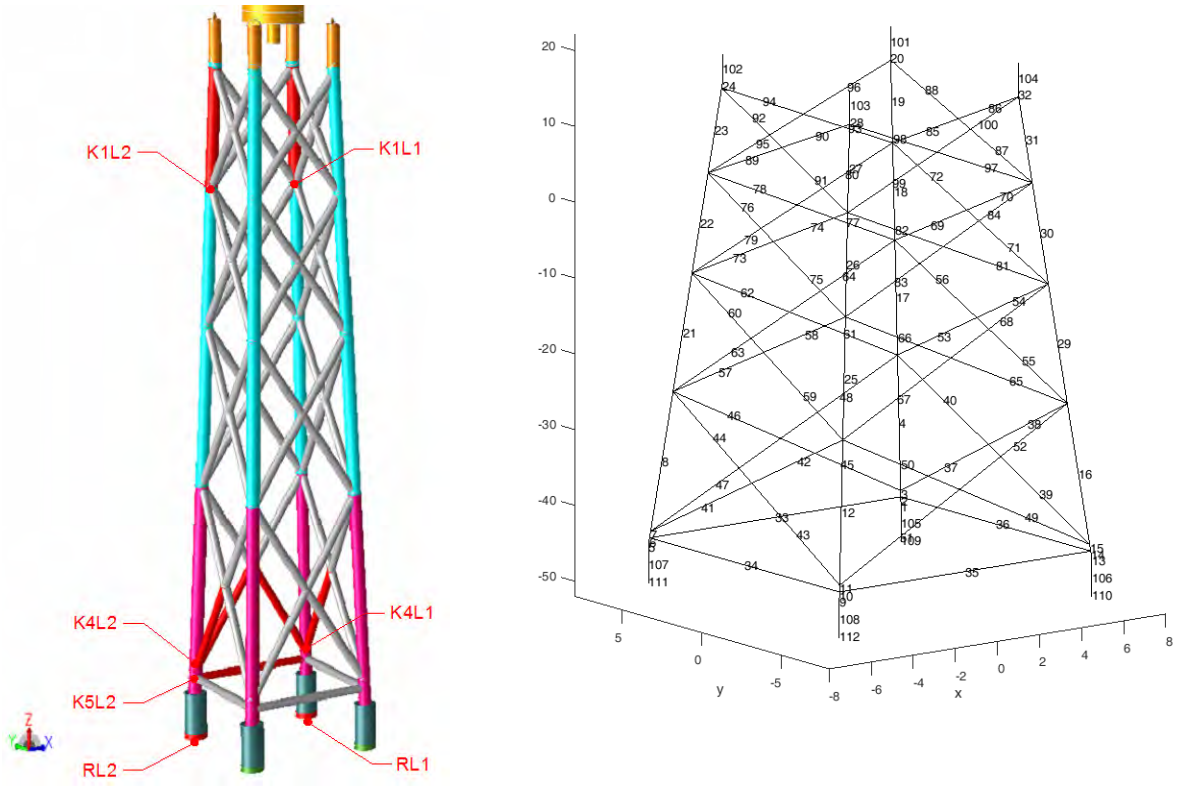

Figure 12. Nodes of interest for the jacket substructure from which loads were extracted and compared between the two approaches (left); member numbers (right)

5.3 Exchange Data Format

All data were exchanged via either text (ASCII) or Microsoft Excel files. Version control of all of the files was implemented to account for modifications and iterations among all parties involved.

5.4 Design Load Cases

The DLCs presented in Table 13 are a subset of those prescribed by the IEC design standard 61400-3 (International Electrotechnical Commission 2008); these DLCs are generally driving cases for offshore wind turbine design and were selected for this study because they should provide the most relevant information to emphasize differences in the methodology (fully coupled vs. sequentially coupled). Two main categories are selected: a power production set (DLC 1.1) and a parked (extreme event) set (DLC 6.1).

The selected wave conditions were based on the site-specific conditions detailed in Section 3.1. The selected 50-year extreme wind speed for DLC 6.1a is based on the requirements for a Class I turbine as specified in the IEC-61400-1 standard. The selected subsurface current speeds are based on ocean surface current data from the National Aeronautics and Space Administration (NASA undated) and further discussions with the partners. The tidal conditions are based on the analysis in (Damiani, Dykes, and Scott 2016) and further discussions with the partners. A Joint North Sea Wave Project spectrum was used for all simulations, with a shape factor of 3.3. The effective simulation length was set at 600 seconds (s); 150 s of transient time was discarded prior to the actual 600-s simulation output. During an actual industry project, at least 6 seeds would be

considered to achieve a statistically sound representation of the entire wave spectrum. Given the limited resources allocated to this project, only one seed was analyzed. However, because the nature of this project is focused on identifying the differences between the two modeling approaches and not on the development of an actual substructure design for a given site, a single seed was deemed sufficient. Subsurface currents were aligned with the wave direction, whereas surface currents were aligned with the wind direction. For the monopile, only the 0-degree wind direction was used, because of the axial symmetry of the structure. Further, note the fact that the wave time series were generated by Moffatt & Nichol and Keystone and used by NREL for both the sequentially coupled and fully coupled approach as direct inputs to the aero-hydro-servo-elastic software. To minimize potential issues related to different hydrodynamic modeling approaches, simple linear airy wave theory without any additional free-surface treatment was used by all project partners.

To have a common nomenclature among all parties and distinguish the results from various load cases, Table 14 and Table 15 show the identifiers used for the DLCs, together with the simulated key environmental parameter values.

Table 13. Load Cases Analyzed in This Study

DLC-1.1 (Normal Power Production):		
Wind Model:	Normal Turbulence Model	
Wind Speeds (WS):	12 m/s at hub height (90 m)	
Wind Direction (WD):	0, 45	
Wave Model:	Normal Sea State (NSS)	
	Jacket:	Significant Wave Height (Hs)=1.3410 m
		Peak Period (Tp)=6.4792 s
	Monopile:	Hs=1.3813 m, Tp=6.9695 s
Wave Direction:	0, 45, 90, 135	
Current Model:	Normal Current Model	
	Jacket:	Subsurface current at still water level: 0.6 m/s
		Near-surface current (20-m reference depth): 0.0838 m/s
	Monopile:	Subsurface current at still water level: 0.6 m/s
		Near-surface current (20-m reference depth): 0.0838 m/s
Tidal Conditions:	Normal Water Level Range	
	Jacket:	0 m tidal offset
	Monopile:	0 m tidal offset
Sim. Length:	10min	
Max (*) Number of Simulations:	1 Wind Seed (WS) x 2 Wind Direction (WD)	
	x 4Wave Direction (WVD) = 8 (Jacket)	
	1WS x 1WD x 4WVD= 4 (Monopile)	
DLC-6.1a (Parked with Grid Loss, 50-year Extreme Conditions):		
Wind Model:	Extreme Wind Speed Model	
Wind Speeds (WS):	50 m/s at hub height (90 m)	
Wind Direction (WD):	0, 45 degrees	
Wave Model:	Extreme Sea State (ESS)	
	Jacket:	Hs=09.5 m, Tp=12.5 s
	Monopile:	Hs=10.8 m, Tp=13.3 s
Wave Orientations:	Co-directional and Misaligned) 90	
Current Model:	Extreme Current Model	
	Jacket:	Subsurface current at still water level: 1.2 m/s
		Near-surface current (20-m reference depth): 0.349 m/s
	Monopile:	Subsurface current at still water level: 1.2 m/s
		Near-surface current (20-m reference depth): 0.349 m/s
Tidal Conditions: Extreme Water Level Range		
	Jacket:	+2.50m combined surge/tidal offset
	Monopile:	+1.25m combined surge/tidal offset
Sim. Length:	10min	
Yaw Misalignments [deg]:	0, 10	
Max (*) Number of Simulations:		1WS x 2 WD x 2 WVD x 2YawErrors = 8 (Jacket)
		1WS x 1 WD x 2 WVD x 2YawErrors = 4 (Monopile)

Table 14. Load Case Identifiers and Key Parameters for the Monopile Analysis

Design Load Case	Identifier	Wind Speed, Vhub	Wave & Subsurface Current Direction	Yaw Error	Sea State	Significant Wave Height	Peak Spectral Period	Storm Surge
		[m/s]	[deg]	[deg]		[m]	[s]	[m]
1.1	A001	12	0	0	NSS	1.3813	6.9695	0
1.1	A002	12	45	0	NSS	1.3813	6.9695	0
1.1	A003	12	90	0	NSS	1.3813	6.9695	0
1.1	A004	12	135	0	NSS	1.3813	6.9695	0
6.1a	B001	50	0	0	ESS	10.8000	13.3000	1.25
6.1a	B002	50	0	10	ESS	10.8000	13.3000	1.25
6.1a	B003	50	90	0	ESS	10.8000	13.3000	1.25
6.1a	B004	50	90	10	ESS	10.8000	13.3000	1.25

Table 15. Load Case Identifiers and Key Parameters for the Jacket Analysis

Design Load Case	Identifier	Wind Speed, Vhub	Wind Direction	Wave & Subsurface Current Direction	Yaw Error	Sea State	Significant Wave Height	Peak Spectral Period	Storm Surge
		[m/s]	[deg]	[deg]	[deg]		[m]	[s]	[m]
1.1	A001	12	0	0	0	NSS	1.341	6.4792	0
1.1	A002	12	0	45	0	NSS	1.341	6.4792	0
1.1	A003	12	0	90	0	NSS	1.341	6.4792	0
1.1	A004	12	0	135	0	NSS	1.341	6.4792	0
1.1	A005	12	45	0	0	NSS	1.341	6.4792	2.5
1.1	A006	12	45	45	0	NSS	1.341	6.4792	2.5
1.1	A007	12	45	90	0	NSS	1.341	6.4792	2.5
1.1	A008	12	45	135	0	NSS	1.341	6.4792	2.5
6.1a	B001	50	0	0	0	ESS	9.500	12.5000	2.5
6.1a	B002	50	0	0	10	ESS	9.500	12.5000	2.5
6.1a	B003	50	0	90	0	ESS	9.500	12.5000	2.5
6.1a	B004	50	0	90	10	ESS	9.500	12.5000	2.5
6.1a	B005	50	45	45	0	ESS	9.500	12.5000	2.5
6.1a	B006	50	45	45	10	ESS	9.500	12.5000	2.5
6.1a	B007	50	45	135	0	ESS	9.500	12.5000	2.5
6.1a	B008	50	45	135	10	ESS	9.500	12.5000	2.5

6 Model-to-Model Verification

Prior to initiating the load simulations for the selected DLCs, the team performed a set of dedicated analyses to verify that the respective models were consistent in terms of overall mass and inertial properties. These analyses required extensive quality control activities by all parties and were particularly time consuming as they required several iterations to arrive at a common basis among all models. This process involved several modifications to the inputs and assumptions (e.g., coordinate systems; retained degrees of freedom; member flooding; units; and definition of wave, wind, and current directions and profiles) among the various software programs. The first set of comparisons was done between the standalone SubDyn (FAST v8's substructure structural dynamics module) and SACS/EDP. Mass, buoyancy, center of gravity (CG) location, and eigenfrequencies of the substructures above the mudline were compared, while also considering stiffness effects at the pile heads. A brief summary of this initial validation step is given in Table 16 and Table 17. The difference in dry mass for the jacket is simply caused by the way the transition piece is modeled in FAST v8 (included as a lumped mass in the ElastoDyn module input and transparent to SubDyn) and in SACS (included in the jacket model), and was therefore expected and did not cause any issues. Eigenfrequencies were also assessed for the entire offshore wind turbine, and in this case, the FAST v8 results were postprocessed via spectral analysis and compared to Moffatt & Nichol's and Keystone's model data (see Table 18).

Table 16. Comparison of Overall Inertial Properties Among Different Models

Parameter	Monopile			Jacket		
	FAST	EDP	**Delta (%)**	FAST	SACS	**Delta (%)**
Tower Mass [kg]	237,098	237,001	0.04	216,614	219,800	-1.47
Tower Z-CG abv. Still Water Line [m]	43.821	43.87	-0.11	50.55	49.83	1.43
RNA Mass [kg]	350,000	350,000	0.00	350,000	350,000	0.0001
RNA Z-CG abv. Still Water Line [m]	89.571	89.57	0.00	89.57	89.57	0.0015
Substructure Mass (dry) [kg]	2.86E+05	285,432	0.03	6.74E+05	6.86E+05	-1.80
Substructure Z-CG (dry) abv. Still Water Line [m]	-5	-5	0.00	-21.90	-22.36	-2.08
Transition Piece Mass [kg]					666,000	-
Overall Mass (dry) [kg]	8.73E+05	872,433	0.02	1.24E+06	1.92E+06	-54.92
Submerged Volume [m^3]	5.65E+02	565.49	0.00	497.36	497.31	0.01
Ballasted Volume [m^3]	0.00E+00	0	0.00	199.59	199.55	0.02
Buoyant Volume [m^3]				297.77	297.76	0.00

Table 17. Comparison of First Eigenfrequencies for the Monopile and Jacket Among Different Models

	Monopile (Only Substructure)			Jacket (Only Substructure)		
	FAST	EDP	**Delta %**	FAST	SACS	**Delta %**
Eigenfrequency [Hz]	2.75	2.76	-0.27	2.76	2.68	2.89
	2.75	2.76	-0.27	2.76	2.68	2.89
	5.93	5.93	0.02	5.00	5.25	-4.92
	16.3	16.78	-2.98	5.41	-	-
	16.3	16.78	-2.98	7.63	7.43	2.71

Table 18. Comparison of First Eigenfrequencies for Monopile- and Jacket-Based Offshore Wind Turbine Systems Among Different Models

	Monopile Offshore Wind Turbine			Jacket Offshore Wind Turbine		
	FAST	EDP	**Delta %**	FAST	SACS	**Delta %**
Eigenfrequency [Hz]	0.23	0.25	-7.05	0.3	0.3	-1.04
	0.24	0.25	-2.59	0.3	0.3	-1.54
	1.42	1.47	-3.5	0.94	0.9	4.21
	1.33	1.47	-10.51	0.93	0.91	1.80
				2.06	1.73	15.97

Overall differences were less than about 3%, except for eigenfrequencies above the fourth mode.

A second level of verification entailed comparing the dynamic response of NREL's FAST v8 full offshore wind turbine model to Moffatt & Nichol's and Keystone's models for a few simple cases. In fact, because the hydrodynamic loads were to be computed by Moffatt & Nichol and Keystone for the sequentially coupled approach and by NREL for the fully coupled approach, we had to ensure that all team members utilized a consistent hydrodynamic modeling approach. A comparison of the hydrodynamic loads time series for a simple test case for the monopile and jacket are shown in Figure 13 through Figure 16.

For the monopile, we considered a power production case (e.g., A001) with a regular (sinusoidal) wave with a 1.3813-m height and 6.9695-s period. For the jacket, we performed the verification on DLC A001-A003 and B001, B003, and B005.

As shown in Figure 13 through Figure 16, relatively good agreement was achieved in the loads calculated in the substructures, which instilled confidence in both the overall calculation process and the hydrodynamic modeling assumptions.

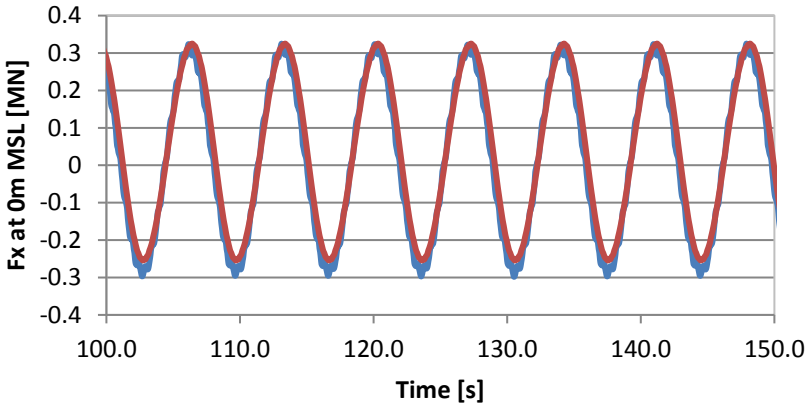

Figure 13. Monopile shear at MSL as calculated by NREL (in red) and Moffat & Nichol (in blue) for a simple test case (H=1.3813 m, Tp=6.9695 s)

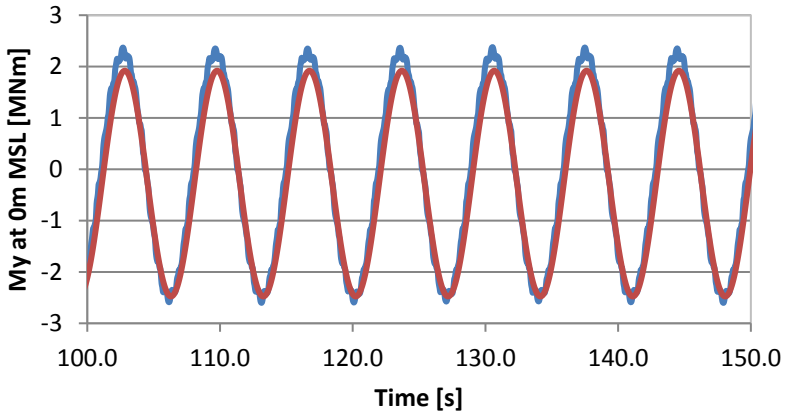

Figure 14. Monopile MSL overturning moment calculated by NREL (in red) and Moffat & Nichol (in blue) for a simple test case (H=1.3813 m, Tp=6.9695 s)

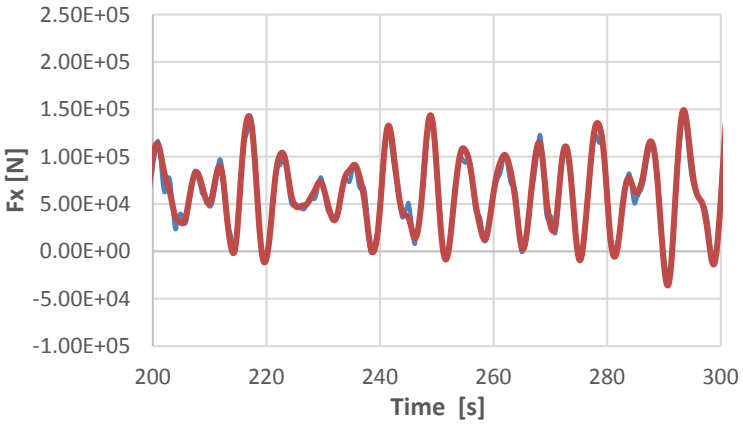

Figure 15. Equivalent hydrodynamic load Fx (NREL [in red] and Moffat & Nichol [in blue]) to be applied at the tower base for the verification case discussed in the text (same wave conditions as described for load case A002)

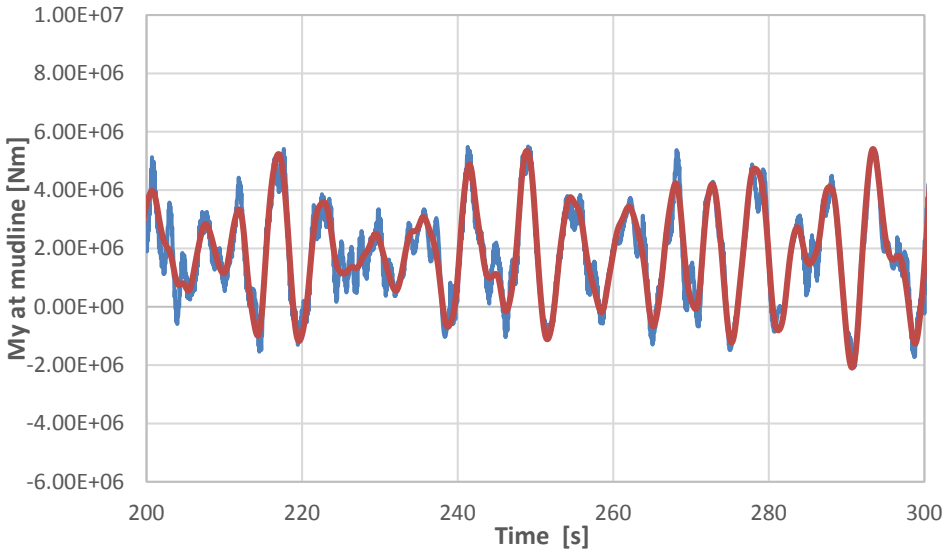

Figure 16. Overall moment reaction My (NREL [in red] and Moffat & Nichol [in blue]) at the mudline for the verification case discussed in the text (same wave conditions as described for load case A002)

7 Maximum Loads Comparison for ULS Load Cases

In this section, we provide comments on the observed results for the maximum loads as calculated with the two approaches for various components and under the ULS design load cases listed in Table 13 through Table 15. We separated the power production and parked cases into two subsections for the monopile and jacket offshore wind turbine, respectively. For a complete gallery of the results in terms of calculated ULS loads and differences between FC and SC methods, see Appendix A. The symbols used in those graphs are explained in Section 5.2.1. In this section, we also provide summary tables that compile the differences in overall maxima across all power production and parked cases, respectively; the summary tables help assess whether one method is more conservative overall than the other for a specific load channel. The differences are given in terms of errors relative to the FC results (i.e., ((SC-FC)/FC)*100), which we assumed closer to the expected actual loads. The difference between FC and SC is color coded in the tables below. Green indicates situations in which the SC approach is more conservative and red indicates situations in which the FC approach is more conservative. A color scale ranging from green, yellow, and red is used to qualitatively indicate the magnitude of the observed differences (e.g., yellow indicating relatively small differences with the FC approach being conservative, and orange indicating relatively small differences with the SC approach being conservative).

7.1 Monopile–Power Production: Comparison of Overall Maximum Loads

Overall, there was good agreement among the SC and FC results (see Table 19, Table 20, and Table 21). SC tends to give results that are more conservative than FC in most cases, which implies that the designs evaluated with the SC approach should at least be as safe as those that are verified via the more rigorous FC approach, though designs might therefore be overconservative. Nonetheless, the FC approach is more conservative in several channels: shaft *LSSMy*, tower-top *YawBearingMx*, *YawBearingFy*, tower-base *TowerBaseFy*, and *TowerBaseMx*. The large difference between FC and SC for *BladeRootMz* shown in Table 19 is related to an artifact in the *BladeRootMz* signal that is discussed in Section 7.1.1.

Table 19. Maximum Turbine Loads During Power Production (Monopile); Part 1

	BladeRootFx	BladeRootFy	BladeRootFz	BladeRootMx	BladeRootMy	BladeRootMz	LSSMy	LSSMz	YawBearingFx	YawBearingFy
Fully Coupled	395	245.4	860.1	6,031	14,020	3,430	7,303	6,824	942.9	237
Sequentially Coupled	400.3	261.1	858.2	6,093	14,070	118.4	6,837	6,809	954.3	222.4
Delta (%)	1.3	6.4	-0.2	1.0	0.4	-96.5	-6.4	-0.2	1.2	-6.2

Color code explained in Section 7.

Table 20. Maximum Turbine Loads During Power Production (Monopile); Part 2

	YawBearingFz	YawBearingMx	YawBearingMy	YawBearingMz	TowerBaseFx	TowerBaseFy	TowerBaseFz	TowerBaseMx	TowerBaseMy	TowerBaseMz
Fully Coupled	3,566	5,274	5,653	5,974	981.4	282.6	5,900	23,530	72,470	5,974
Sequentially Coupled	4,328	5,014	5,842	6,036	1,012	271.8	7,245	22,120	72,900	6,036
Delta (%)	21.4	-4.9	3.3	1.0	3.1	-3.8	22.8	-6.0	0.6	1.0

Table 21. Maximum Substructure Loads During Power Production (Monopile)

	MSL_Mx	MSL_My	Mx_10m_depth	My_10m_depth	Fx_mudline	Fy_mudline	Fz_mudline	Mx_mudline	My_mudline	Mz_mudline
Fully Coupled	25.9	81.9	28.9	91.9	1.4	0.6	8.7	33.8	103.4	6.0
Sequentially Coupled	24.6	82.3	27.7	92.2	1.4	0.6	9.7	32.3	104.0	6.0
Delta (%)	-4.8	0.6	-4.2	0.3	-2.8	-0.9	11.9	-4.5	0.6	0.1

7.1.1 Blade Loads

The blade loads agree relatively well between the FC and SC approaches (see Appendix A: ULS Result Gallery). The largest differences are in the Fy shear force (an approximate 6% difference). The extremely large differences observed for the maximum blade torsion loads (BladeRootMz) are caused by an artifact in the FC simulation that pushes the maximum for this channel to unrealistic values. This issue is only observed for the monopile simulations during power production. A time series plot of the Mz signal is shown in Figure 17, wherein a single isolated spike in the signal is shown, and which is not accompanied by similar spikes in the other load channels investigated within this project. Also, it is important to note that, as mentioned earlier, these results do not include the dynamic response of the blades along the torsional degree of freedom, as typical blades are very stiff in torsion. More analysis is needed to identify the cause for this numerical artifact in the BladeRootMz signal.

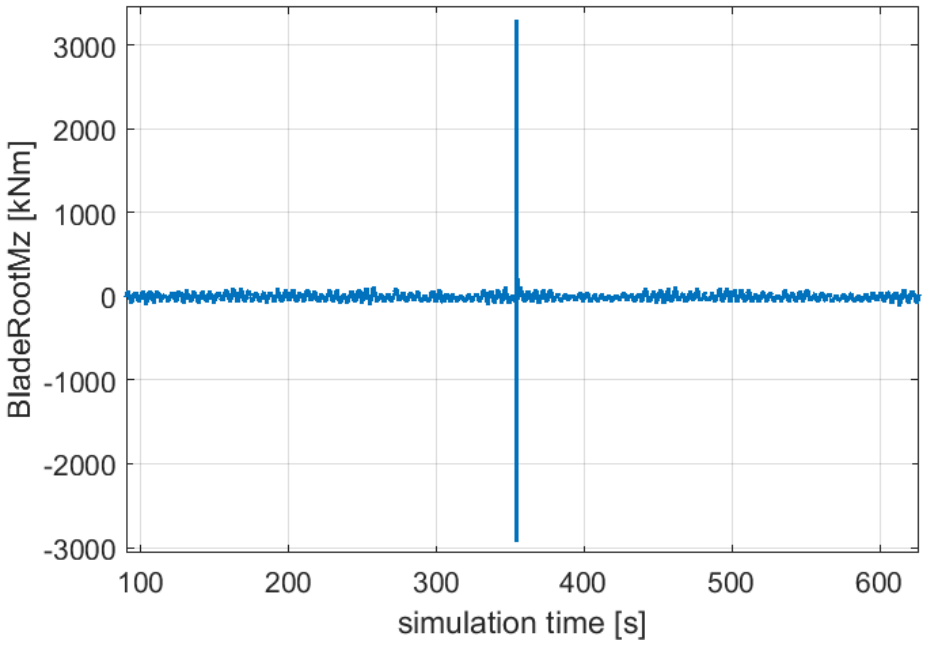

Figure 17. Typical time series of the torsional moment at the blade root as observed in the simulations

7.1.2 Shaft Loads

Relatively good agreement between FC and SC was also observed for the low-speed-shaft bending moments (differences on the order of ~6% and ~1% for My and Mz, respectively). See Appendix A for more detail.

7.1.3 Tower-Top (Yaw-Bearing) Loads

The largest differences for the yaw-bearing loads are observed in the force aligned with global z. This difference is related to the fact that no significant damping in the z direction was specified for the SC approach. The lightly damped initial transient for the *YawBearingFz* signal is illustrated in Figure 18; it is responsible for the relatively large maximum loads for the SC approach and could be reduced by selecting an appropriate linear damping coefficient. Other noticeable differences that could affect the design of a fixed-bottom offshore wind system are observed for *YawBearingFy* (~10%) and *YawBearingMy* (~6%). See Appendix A for more detail.

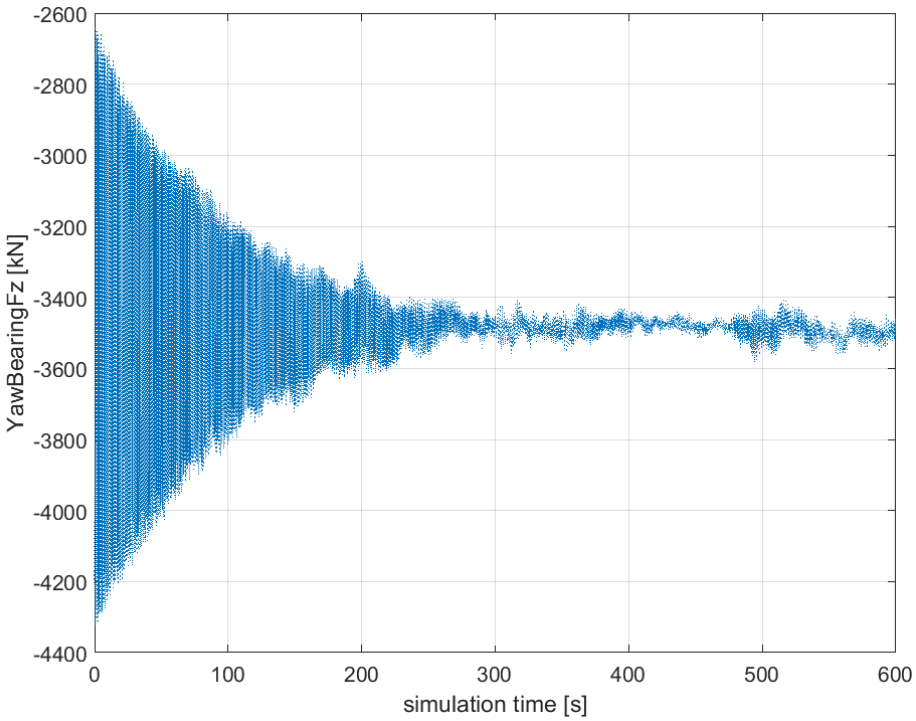

Figure 18. Typical time series of yaw-bearing force along global z (note the transient has not settled after more than 300 s [including 150 s of discarded data])

7.1.4 Tower-Base Loads

Tower-base loads (shown in Appendix A) behaved similarly to what was seen for the tower-top loads. Relatively large differences in the *TowerBaseFz* signal are caused by an insufficiently damped initial transient oscillation, whereas differences around 10% in the *TowerBaseFy* shear were noted.

7.1.5 Substructure Loads

For the substructure loads (shown in Appendix A), differences amounted to some 5% for the bending moments about the global x-axis and approximately 10% for the shear force in the x-direction at the mudline. SC and FC loads for the mudline shear force in the y-direction differed up to 30% for certain wind/wave orientations.

7.2 Monopile–Extreme Conditions: Comparison of Overall Maximum Loads

Overall, the differences between the SC and FC monopile results were larger for the extreme load cases than for the power production cases. Even more importantly, the FC approach seems to be more conservative for the majority of the analyzed channels for DLCs B001–B004. A comparison of the overall maximum turbine and tower loads for all parked DLCs (B001–B004) (see Table 22 and Table 23) shows agreement within 10% between SC and FC. In Table 24, for the respective substructure loads, the calculated relative errors are on the order of 13%, with the SC less conservative than the FC approach.

Table 22. Maximum Turbine Loads During Extreme Conditions (Monopile); Part 1

	BladeRootFx	BladeRootFy	BladeRootFz	BladeRootMx	BladeRootMy	BladeRootMz	LSSMy	LSSMz	YawBearingFx	YawBearingFy
Fully Coupled	98.71	347.2	177.1	9,991	1,969	152.5	4,570	5,709	514.7	779.4
Sequentially Coupled	97.91	349.3	186	10,030	2,102	148.3	4,705	5,453	507.6	818.1
Delta (%)	-0.8	0.6	5.0	0.4	6.8	-2.8	3.0	-4.5	-1.4	5.0

Table 23. Maximum Turbine Loads During Extreme Conditions (Monopile); Part 2

	YawBearingFz	YawBearingMx	YawBearingMy	YawBearingMz	TowerBaseFx	TowerBaseFy	TowerBaseFz	TowerBaseMx	TowerBaseMy	TowerBaseMz
Fully Coupled	3,429	2,697	3,941	6,086	1,057	860.9	5,764	65,050	62,680	6,086
Sequentially Coupled	3,526	2,842	3,943	5,661	1,008	893.8	5,981	69,260	58,550	5,661
Delta (%)	2.8	5.4	0.1	-7.0	-4.6	3.8	3.8	6.5	-6.6	-7.0

Table 24. Maximum Substructure Loads During Extreme Conditions (Monopile)

	MSL_Mx	MSL_My	Mx_10m_depth	My_10m_depth	Fx_mudline	Fy_mudline	Fz_mudline	Mx_mudline	My_mudline	Mz_mudline
Fully Coupled	72.9	72.7	83.9	89.0	3.5	3.6	8.6	113.6	111.7	6.1
Sequentially Coupled	78.0	67.6	88.4	80.4	3.5	3.2	8.5	101.9	97.0	5.7
Delta (%)	7.0	-7.0	5.4	-9.7	0.5	-12.7	-1.2	-10.3	-13.2	-7.5

7.2.1 Blade Loads

For the simulated extreme conditions with a parked turbine, differences between the SC and FC blade root loads were larger than what was observed during the power production cases, namely: *BladeRootFx*: ~5%, *BladeRootFz*: ~5%, and *BladeRootMy*: ~10%. Note that the load spike observed in the *BladeRootMz* signal during the power production conditions did not occur in the parked simulations. See Appendix A for more information.

7.2.2 Shaft Loads

Compared to the power production case, the parked case showed larger differences (~10%) for *LSSMz* between the FC and SC results. See Appendix A for more information.

7.2.3 Tower-Top (Yaw-Bearing) Loads

For the tower-top yaw-bearing loads, larger differences were observed when comparing to the power production case, specifically *YawBearingFx* ~4% and *YawBearingMz* ~20%. A consideration similar to what was stated for the blade torsion must be emphasized. The torsional

degree of freedom of the tower was not included in the calculations, as towers are normally fairly stiff in torsion, and the torsional moment is not a design driver. See Appendix A for more information.

7.2.4 Tower-Base Loads

Similar levels of differences between the FC and SC results were observed for both the yaw-bearing and tower-base loads. The largest difference (~20%) at the tower base was observed in the *TowerBaseMz* (torsional moment). See Appendix A for more detail.

7.2.5 Substructure Loads

The differences between the FC and SC substructure loads were larger than for the power production cases. Bending moments differed by about 10% between the FC and SC results (compared to about 5% for the power production case). Even larger differences in mudline shear forces (*Fx_mudline* ~200% and *Fy_mudline* ~150%) were noted for the parked case. See Appendix A for more information.

The mudline shear forces are highly influenced by hydrodynamic loads, which points to potential differences between Moffatt & Nichol's and NREL's modeling approach in terms of hydrodynamic load application. Further investigation is needed here.

Note that the comparison of the overall maximum substructure loads for all analyzed parked cases (B001-B004) shown in Table 24 states differences between FC and SC beyond 10%.

7.3 Jacket–Power Production: Comparison of Overall Maximum Loads

Turbine loads were well captured by the SC method when compared to the FC results, and the differences were smaller than for the monopile configurations (less than 5%). For several wind/wave direction combinations, the FC approach appeared to yield more conservative results than the SC approach, especially for the *YawBearingFx, YawBearingFy,* and *TowerBaseFy* load channels.

A comparison of the maximum turbine loads over all analyzed power production load cases (A001–A008) yielded differences between SC and FC approaches below 5% (see Table 25 and Table 26). Table 27 and Table 28 show larger differences (up to 60%) for the jacket member loads, but the SC approach appears to be conservative for all of the member load channels analyzed.

Table 25. Maximum Turbine Loads During Power Production (Jacket); Part 1

	BladeRootFx	BladeRootFy	BladeRootFz	BladeRootMx	BladeRootMy	BladeRootMz	LSSMy	LSSMz	YawBearingFx	YawBearingFy
Fully Coupled	392.6	246.8	837	6,114	14,190	206.6	6,186	7,097	892.3	646.2
Sequentially Coupled	396.4	246.1	836	6,122	14,200	203.1	6,225	7,350	874.5	622.5
Delta (%)	1.0	-0.3	-0.1	0.1	0.1	-1.7	0.6	3.6	-2.0	-3.7

Table 26. Maximum Turbine Loads During Power Production (Jacket); Part 2

	YawBearingFz	YawBearingMx	YawBearingMy	YawBearingMz	TowerBaseFx	TowerBaseFy	TowerBaseFz	TowerBaseMx	TowerBaseMy	TowerBaseMz
Fully Coupled	3,562	7,287	5,993	5,259	894.6	656.3	5,692	47,220	60,680	5,259
Sequentially Coupled	3,560	7,234	6,019	5,141	910.2	637.1	5,691	47,410	60,700	5,141
Delta (%)	-0.1	-0.7	0.4	-2.2	1.7	-2.9	0.0	0.4	0.0	-2.2

Table 27. Maximum Substructure Loads During Power Production (Jacket); Part 1

	K1L1_FZ	K1L2_FZ	K5L2_FZ	RL1_FZ	RL1_FY	RL1_FX	RL1_MZ	RL1_MY	RL1_MX	RL2_FZ	RL2_FY	RL2_FX	RL2_MZ
Fully Coupled	6,643	2,427	249.8	9,225.0	290.1	370.8	224.2	1,974.0	1,434.0	3,232.0	297.1	380.6	1,512.0
Sequentially Coupled	6,660	2,599	271.2	9,568.3	414.8	467.5	342.4	2,301.3	1,954.2	3,629.8	387.8	478.5	1,870.6
Delta (%)	0.3	7.1	8.6	3.7	43.0	26.1	52.7	16.6	36.3	12.3	30.5	25.7	23.7

Table 28. Maximum Substructure Loads During Power Production (Jacket); Part 2

	RL2_MY	K4L1_XZ_FZ	K4L1_XZ_MY	K4L1_XZ_MX	K4L1_YZ_FZ	K4L1_YZ_MY	K4L1_YZ_MX	K4L2_XZ_FZ	K4L2_XZ_MY	K4L2_XZ_MX	K4L2_YZ_FZ	K4L2_YZ_MY	K4L2_YZ_MX
Fully Coupled	1,965.0	755.8	65.1	82.3	800.4	69.6	69.9	563.9	55.1	66.4	557.1	52.4	58.2
Sequentially Coupled	2,303.7	922.0	81.9	106.9	921.6	99.5	88.2	713.2	88.9	96.6	597.7	79.4	90.0
Delta (%)	17.2	22.0	25.9	29.9	15.1	42.9	26.2	26.5	61.4	45.6	7.3	51.7	54.8

7.3.1 Blade Loads

The blade root loads agreed well, with about a 1% difference between the FC and SC results. See Appendix A for more information.

7.3.2 Shaft Loads

About a 4% difference between the FC and SC results can be observed for the *LSSMz* (shaft yawing moment). See Appendix A for more detail.

7.3.3 Tower-Top (Yaw-Bearing) Loads

The largest differences in yaw-bearing loads were found for the *YawBearingFy* (~15%) and *YawBearingFx* (~3%) shear signals for specific load cases. See Appendix A for more information.

7.3.4 Tower-Base Loads

The differences at the tower base are consistent with those noted at the tower top (*TowerBaseFy*: ~15%, *ToweBaseFx*: ~3%). See Appendix A for more information.

7.3.5 Substructure Member Loads

Regarding the substructure member loads (see Appendix A), the SC approach appears to predict maximum loads that are larger than the corresponding values computed based on the FC approach. The observed differences show large variations, depending on load direction and location (~5% - ~120%). The best agreement between SC and FC was found for *K1L1_FZ* and *RL1_FZ* (differences below 5%). With the exception of *K1L1_FZ*, *RL1_FZ*, and *K4L2_YZ_FZ* during certain wind/wave orientations, the SC approach proved to be more conservative for the substructure loads.

The relatively good agreement of the turbine maximum loads and the relatively large differences in substructure member maximum loads (with the SC approach being more conservative) is in line with what was reported in (Seidel and Ostermann 2009). Power spectra of the *RL1_Fx* and *RL1_Fy* (pile head shears) are shown in Figure 19 and Figure 20. The large peaks around 1.7 Hz in the Keystone (SC) response coincide with the first global torsion mode (reported at 1.73 Hz by Keystone). The FC approach appears to predict significantly less excitation for this mode. This higher-order global mode is exciting local member deformations that are not predicted by the FC modeling approach. According to Seidel and Ostermann (2009), this excitation during the recovery run is of an artificial nature and leads to a significant overestimation of the local member loads. In the SC analysis, the global torsion mode was not accurately represented in the FAST simulation because of the applied reduction scheme. In the subsequent recovery run, the tower-base loads from FAST were used as input to the substructure design tool (EDP/SACS), resulting in the possible overexcitation of the higher-order modes, such as the global torsion mode at around 1.7 Hz.

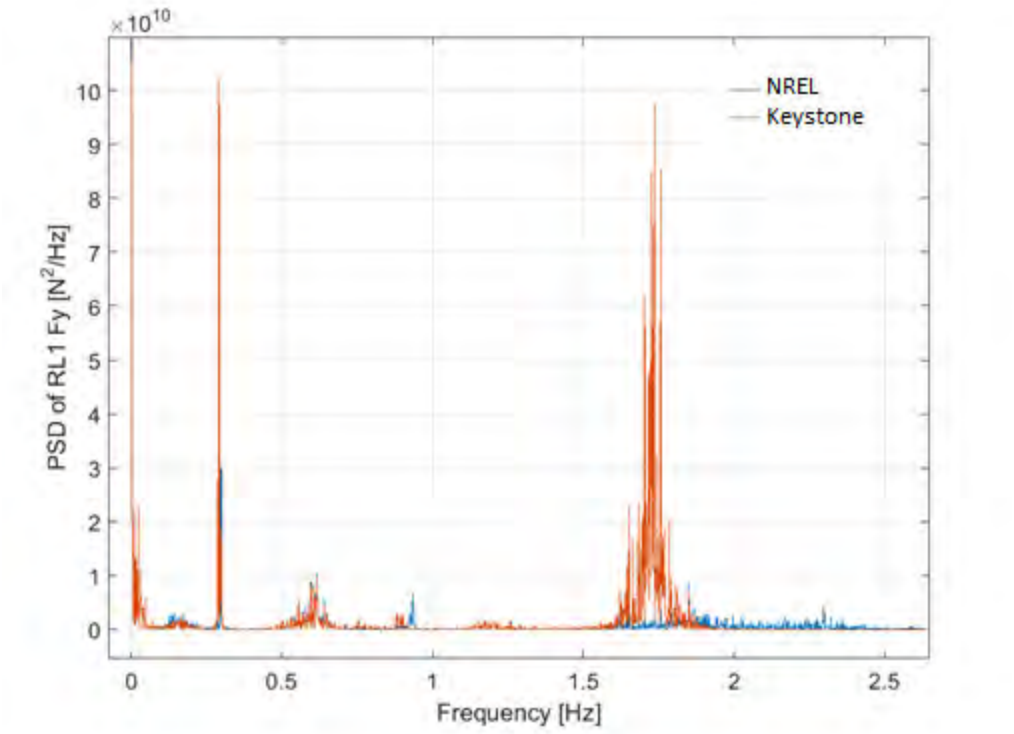

Figure 19. Power spectral density (PSD) plot of the pile head shear *RL1_Fy* as calculated by NREL and Keystone

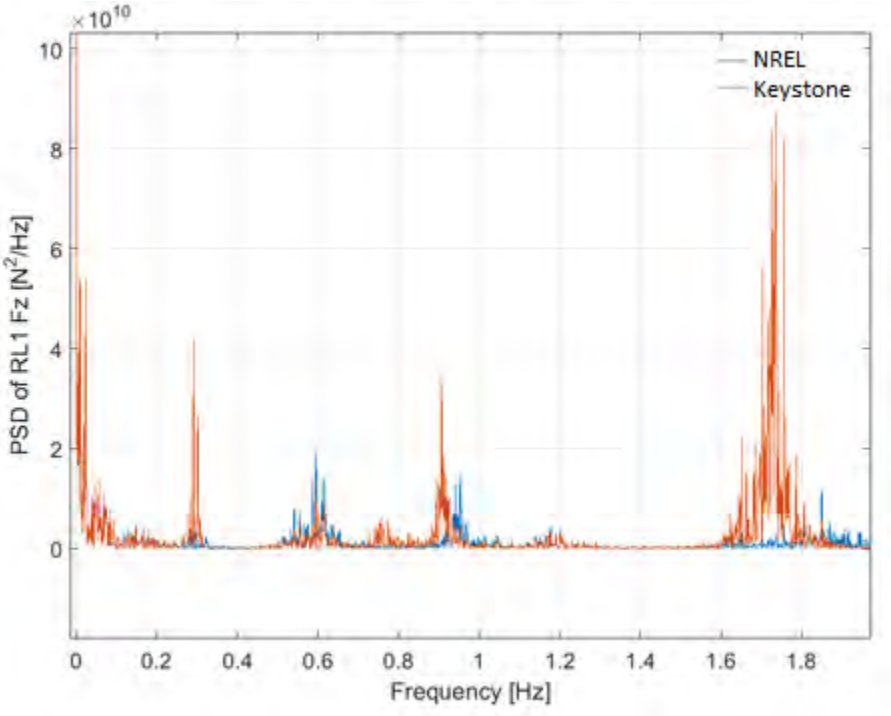

Figure 20. PSD plot of the pile head normal force *RL1_Fz* as calculated by NREL and Keystone

7.4 Jacket–Extreme Conditions: Comparison of Overall Maximum Loads

The differences in the results from the SC and FC approaches are larger under parked DLCs than under the power production cases. As for the maximum turbine loads, the FC and SC approaches alternately predicted higher (more conservative) loads, depending on the load channel and wind/wave direction combination. Compared to the power production case, however, the SC approach appears to predict less conservative maximum turbine loads under extreme condition DLCs. By comparing the overall maxima across all parked cases, the maximum difference in turbine loads (Table 29–Table 30) came to ~13%, and with the SC method showing less conservative results. For the respective substructure loads (Table 31–Table 32), differences on the order of 30%–40% were noted with the SC approach being less conservative, whereas one load channel (K5L2_FZ) showed the overall largest difference (~50%), with the FC approach returning lesser values than the SC approach.

Table 29. Maximum Turbine Loads During Extreme Conditions (Jacket); Part 1

	BladeRootFx	BladeRootFy	BladeRootFz	BladeRootMx	BladeRootMy	BladeRootMz	LSSMy	LSSMz	YawBearingFx	YawBearingFy
Fully Coupled	89.34	160.4	178.8	5,413	1,869	151.5	4,872	5,942	502.4	893.1
Sequentially Coupled	83.72	159.1	179.2	5,340	1,807	147.8	4,933	6,118	464.2	805.7
Delta (%)	-6.3	-0.8	0.2	-1.3	-3.3	-2.4	1.3	3.0	-7.6	-9.8

Table 30. Maximum Turbine Loads During Extreme Conditions (Jacket); Part 2

	YawBearingFz	YawBearingMx	YawBearingMy	YawBearingMz	TowerBaseFx	TowerBaseFy	TowerBaseFz	TowerBaseMx	TowerBaseMy	TowerBaseMz
Fully Coupled	3,382	3,347	3,547	7,035	585.5	962.7	5,511	65,830	37,240	7,035
Sequentially Coupled	3,381	2,891	3,507	7,080	505.8	852.5	5,507	58,860	34,520	7,080
Delta (%)	0.0	-13.6	-1.1	0.6	-13.6	-11.4	-0.1	-10.6	-7.3	0.6

Table 31. Maximum Substructure Loads During Extreme Conditions (Jacket); Part 1

	K1L1_FZ	K1L2_FZ	K5L2_FZ	RL1_FZ	RL1_FY	RL1_FX	RL1_MZ	RL1_MY	RL1_MX	RL2_FZ	RL2_FY	RL2_FX	RL2_MZ
Fully Coupled	5,019	4,491	377	10,440	913.0	916.2	295.5	4,482.0	4,321.0	12,350.0	922.7	924.8	4,351.0
Sequentially Coupled	5,075	4,472	573	11,705	1,089	990.1	278.4	4,784.7	5,256.3	7,660.0	1,206.5	960.7	5,752.1
Delta (%)	1.1	-0.4	51.9	12.1	19.3	8.1	-5.8	6.8	21.6	-38.0	30.8	3.9	32.2

Table 32. Maximum Substructure Loads During Extreme Conditions (Jacket); Part 2

	RL2_MY	K4L1_XZ_FZ	K4L1_XZ_MY	K4L1_XZ_MX	K4L1_YZ_FZ	K4L1_YZ_MY	K4L1_YZ_MX	K4L2_XZ_FZ	K4L2_XZ_MY	K4L2_XZ_MX	K4L2_YZ_FZ	K4L2_YZ_MY	K4L2_YZ_MX
Fully Coupled	4,503.0	1,786.0	69.0	226.9	1,881.0	130.6	226.9	1,867.0	89.5	222.9	1,798.0	104.0	219.7
Sequentially Coupled	4,564.2	1,930.4	71.1	279.7	1,389.6	89.6	264.4	1,600.0	89.2	231.8	1,641.0	63.1	293.0
Delta (%)	1.4	8.1	3.1	23.3	-26.1	-31.4	16.5	-14.3	-0.3	4.0	-8.7	-39.3	33.4

7.4.1 Blade Loads

For the blade loads, the most prominent differences are observed in the shear *BladeRootFx* (~6%) and *BladeRootMy* moment (~10%). For more information, see Appendix A.

7.4.2 Shaft Loads

The differences between the SC and FC shaft loads increased as well, when going to extreme condition DLCs, than to what was observed for the power production DLCs (e.g., ~5% for *LSSMy* and ~14% for *LSSMz, was ~1% for LSSMy and ~3% for LSSMz during power production*). See Appendix A for more detail.

7.4.3 Tower-Top (Yaw-Bearing) Loads

At tower top, differences between SC and FC *YawBearingFx*, *YawBearingMx*, *YawBearingMy*, and *YawBearingMz* exhibited values of about 15%. See Appendix A for more information.

7.4.4 Tower-Base Loads

Similar differences to the tower-top loads were noted for the corresponding tower-base load channels. For more information, see Appendix A.

7.4.5 Substructure Loads

Like the RNA and tower loads, the overall differences between SC and FC member loads are larger than what was observed for the power production case. Although the member loads were conservatively calculated by the SC approach for the power production cases, for the parked conditions the FC approach produced the more conservative estimates in many instances. A time series plot of *K4L1_XZ_MY* (bending moment in the bottom brace, Figure 21a) illustrates that the frequency content between the SC and FC approach appears to be similar. However, the difference in mean value between the two signals eventually causes the differences in maximum loads, with the FC approach being the more conservative solution. This difference in mean value was not observed for the corresponding load channel during power production (see Figure 21b). Further analysis is needed here, but it is outside the scope of this project.

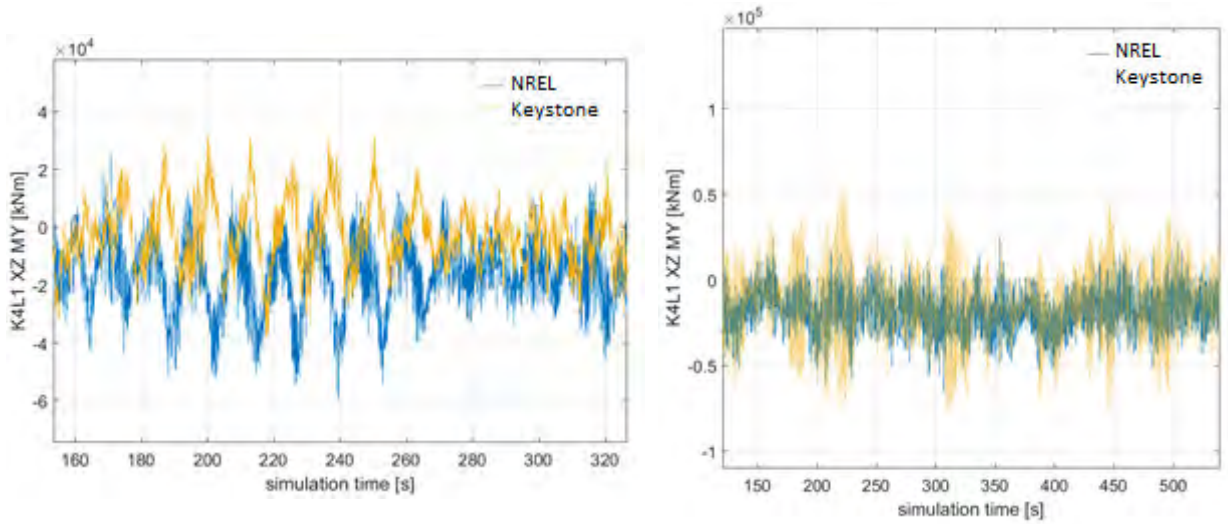

Figure 21. Time series plot of bending moment in brace member 45 for a parked DLC (a) and a power production DLC (b), as calculated by NREL and Keystone

8 Conclusions

The authors conducted a study for BSEE to assess the impact of sequentially coupled modeling approaches on the ULS loads and therefore eventually on the design of offshore wind turbines. The SC approach is commonly used in the industry as it avoids sharing proprietary information between different design groups (turbine OEM and substructure designers), but reservations exist concerning its ability to capture all of the important dynamic coupling aspects associated with offshore wind turbines. In this study, we compared results in terms of maximum ULS loads as predicted from power production and parked (extreme event) case simulations when using either SC or FC methods. Although the comparison is quite involved and significant details exist for the various component load channels, a few general statements can be made.

For the turbine RNA and tower, we observed good agreement between the two methods for the analyzed power production cases. Larger differences were observed for the extreme condition cases as compared to operational cases. The overall level of differences in turbine loads during extreme conditions was larger for the jacket-based offshore wind turbine (~5%-20%) than for the monopile-based offshore wind turbine (~5%-10%). For power production conditions, larger differences in turbine loads were observed for the monopile offshore wind turbine (~%5-10%), whereas results for the jacket offshore wind turbine showed relatively small differences (~1%-5%).

For the monopile loads, the ultimate bending moments under power production DLCs agreed within about 5% between the SC and FC results, whereas the shear forces at the mudline exhibited some larger differences (~10%–30%). For the extreme condition DLCs, these differences increased (~10% for bending moments and +100% for shear forces at the mudline). This outcome could potentially be related to issues in the hydrodynamic load definition/application and should be investigated further. The SC approach does not consistently return more conservative load estimates for the monopile.

For the jacket member loads under power production DLCs, the SC approach appears to be generally more conservative with respect to the FC approach when estimating the ULS loads (maximum jacket member loads increased by ~+20% for the SC approach). A frequency domain analysis of substructure member load signals demonstrated that the SC coupled approach showed more contributions from the higher-order global deformation modes. This finding is consistent with the data presented in Seidel and Ostermann (2009), which identifies the SC approach as overly conservative because of the artificial excitation of these higher-order modes. For the extreme condition DLCs, the differences between the SC and FC approaches for the jacket loads are larger (+40%) than what was observed for the power production DLCs, and the SC approach produced less conservative estimates in several instances. A potential discrepancy in member mean loads between FC and SC approaches during parked DLCs needs to be further investigated.

When considering the maximum load values across all operational cases (A001–A008), the RNA and tower loads were found to be within 3% and 6% for the jacket and monopile configurations, respectively. When considering the maximum load values across all parked cases (B001–B008), the RNA and tower loads were within 13% and 7% for the jacket and monopile configurations, respectively, and with the SC results being less conservative than the FC results. For the

substructure loads across all power production cases, results showed differences of up to 60% for the jacket members, and with the SC approach overestimating the loads; the monopile maximum loads were in close agreement (6%–11%) and with no clear over/underestimation by any particular method. Across all the parked cases (B001–B008), one jacket member load channel was overestimated by ~50% under the SC approach, whereas several other member loads were underestimated by up to 39% when compared to the FC approach; the monopile loads were underestimated by up to 11% by the SC method.

Some of these differences can have important consequences on the design of the support structures, with potentially either overdesigned or underdesigned components, and should be further investigated. It can be stated, however, that including the modal content of the hydrodynamic forces in the SC aeroelastic simulations that can be accomplished using larger superelement matrices that include modal degrees of freedom, could further improve the agreement between the SC and FC modeling approaches.

This study highlighted how the SC approach requires a thorough and time-intensive model verification, a rigorous data exchange protocol, and extensive and critical quality control. Also for this reason, the SC method limits the opportunity for design optimization. The FC approach, on the other hand, is more direct and rigorous, but, often times, not as practical because of the division of responsibility and intellectual property.

Our findings yield some significant differences that require further investigation to address any remaining concern regarding the practicability of the SC analysis method for the design of offshore wind systems. More analysis is needed to clearly identify the sources of the observed differences and devise potential mitigation strategies.

8.1 Recommended Follow-On Studies

Given the level of differences observed between the FC and SC modeling approach, the authors recommend further follow-on studies that focus on the characterization and mitigation of the observed differences. A comparative study that relates the observed differences in ultimate load predictions between the SC and FC approach to the commonly utilized safety factors is also recommended.

Additional future research recommendations include:

- Performing targeted calibration efforts to minimize possible errors because of the use of different software packages. This work will add significant value to the initial study presented in this document, and a focus will be set on the observed differences mentioned earlier. These differences will then be mitigated/explained through targeted model calibration and verification cases.

- Expanding the results to fatigue load cases to analyze the impact of the modeling approach on fatigue loads and potentially other load cases for ultimate loads, including constrained wave cases

- Expanding the substructure superelement to include additional model degrees of freedom (Craig-Bampton method) to help reduce the observed differences

- Conducting a complete design iteration to compare the effect of the observed differences in load predictions on structural mass

- Assessing the effects of higher-order hydrodynamics, and employing larger and more flexible turbine models to verify the effects on the RNA loads.

There has been some evidence that the importance of a coupled analysis may become even more important for floating substructures. The industry for floating offshore wind substructures is just getting started with only five commercial floating offshore wind turbines operating today, but the pipeline for tracking this development indicates that a commercial industry may be forming in the next 5 years. Assessing this issue for floating offshore wind substructures is beyond the scope of this project, but is recommended for future research.

8.2 Final Question and Answer with BOEM and BSEE

The following questions were submitted to NREL after BOEM/BSEE reviewed a draft version of this report. The corresponding answers were provided by the NREL authors.

Q. Do you have any recommendations for BOEM/BSEE as to how we review project structural designs? We feel we should require the certified verification agent (CVA) to verify at least one FC analysis for each project. If no FC analysis is available for CVA verification, the CVA should perform an independent FC analysis for comparison to the SC analysis results.

A. Based on the differences in ULS loads that were observed during the course of the project, requiring a cross check against a FC model for certain load cases is appropriate. However, additional guidance on the selection of the load cases and the follow-on comparison of FC and SC results is needed. Furthermore, additional evidence and guidance can stem from the analysis of FLS cases. The development of a FC model, however, will require additional time and resources and will eventually increase the cost of the certification process.

Q. How does this study impact current technical standards (e.g., IEC 61400-3)?

A. Based on the results observed so far, the SC and FC approach could eventually lead to different safety factors and implied levels of structural reliability. Further research is needed to further quantify this potential impact on technical standards.

Q. Which method would be best for avoiding potential resonance in monopile structures?

A. Resonance issues would likely be captured more accurately by the FC approach because of more rigorous treatment of coupled modes.

Q. Should geotech (finite-element analysis and actual pile section modulus to simulate pile-soil interaction) be included in follow-on studies (or considered for an eventual optimized design tool)? Is a linearized soil stiffness approximation acceptable for a true dynamic analysis?

A. Further follow-on studies should first focus on the differences that were observed in ultimate loads, using the same models as used in this study. Once these differences are analyzed and explained sufficiently, more complexity can be introduced (e.g., more complex soil-structure

interaction and modal representation of the substructure). In general, further analysis with a focus on the effect of nonlinear soil/pile interaction, especially for larger systems in deeper waters, is recommended.

Q. Does the investigative team have an opinion on how many eigenfrequencies the designers should check to ensure avoidance of harmonic amplification?

A. The frequency cutoff will differ from system to system. A preliminary FC analysis could be used to determine the upper frequency limit of the system response based on spectral analysis of key response load channels (e.g., overturning moment at the top or base of the tower and substructures).

Q. Would the observed differences between the methods change significantly with larger turbines (8 to 10 MW)?

A. Larger differences between the FC and SC approach are expected for larger systems because of stronger coupling between turbine, substructure, and pile/soil interaction responses.

Q. How would twisted jackets compare to standard jackets with the two methods?

A. In twisted jackets, more complex coupling of eigenmodes can be expected, thus it can be speculated that the FC analysis could be even more important than for standard jackets, but only a dedicated analysis could further answer this question.

Q. What about gravity-based foundations or suction caissons? Any thoughts on how they would compare?

A. Generally speaking, substructures with a larger number of modes situated at lower frequencies tend to exhibit significant differences between the FC and SC modeling approaches. Gravity-based foundations are usually very stiff and their structural response should be concentrated on the first 1 to 2 modes. These modes should be captured relatively well by both approaches. For suction caissons and other types of anchoring configurations, the issues lie on the degree of stiffness that the foundation can guarantee as a boundary condition to the remainder of the system, especially when considering the damaging effect of scouring. These effects are better captured in an FC approach, but methods could be devised to appropriately account for these effects also in an SC fashion.

Q. How can BOEM/BSEE or the industry help reduce proprietary design issues to promote FC analysis?

A. One way to overcome these issues could reside in the involvement of an entity that is not associated with either party (OEMs) or the CVA, and that would be a subcontractor to BOEM and BSEE. The certification of a new project should then require that the substructure and turbine OEMs provide the necessary information, potentially combined with asymmetric encryption technology, to this entity for conducting FC analyses on a select number of load cases to validate the design approach employed by the OEMs.

References

Airy, G. 1841. *Tides and waves.* London: Encyclopaedia Metropolitana.

BOEM. 2014. *Map of the North Carolina Call Areas.* Retrieved July 1, 2017 from https://www.boem.gov/North-Carolina/.

BOEM. 2016. *New York Activities.* Retrieved July 1, 2017 from https://www.boem.gov/New-York.

Damiani, R., K. Dykes, and G. Scott. "A comparison study of offshore wind support structures with monopiles and jackets for U.S. waters." The Science of Making Torque from Wind. Munich, Germany. 2016.

Damiani, R., F. Wendt, W. Musial, Z. Finucane, L. Hulliger, S. Chilka, D. Dolan, J. Cushing, D. O'Connel and S. Falk. "Fully vs. Sequentially Coupled Loads Analysis of Offshore Wind Turbines." Poster at AWEA WINDPOWER. Anaheim, California. 2017.

International Electrotechnical Commission. 2008. IEC 61400-3 Wind Turbines – Part 3: Design Requirements for Offshore Wind Turbines. Geneva, Switzerland.

Jokman, J., and W. Musial. 2010. *Offshore Code Comparison Collaboration (OC3) for IEA Task 23 Offshore Wind Technology and Deployment* (Technical Report). NREL/TP-500-48191. National Rewewable Energy Laboratory (NREL), Golden, CO (US). https://www.nrel.gov/docs/fy11osti/48191.pdf.

Jonkman, J., W. Butterfield, W. Musial, and G. Scott. 2009. *Definition of a 5-MW Reference Wind Turbine for Offshore System Development* (Technical Report). NREL/TP-500-38060. National Renewable Energy Laboratory (NREL), Golden, CO (US). https://www.nrel.gov/docs/fy09osti/38060.pdf.

Kooijman, H., C. Lindenburg, D. Winkelaar, and E. van der Hooft. 2003. *DOWEC 6 MW PRE-DESIGN Aero-elastic modelling of the DOWEC 6 MW pre-design in PHATAS. ECN* DOWEC-F1W2-HJK-01-046/9.

National Aeronautics and Space Administration. Undated. "Ocean Surface Currents (OSCAR)." Accessed April 10, 2016. http://oceanmotion.org/html/resources/oscar.htm.

National Renewable Energy Laboratory. 2016. "*NWTC Information Portal*." Accessed May 24, 2017, from FAST v8. https://nwtc.nrel.gov/FAST8.

Popko, W., F. Vorprahl, A. Zuga, M. Kohlmeier, J. Jonkman, and A. Robertson. 2012. "Offshore Code Comparison Collaboration Continuation (OC4), Phase I - Results of Coupled Simulation of Offshore Wind Turbine with Jacket Support Structure." International Offshore and Polar Engineering Conference (pp. Vol. 1, pp. 337-346). Rhodes, Greece: International Society of Offshore and Polar Engineers.

Rainey, P., and T. Camp. 2007. “Constrained non-linear waves for offshore wind turbine design.” *Journal of Physics*: Conference Series, Volume 75. http://iopscience.iop.org/article/10.1088/1742-6596/75/1/012067/meta.

Rodenbusch, G., and G. Forristall. 1986. “An Empirical Model for Random Directional Wave Kinematics Near the Free Surface.” Offshore Technology Conference. Houston, Texas.

Seidel, M., and F. Ostermann. 2009. “Validation of Offshore Load Simulations Using Measurement Data from the DOWNVInD project.” European Offshore Wind Conference. Stockholm, Sweden.

Vorprahl, F., W. Popko, and D. Kaufer,. (2013). “Description of a basic model of the 'UpWind Reference Jacket' for code comparison in the OC4 Project under IEA Wind Annex 30.” Bremerhaven, Germany: Fraunhofer IWES.

Appendix A: Ultimate Limit State Result Gallery

Power production ULS turbine loads for monopile configuration are provided in Figure A1 through Figure A4.

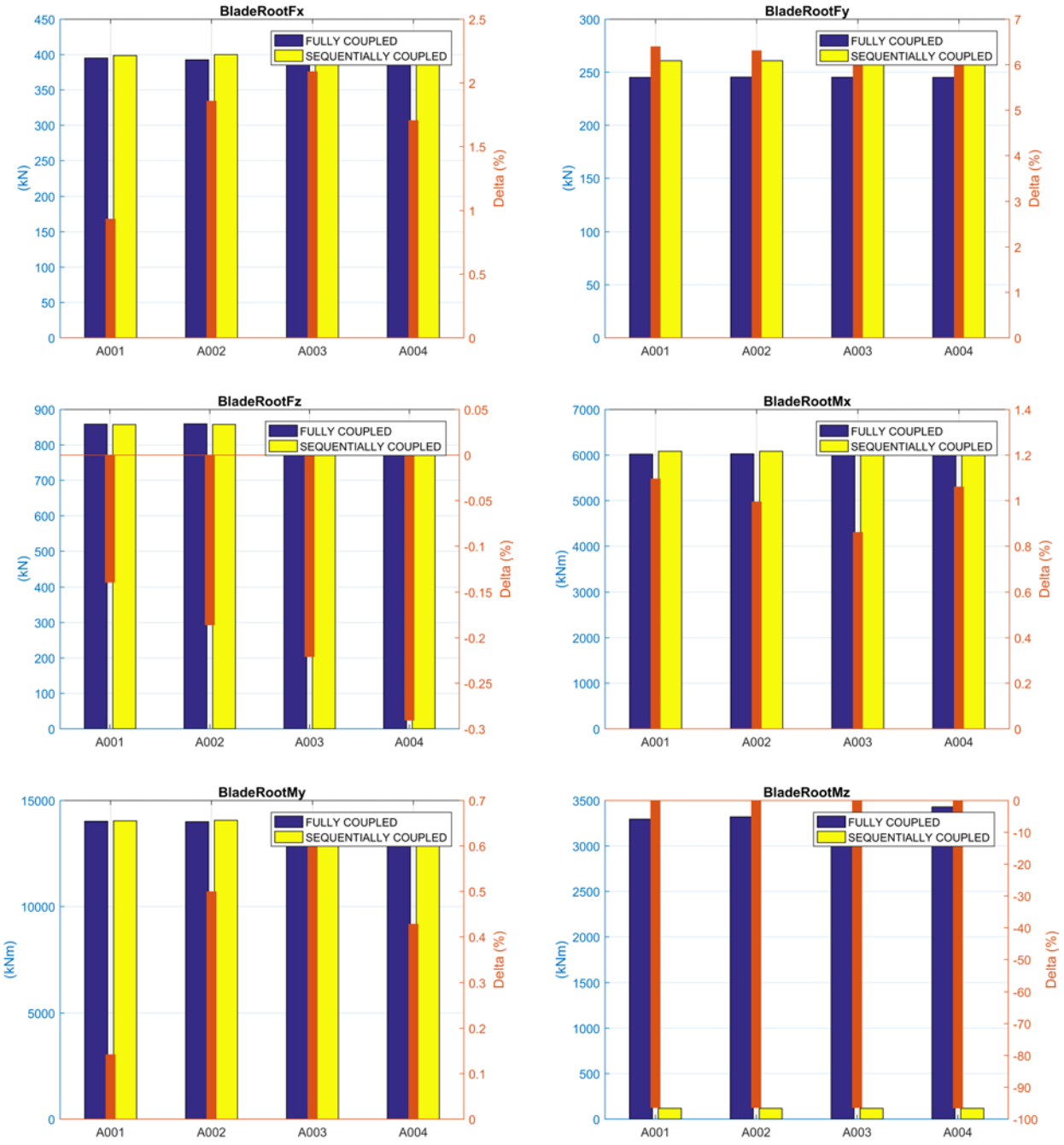

Figure A1. Blade root loads

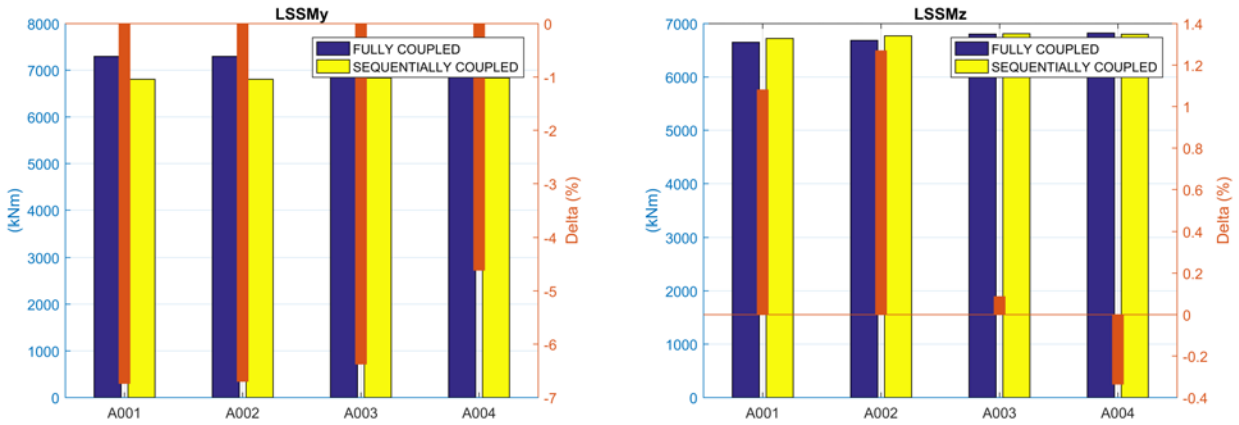

Figure A2. Low-speed-shaft loads

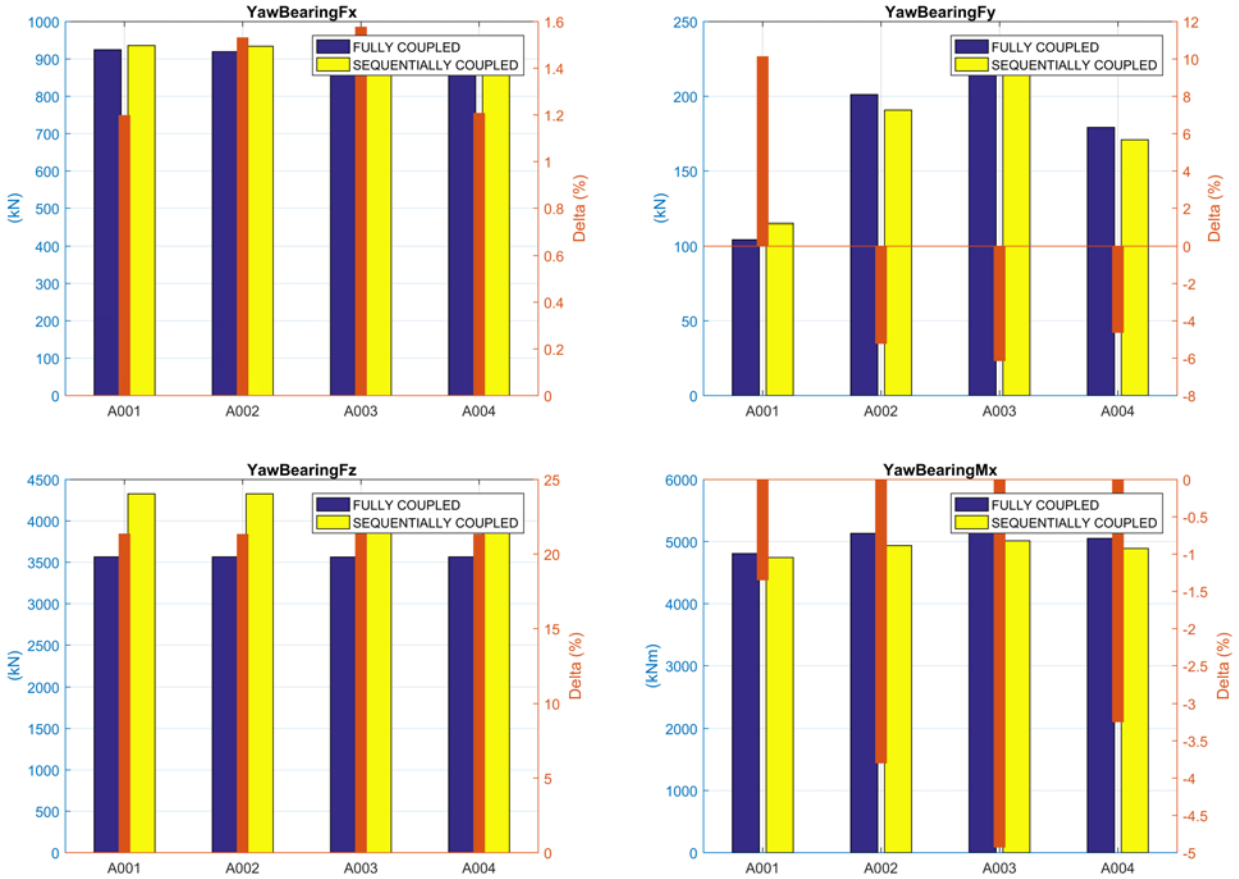

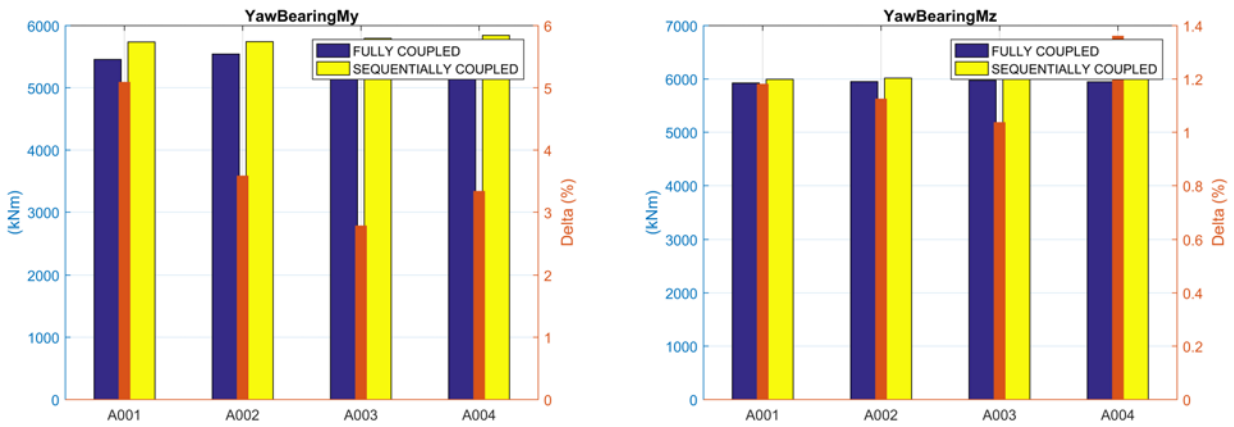

Figure A3. Yaw-bearing loads

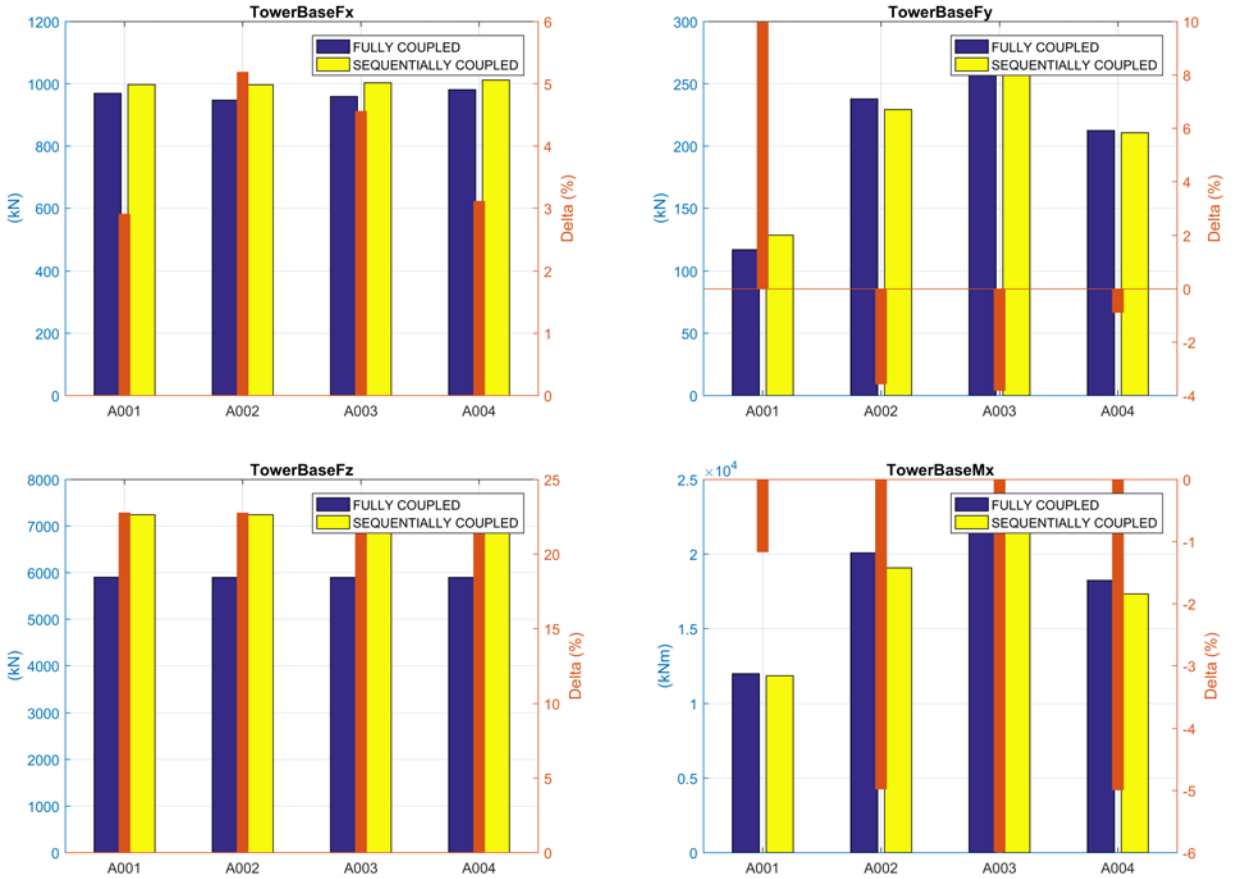

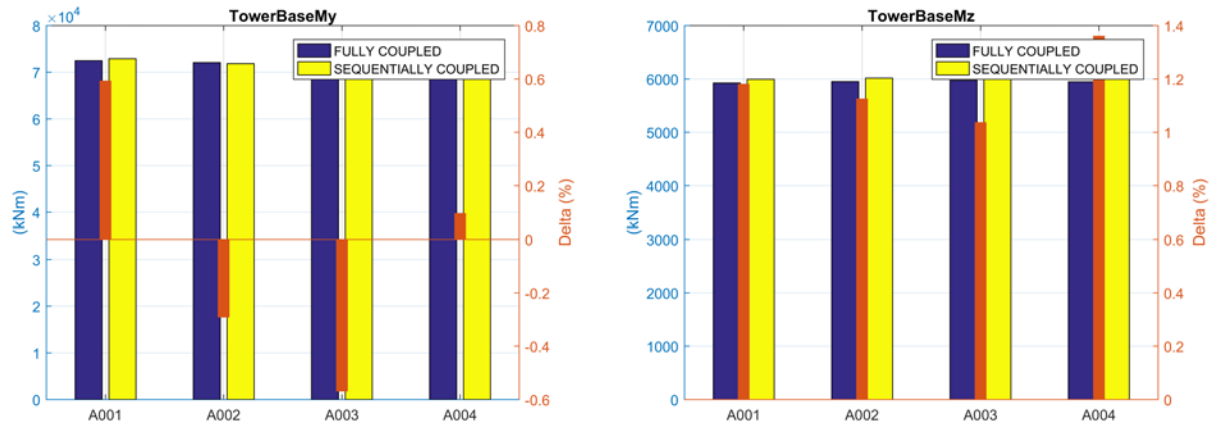

Figure A4. Tower-base loads

Power production ULS loads for monopile substructure are provided in Figure A5 through Figure A7.

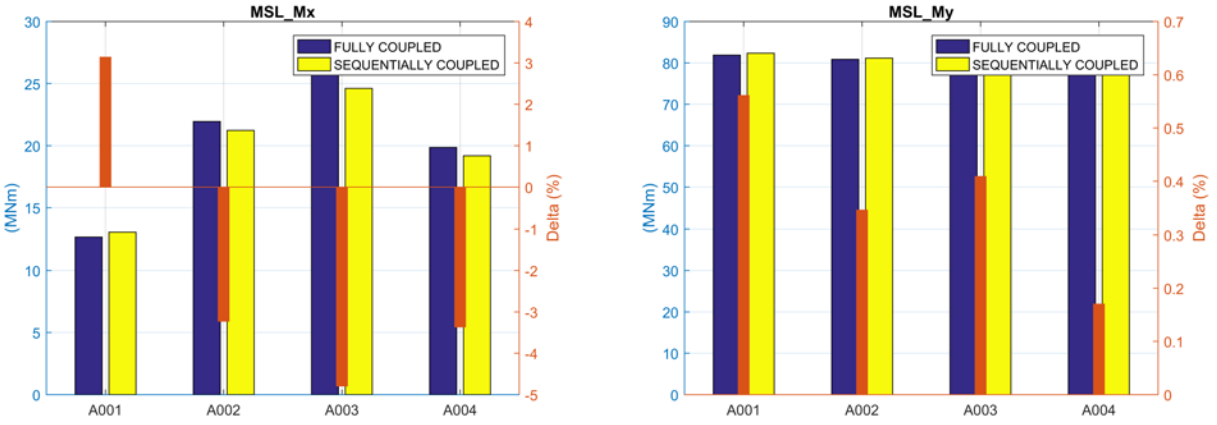

Figure A5. Bending moments at mean sea level (MSL)

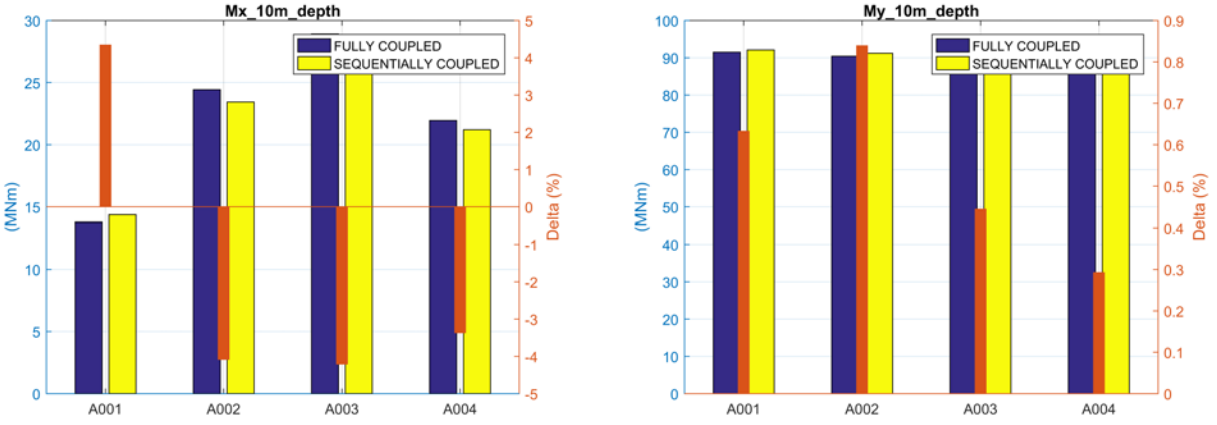

Figure A6. Bending moments at a 10-m water depth

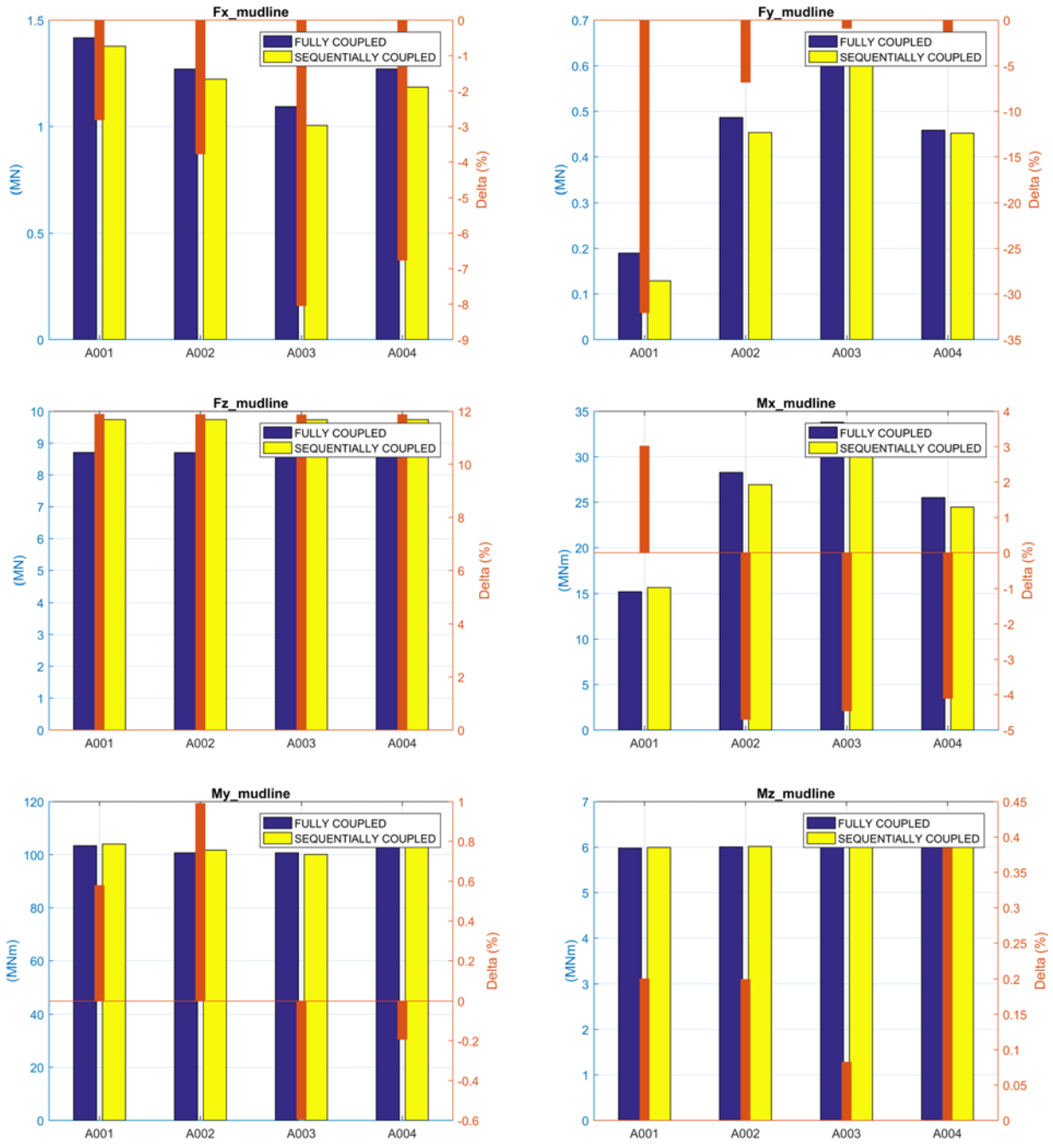

Figure A7. Pile loads at mudline

ULS loads turbine loads for monopile configuration under extreme conditions are provided in Figure A8 through Figure A11.

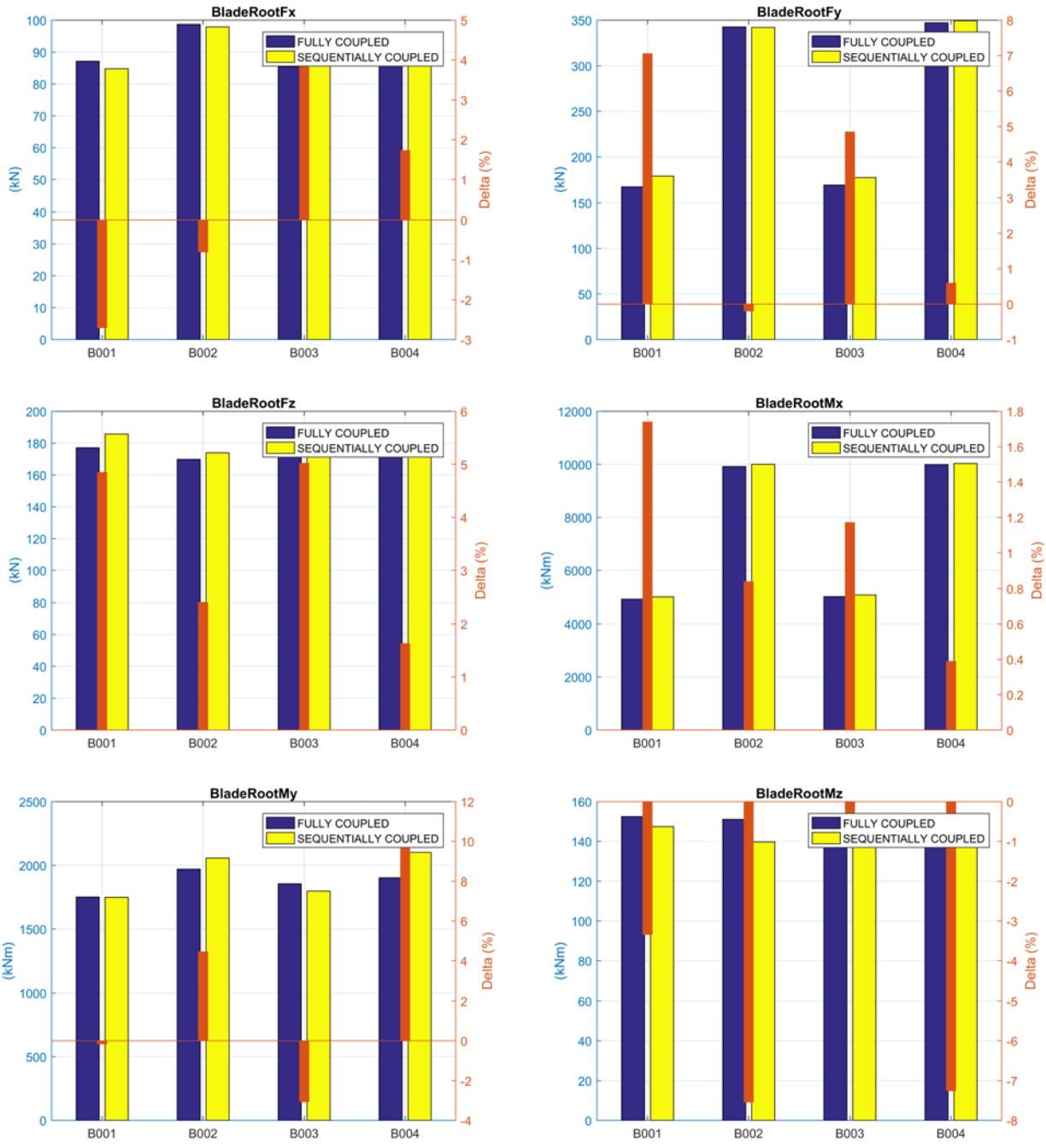

Figure A8. Blade root loads

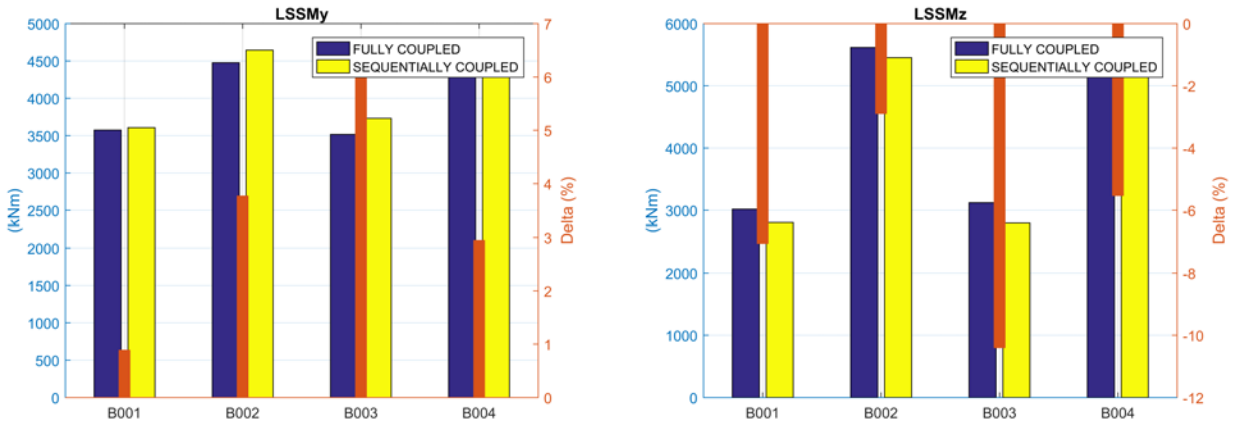

Figure A9. Low-speed-shaft loads

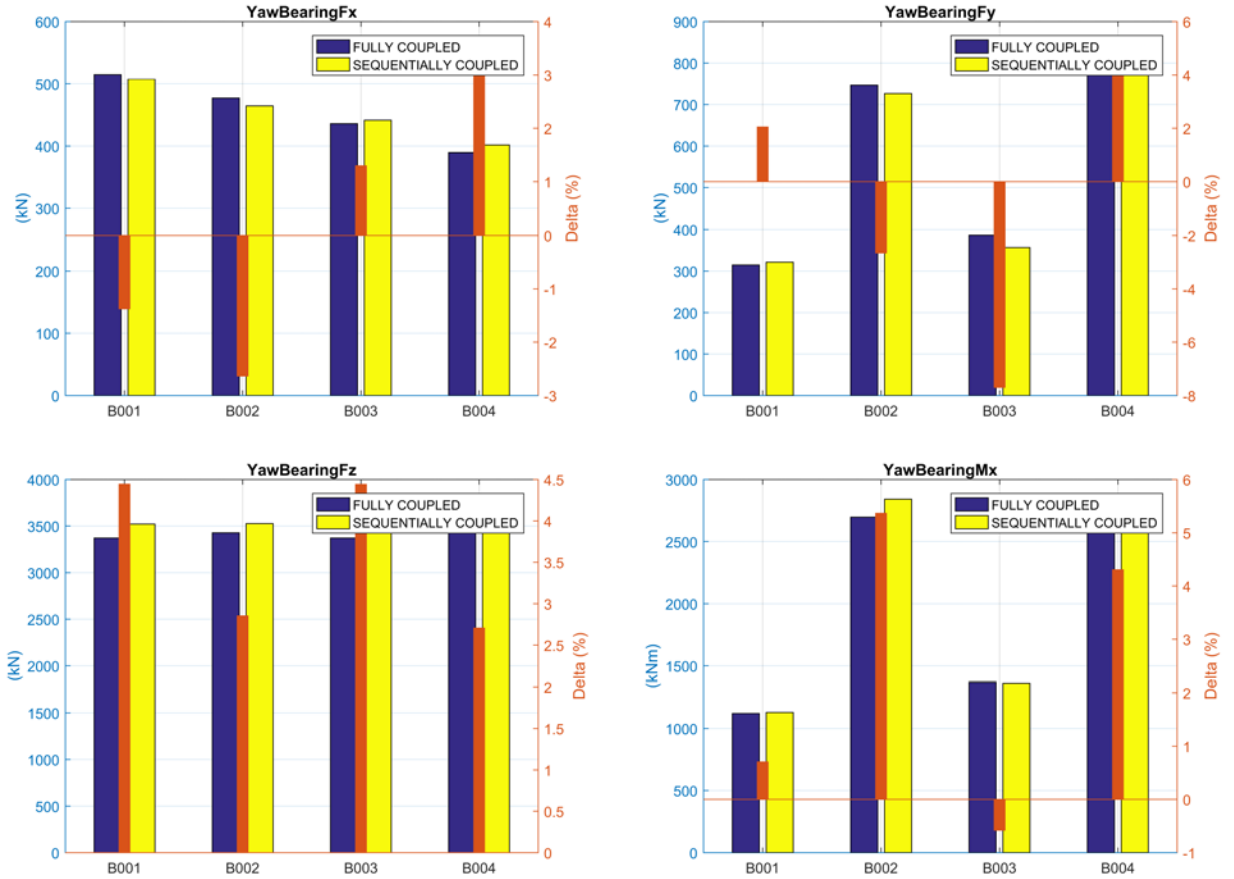

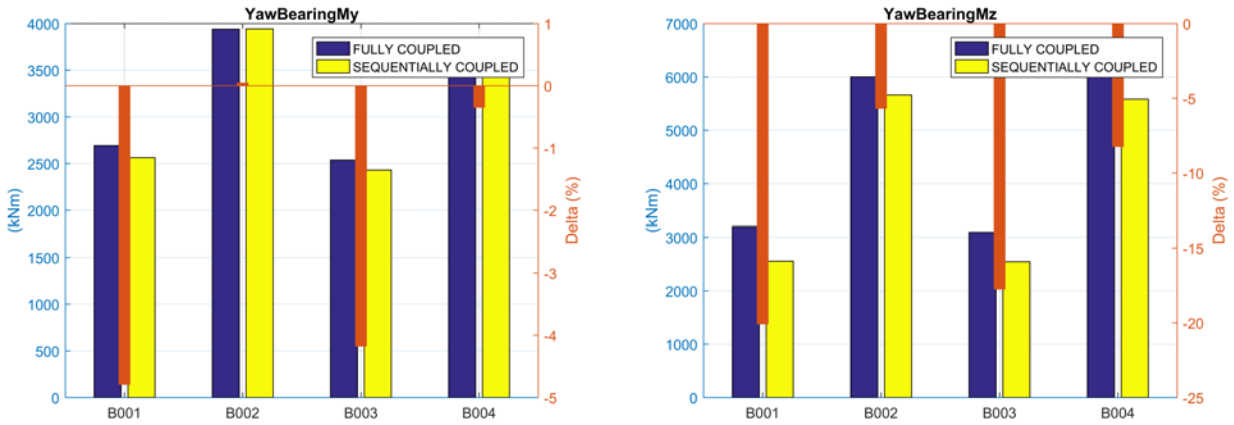

Figure A10. Yaw-bearing loads

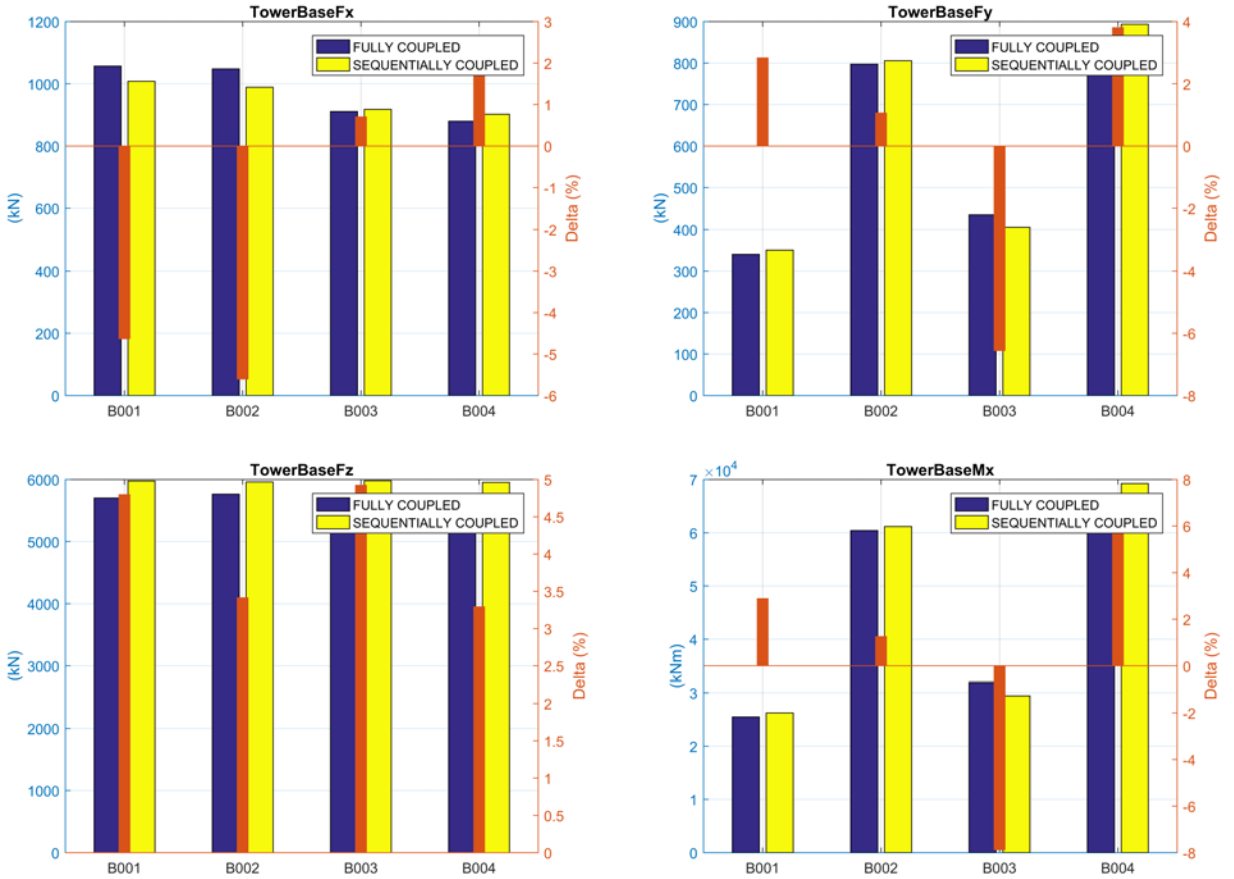

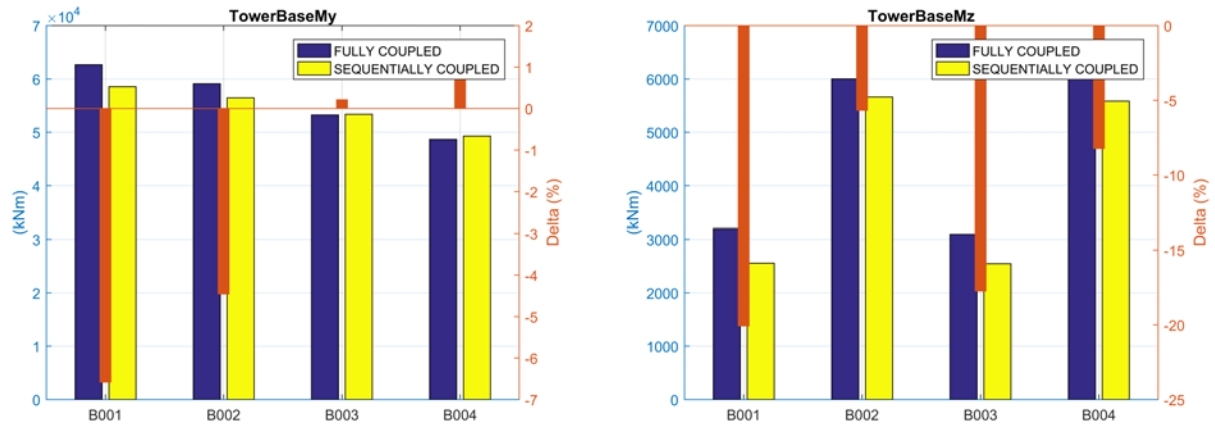

Figure A11. Tower-base loads

ULS loads for monopile substructure under extreme conditions are provided in Figure A12 through Figure A14.

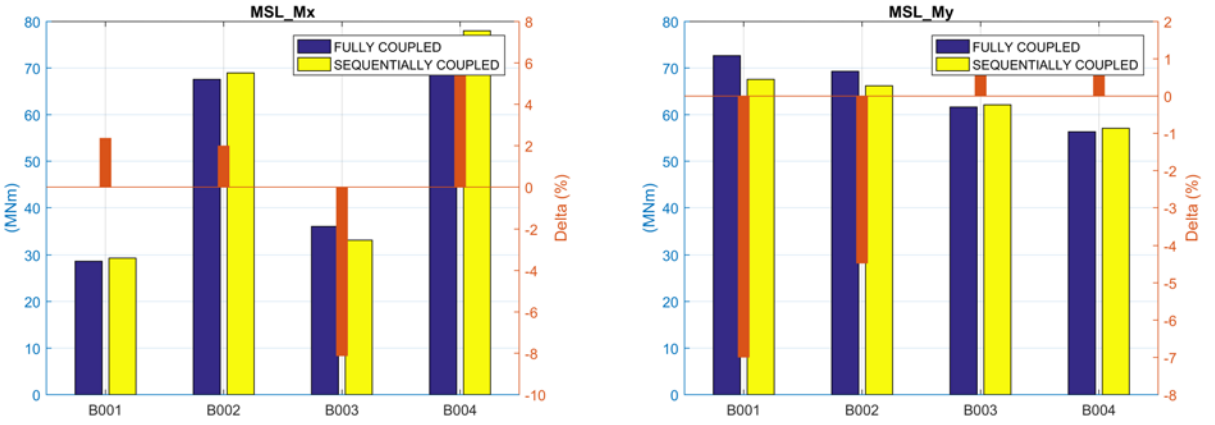

Figure A12. Bending moments at mean sea level

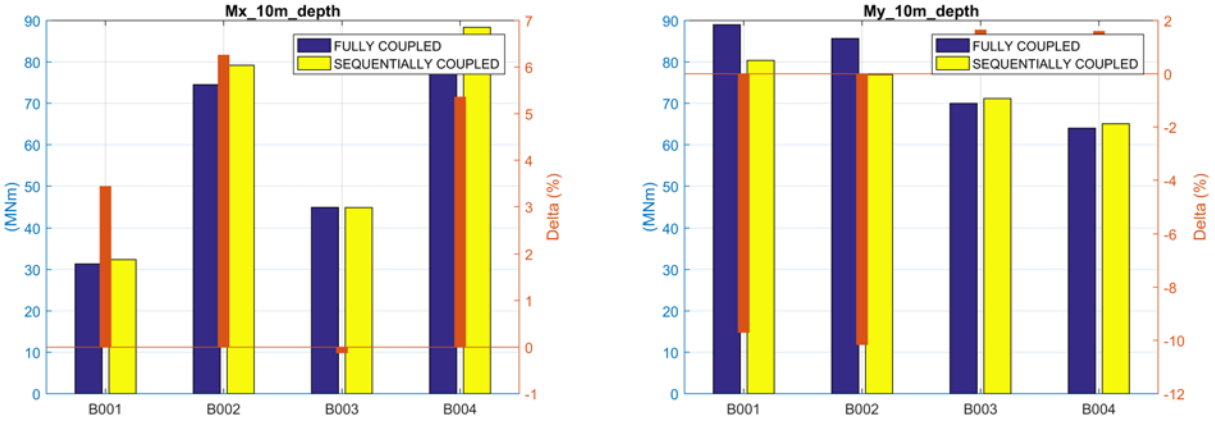

Figure A13. Bending moments at a 10-m water depth

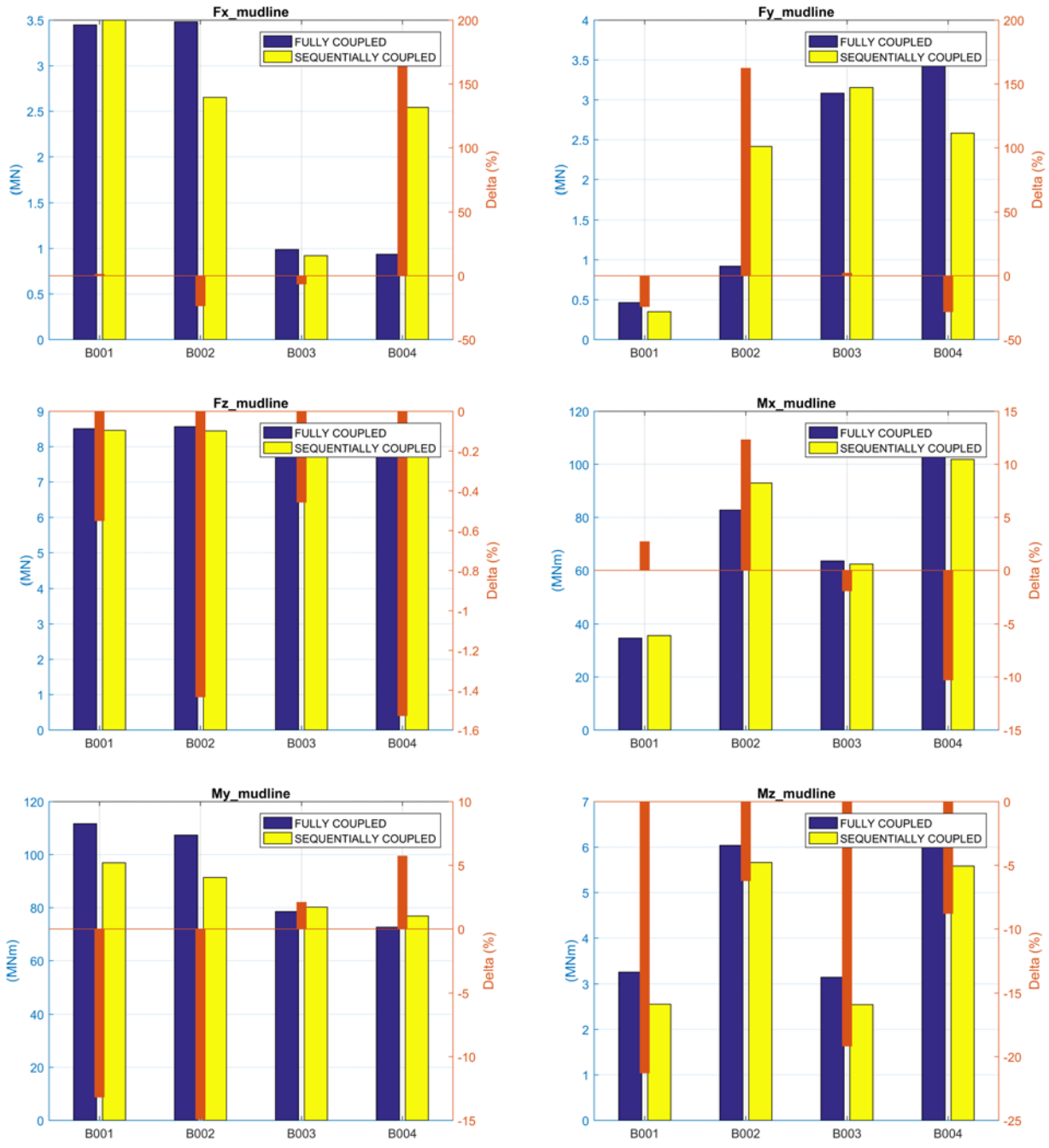

Figure A14. Piled loads at mudline

ULS turbine loads during power production for jacket configuration are provided in Figure A15 through Figure A18.

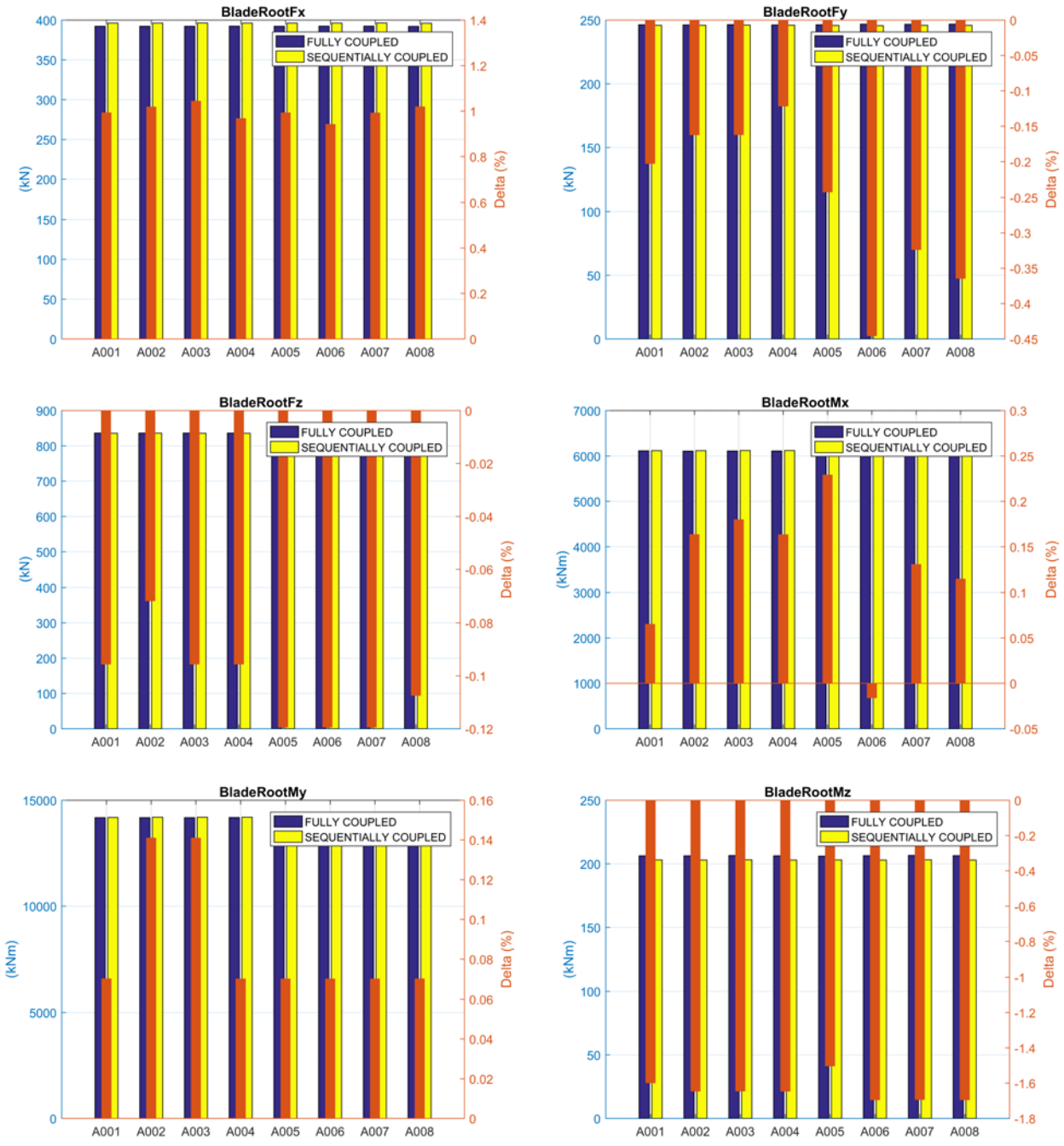

Figure A15. Blade root loads

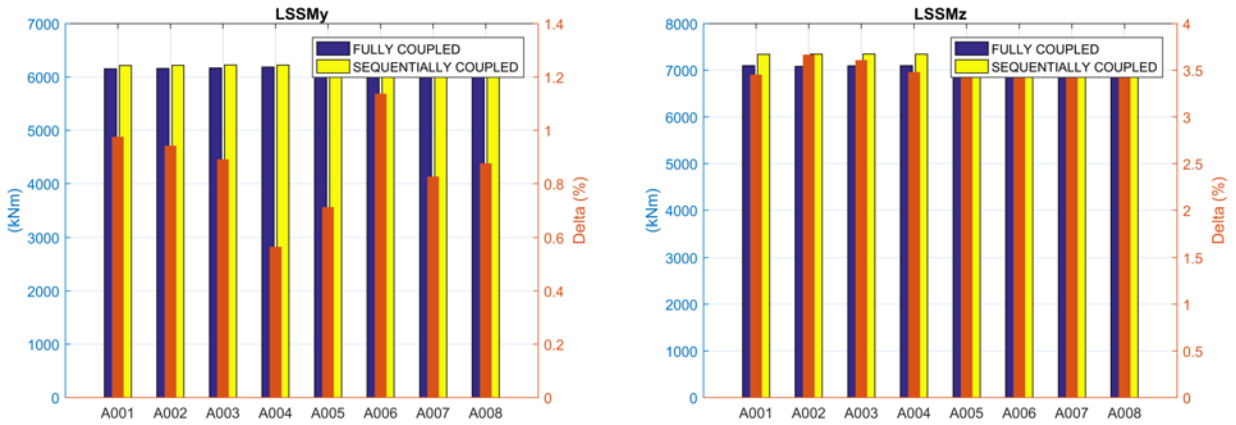

Figure A16. Low-speed-shaft loads

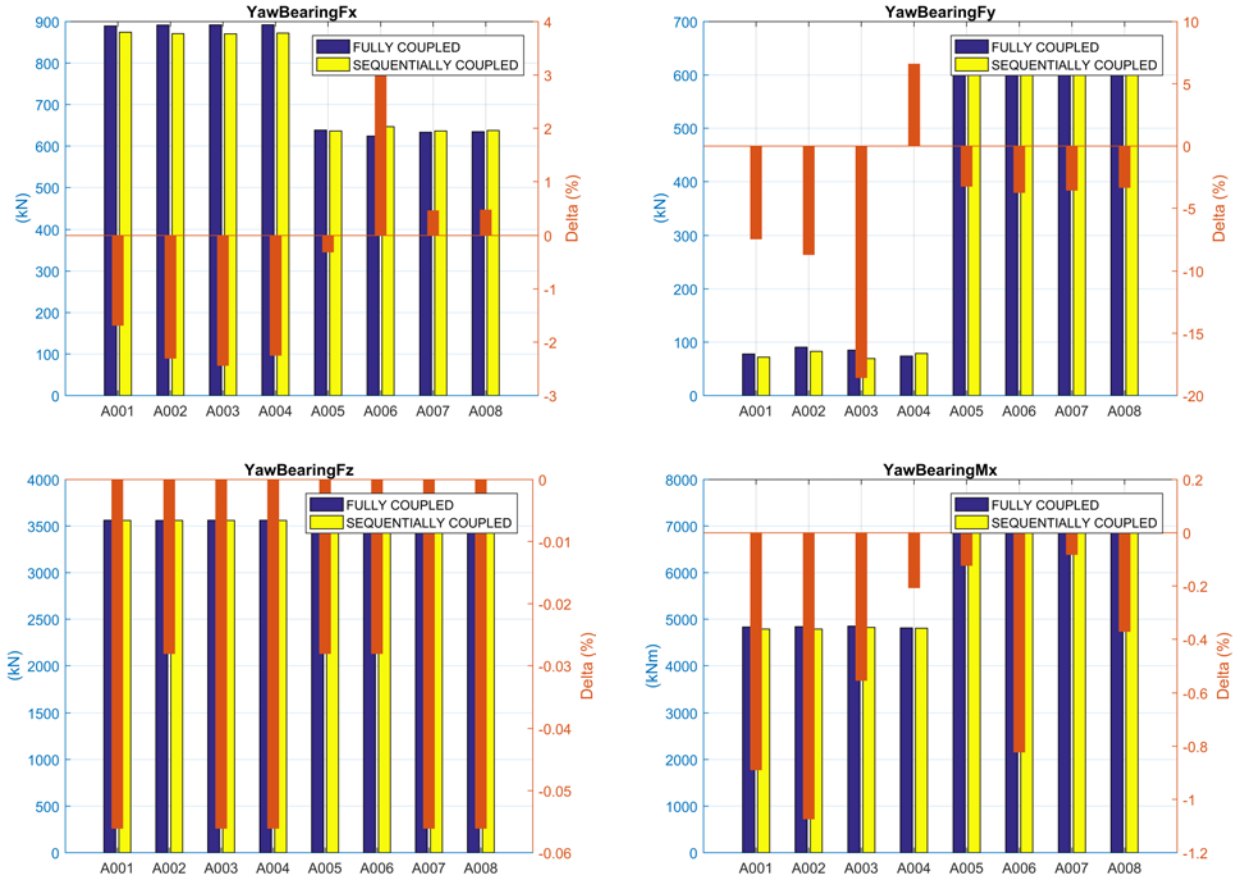

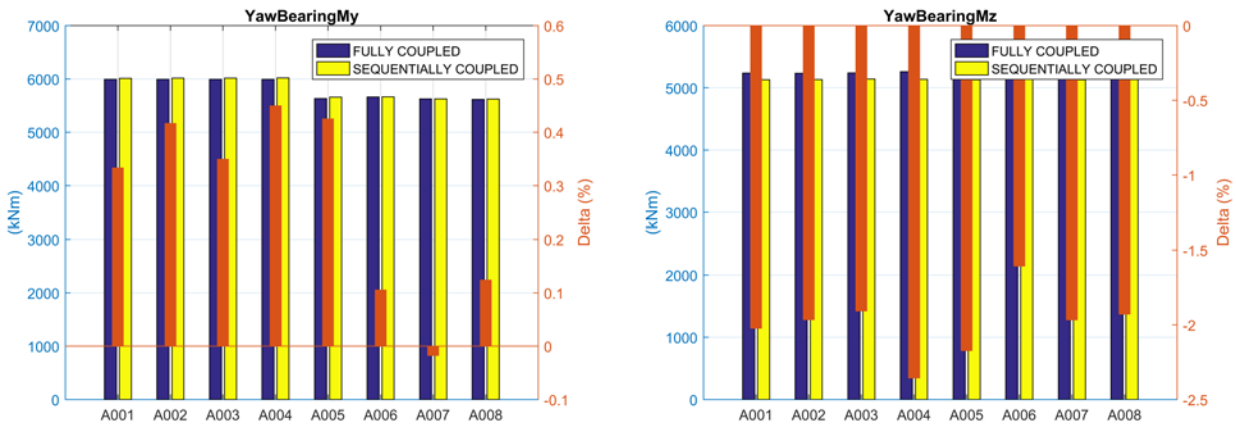

Figure A17. Yaw-bearing loads

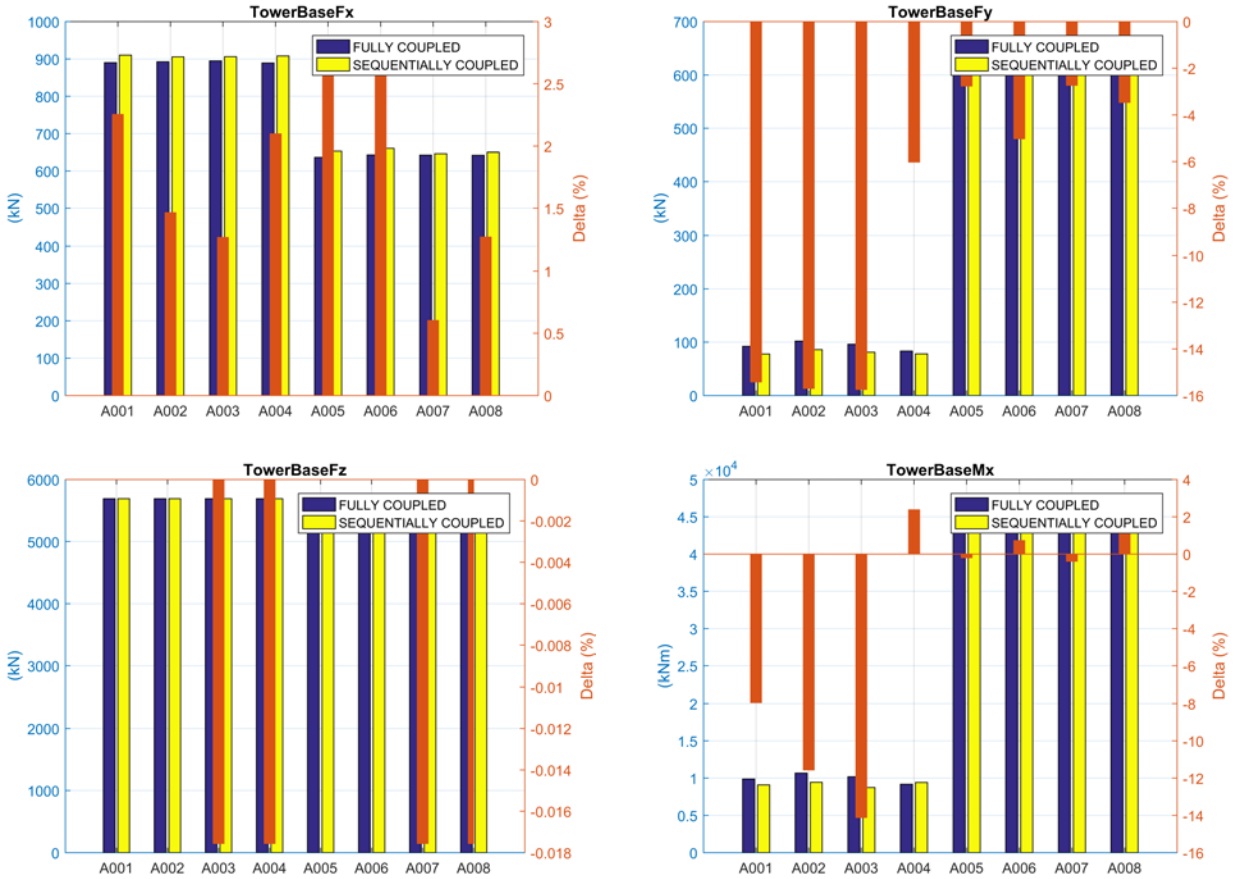

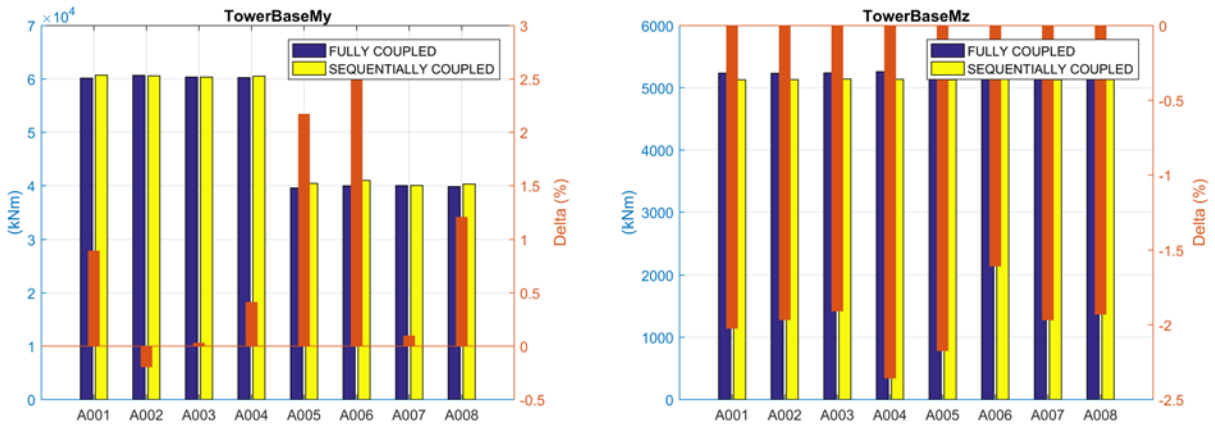

Figure A18. Tower Base Loads

ULS jacket substructure member loads during power production are provided in Figure A19.

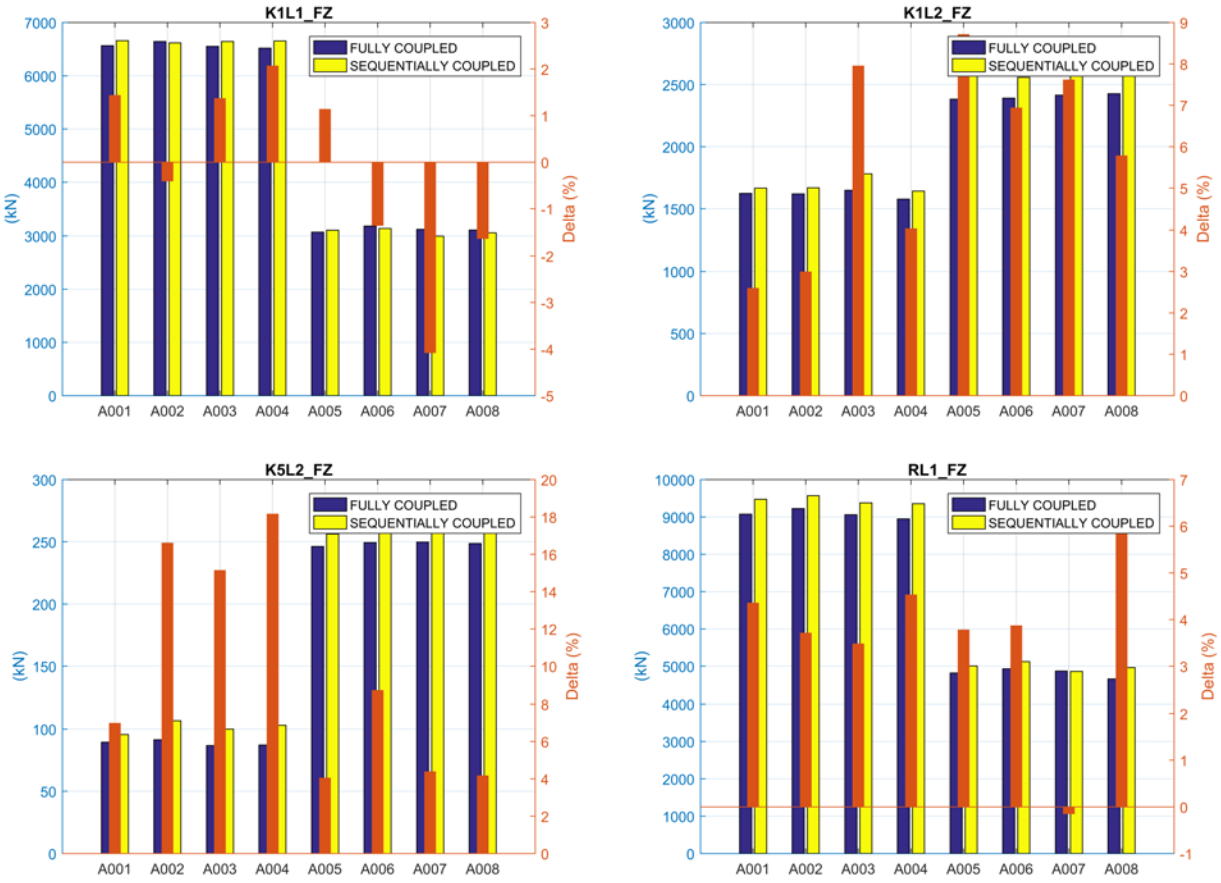

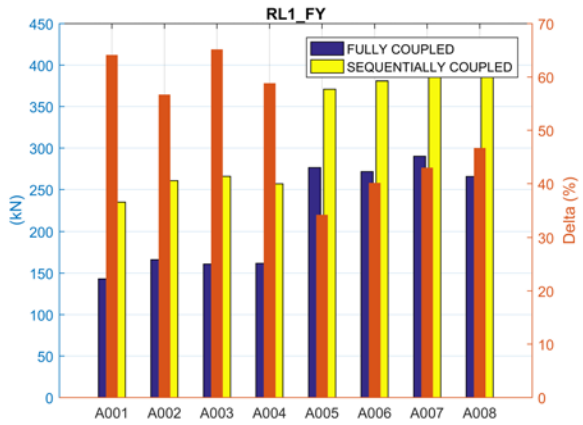

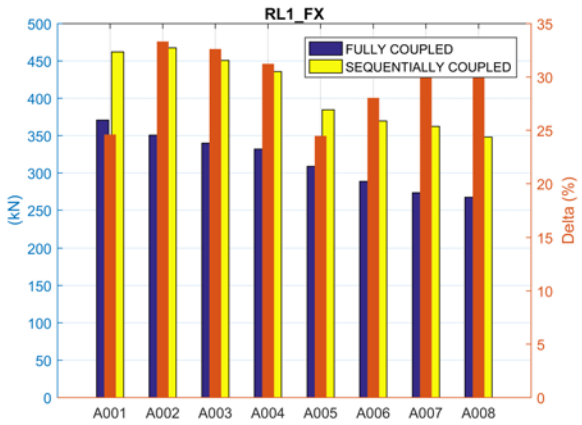

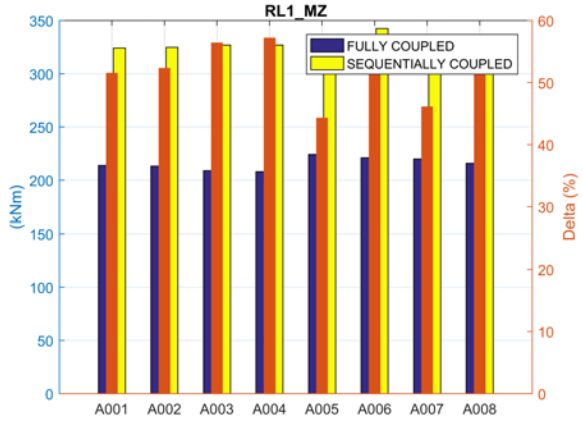

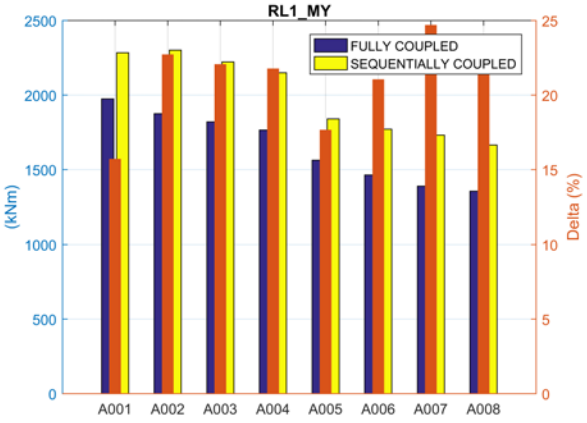

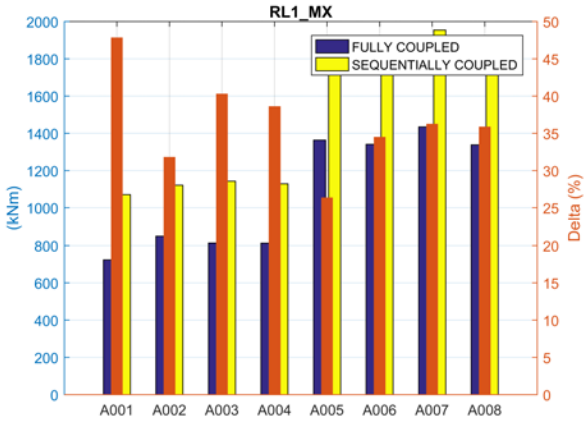

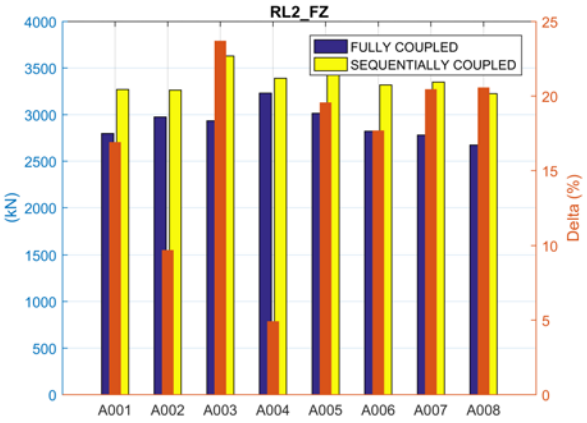

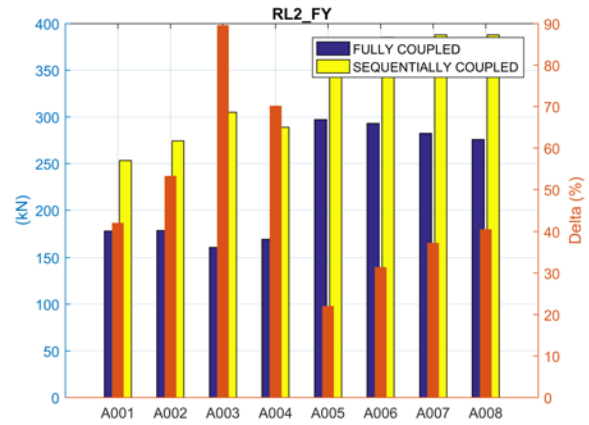

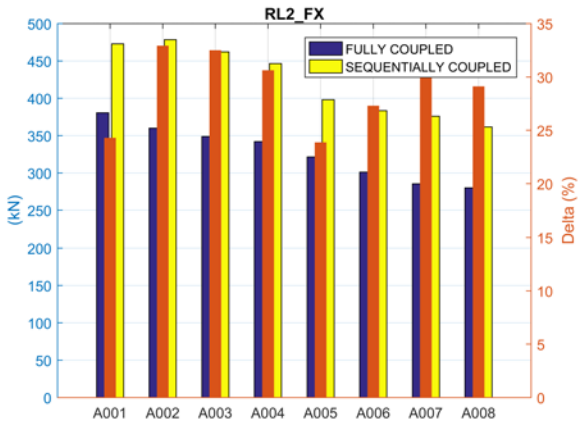

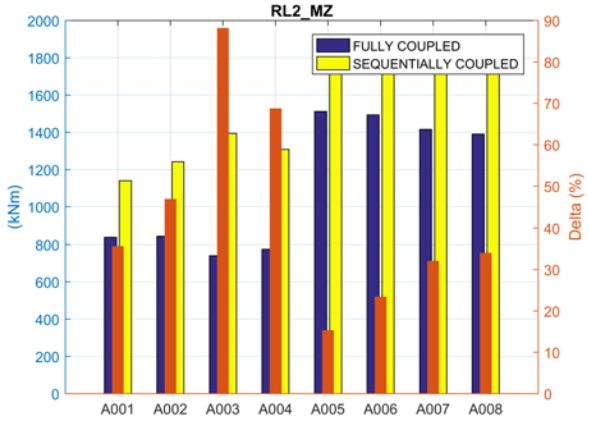

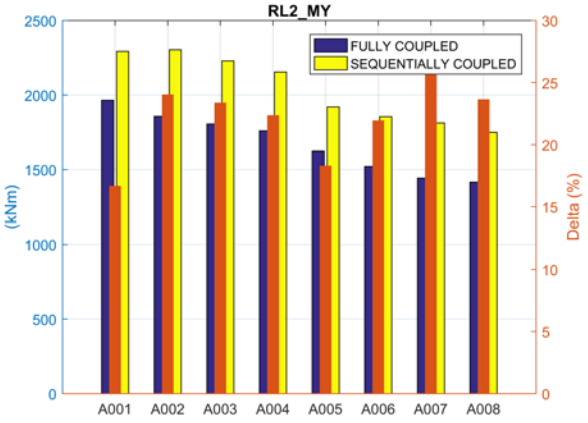

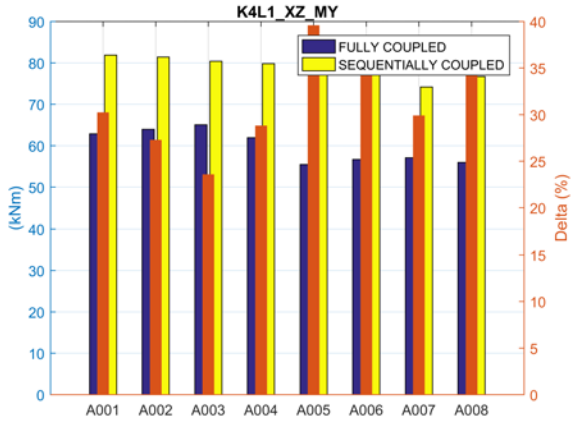

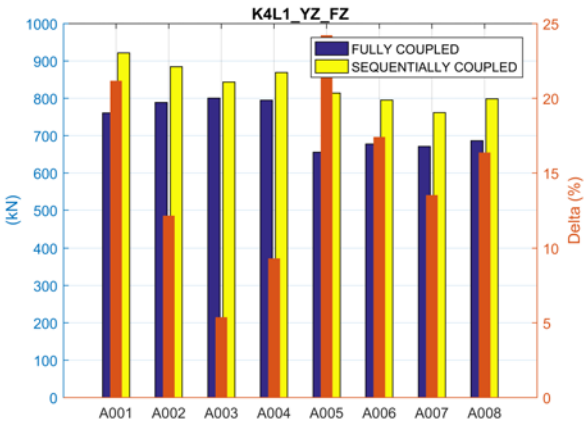

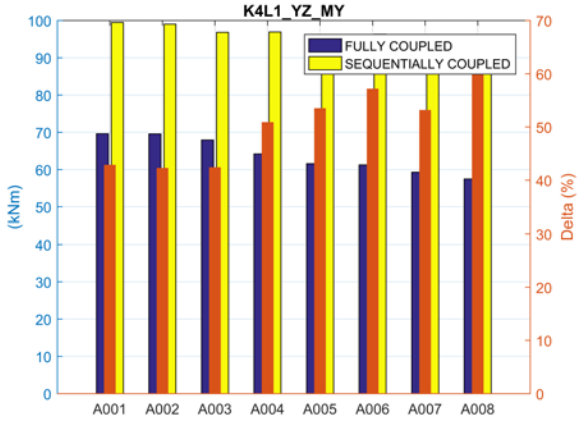

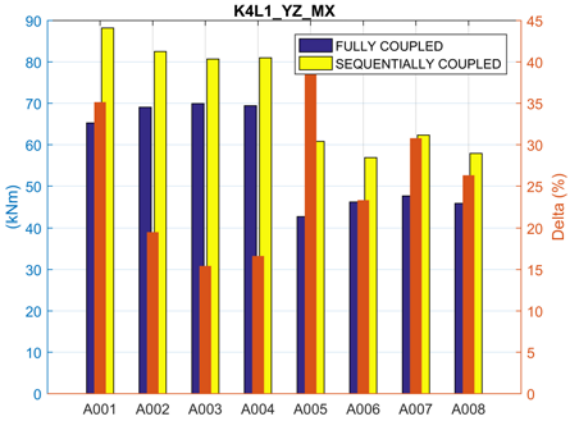

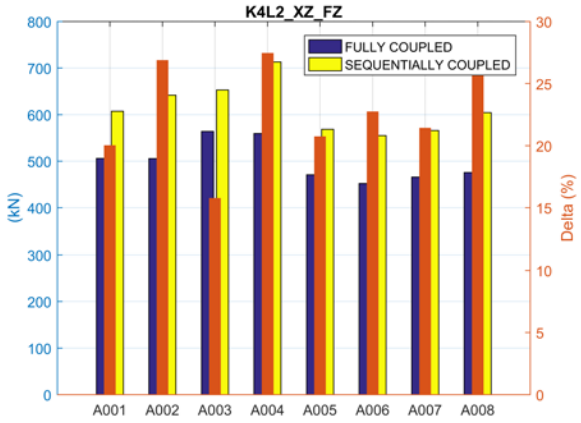

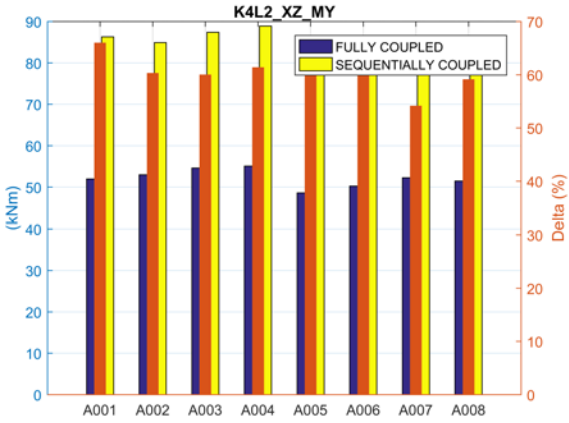

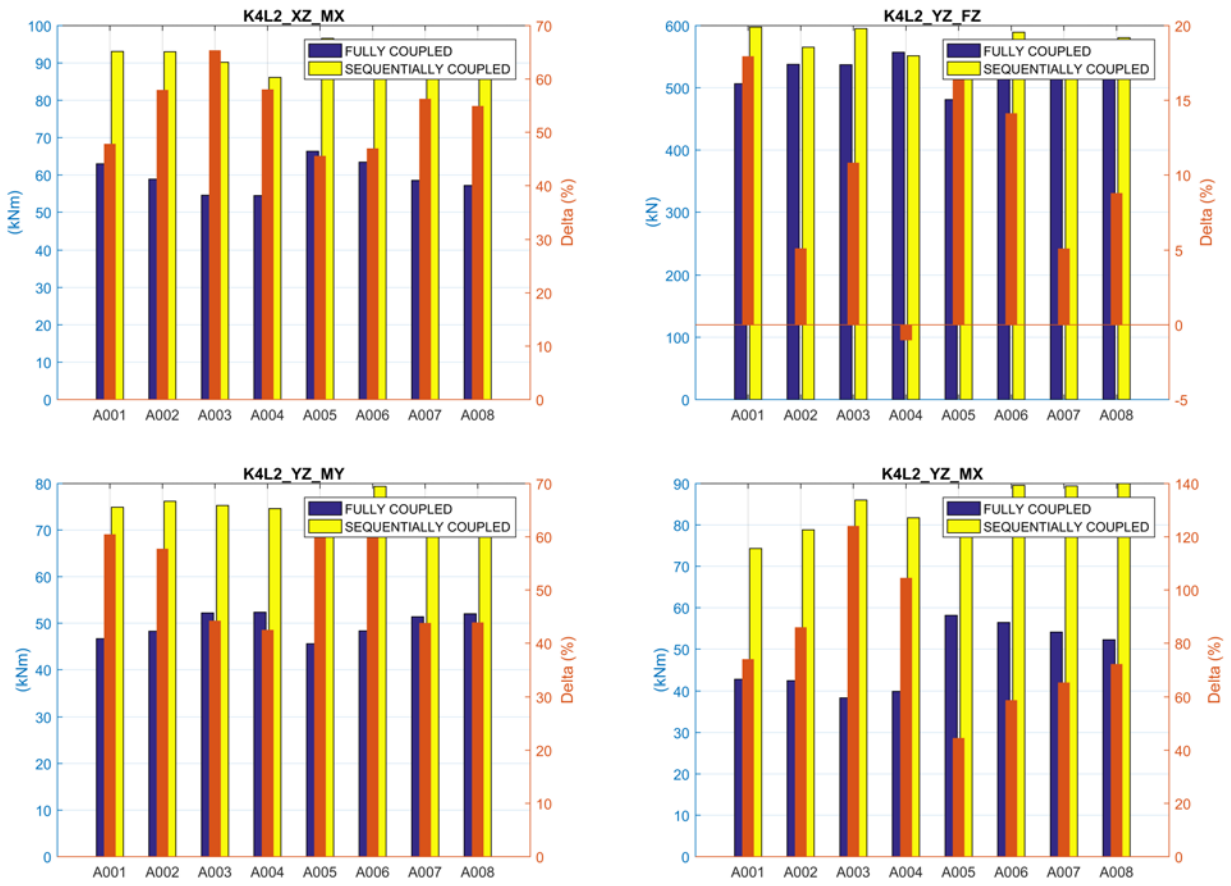

Figure A19. ULS loads of the jacket substructure members during power production

ULS turbine loads for the jacket configuration under extreme conditions are provided in Figure A20 through Figure A21.

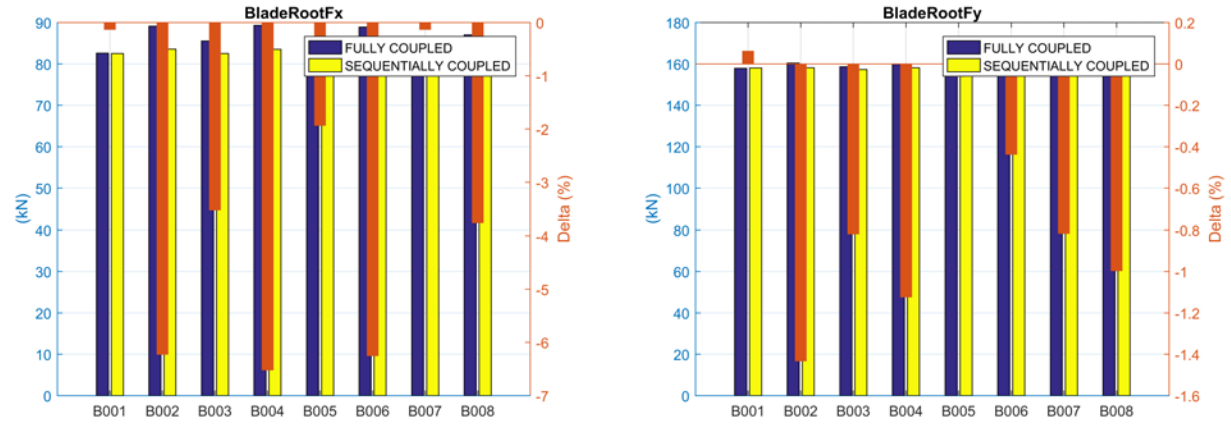

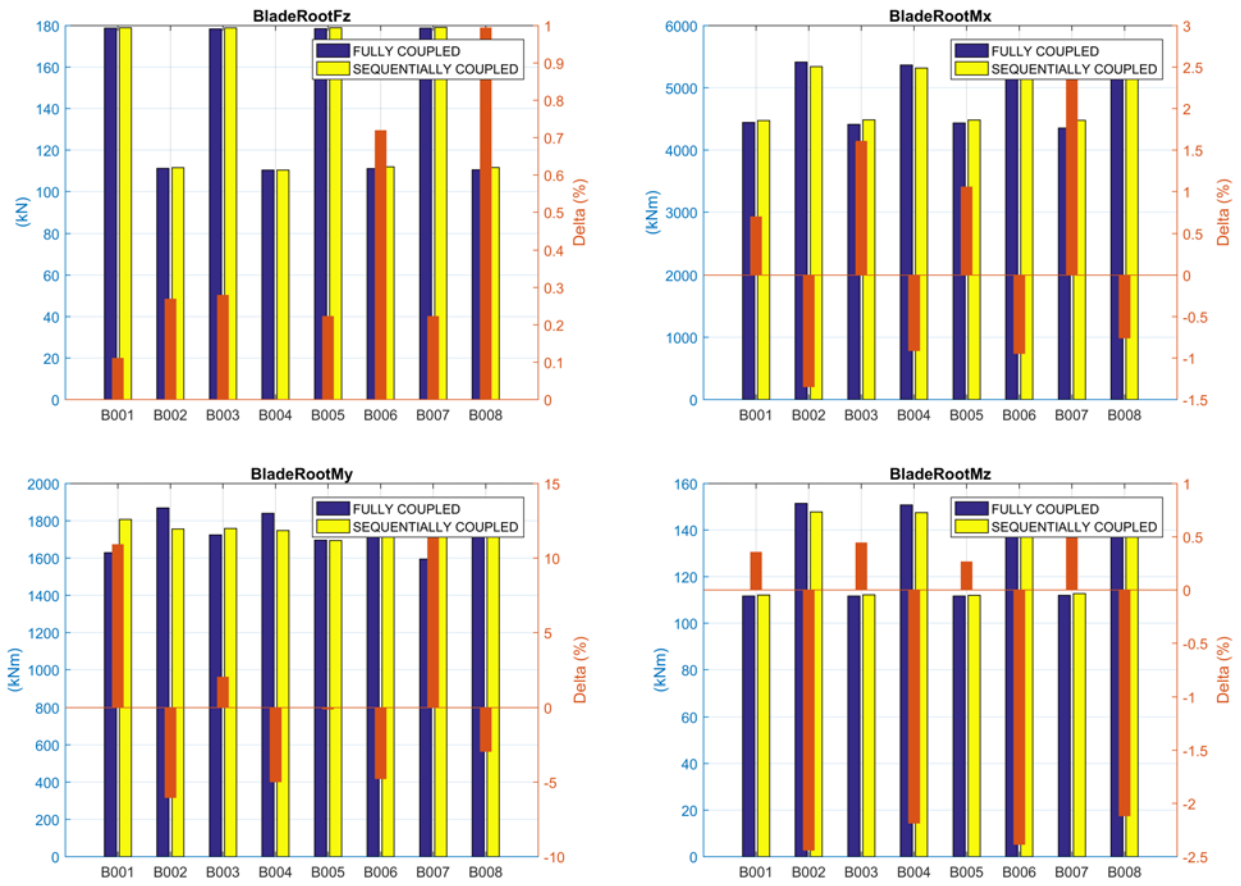

Figure A19. Blade root loads

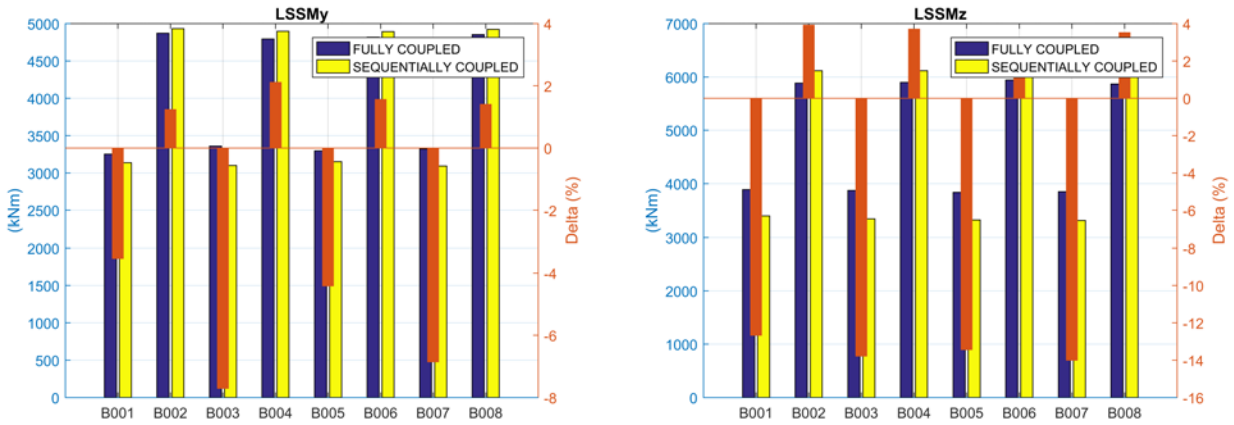

Figure A20. Low-speed shaft loads

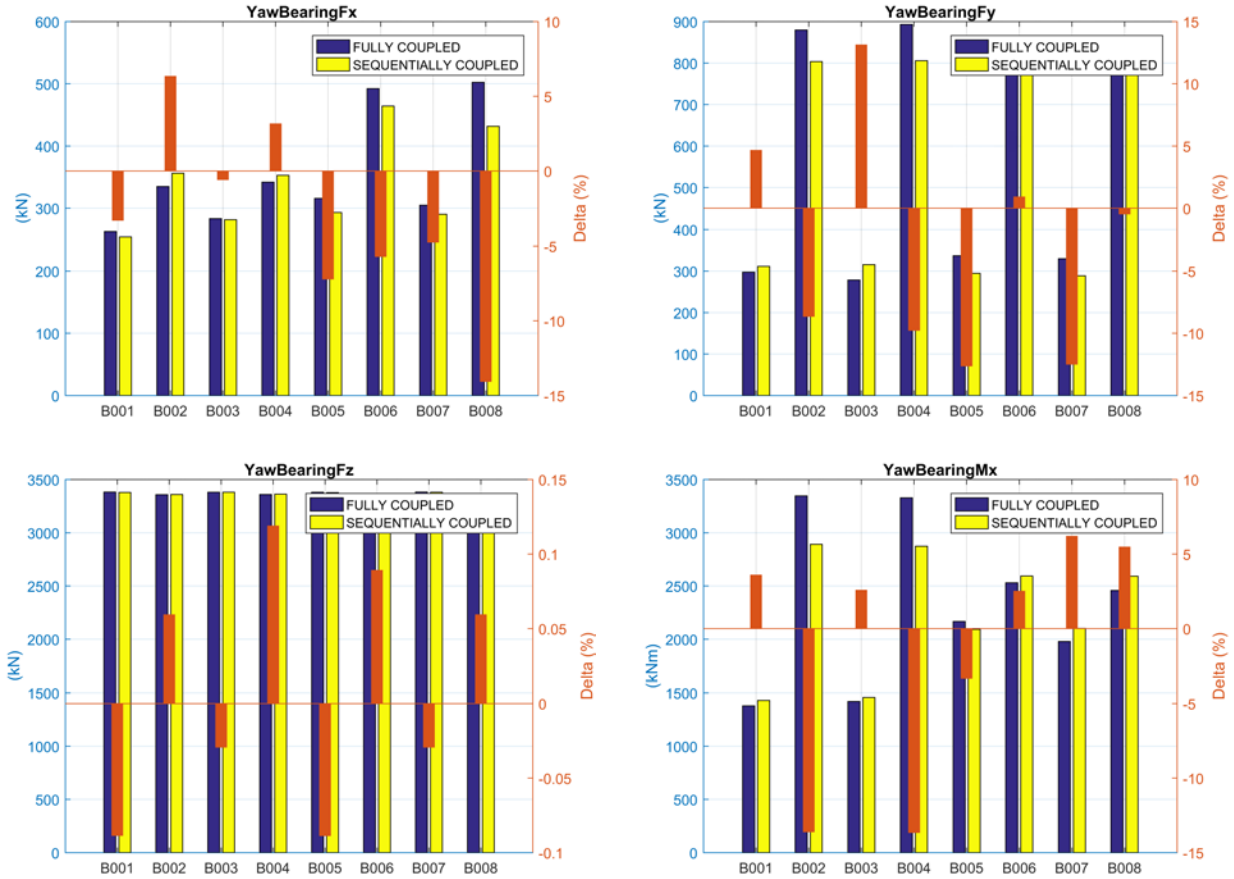

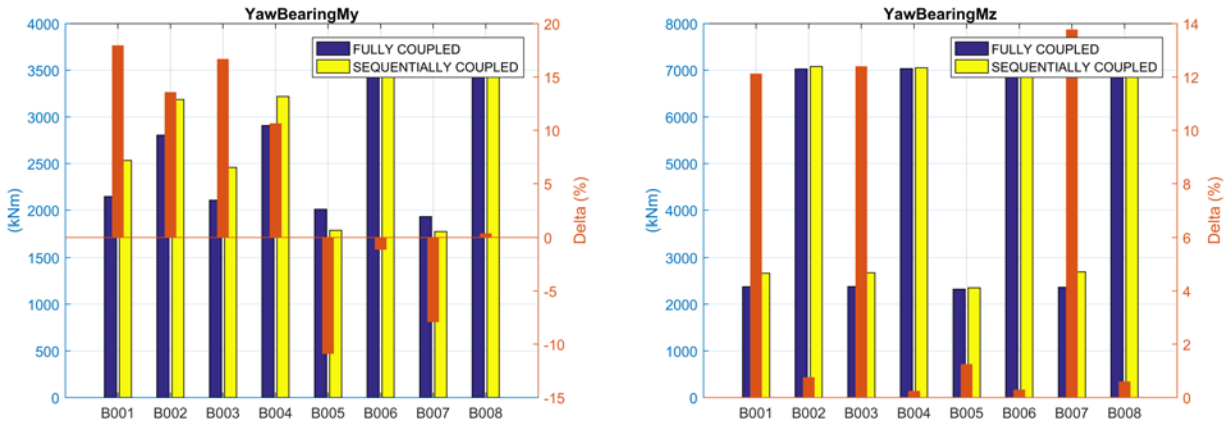

Figure A21. Yaw-bearing loads

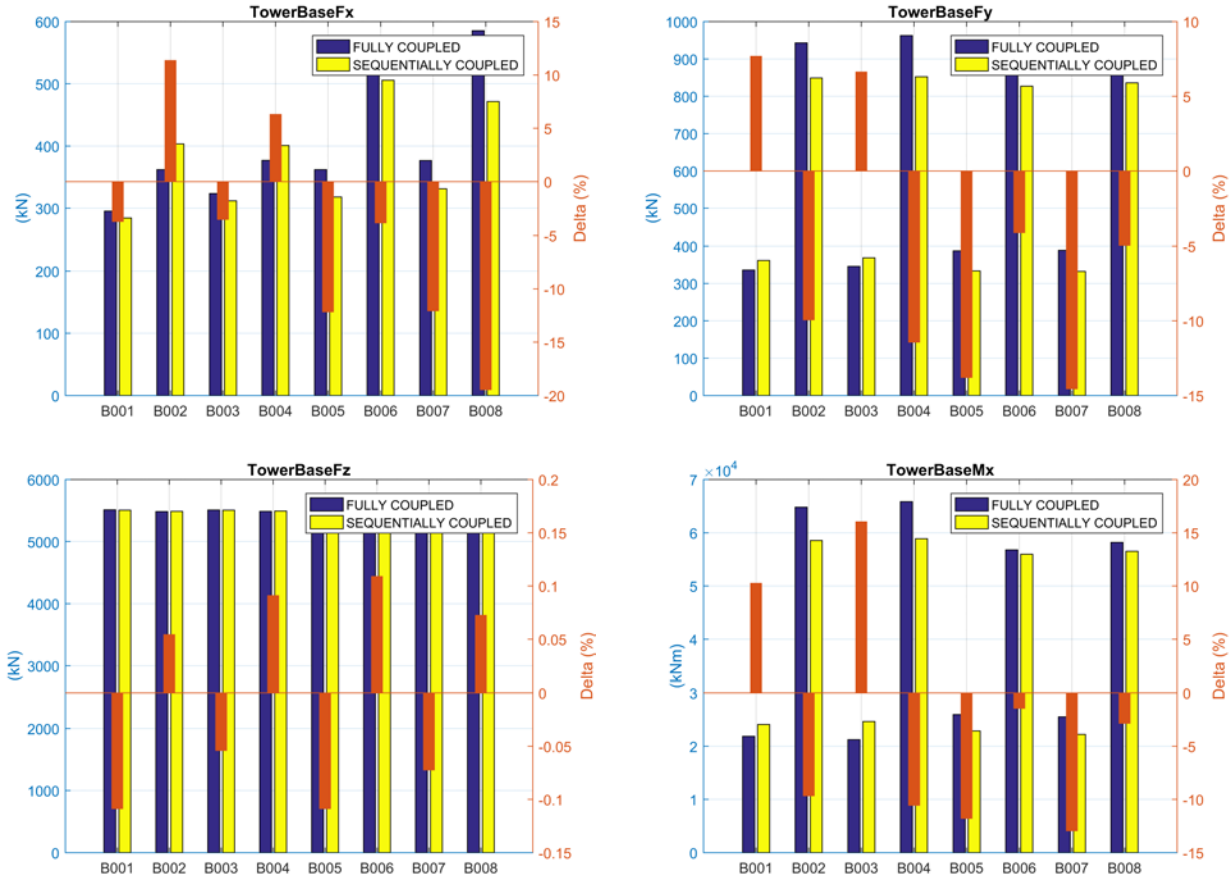

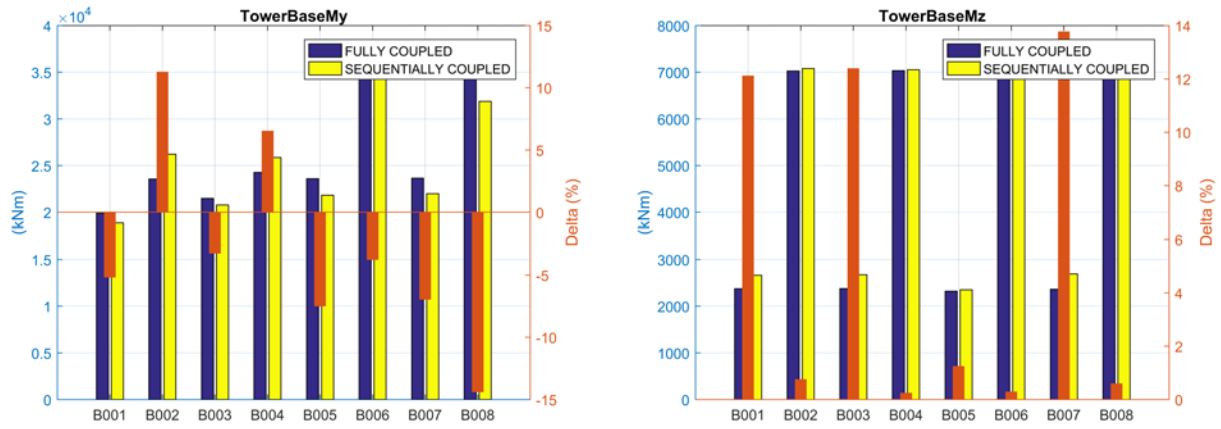

Figure A22. Tower-base loads

ULS jacket substructure member loads during extreme conditions are provided in Figure A23.

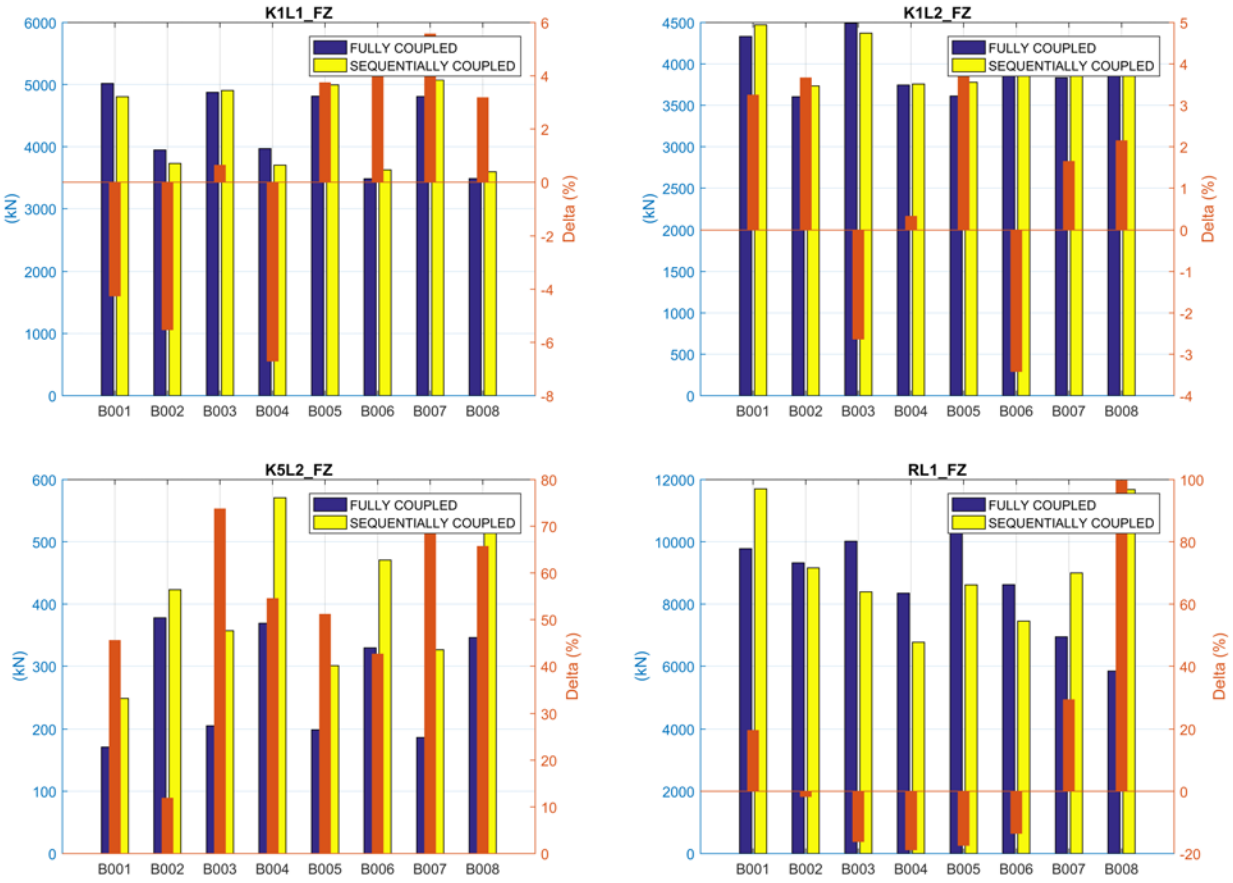

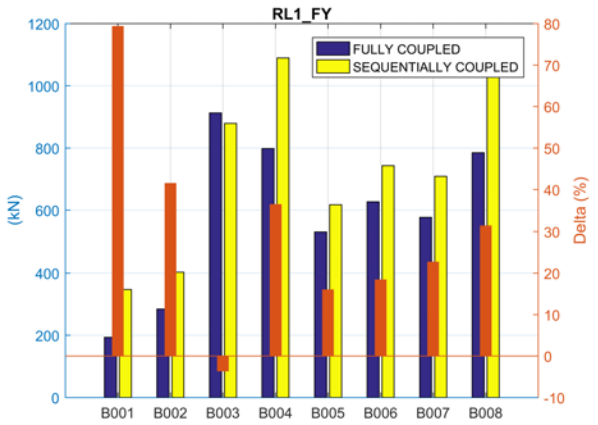

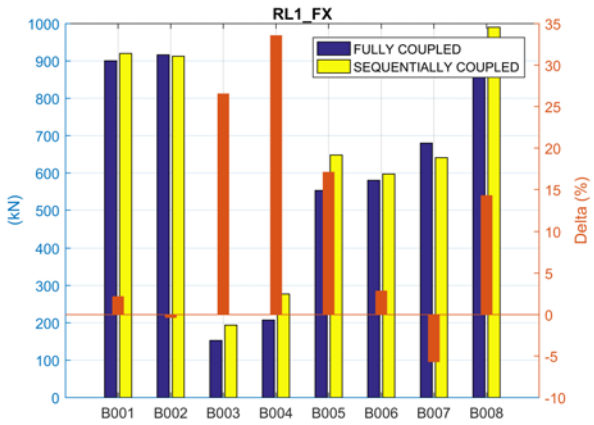

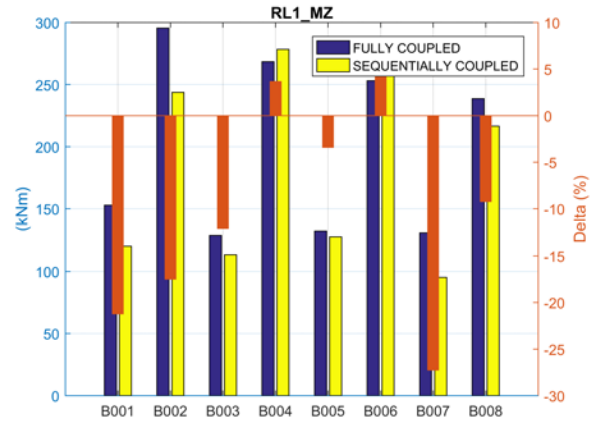

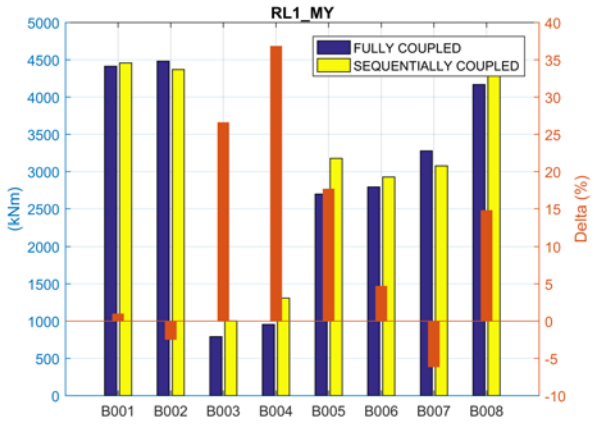

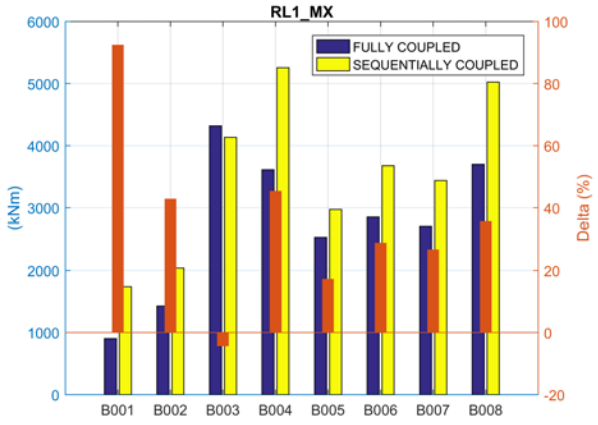

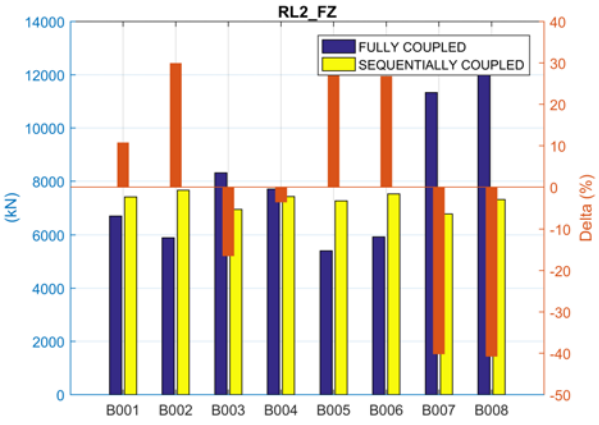

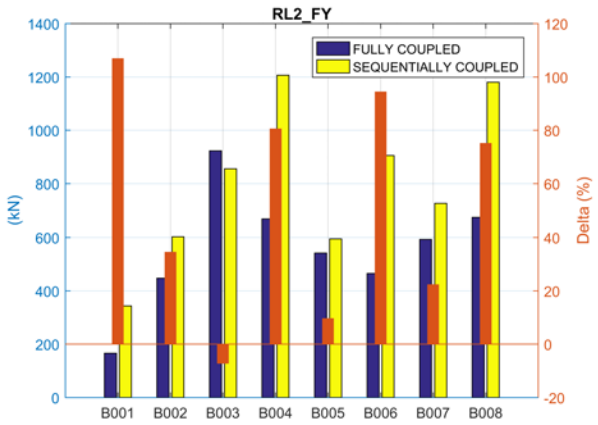

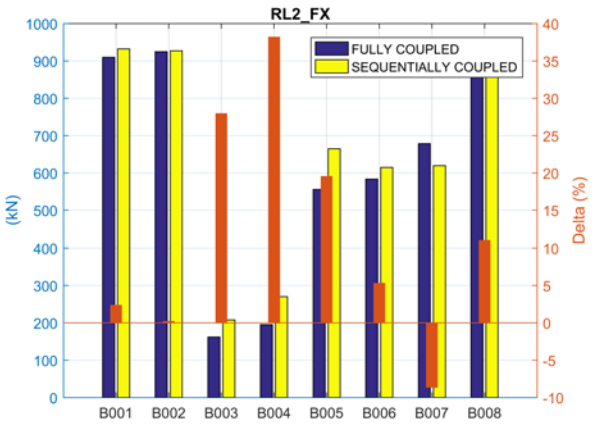

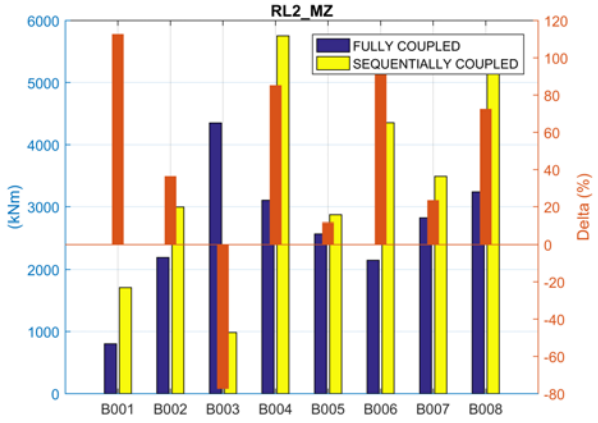

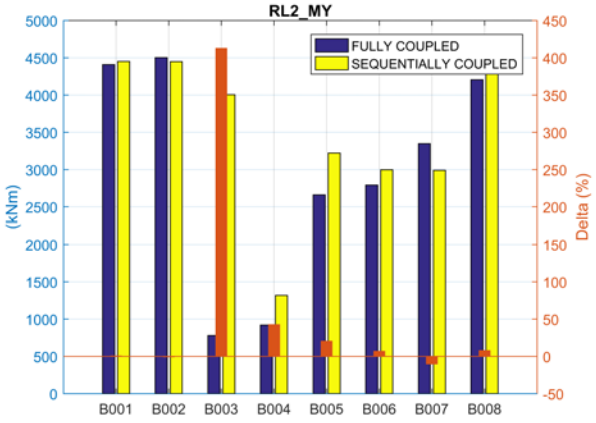

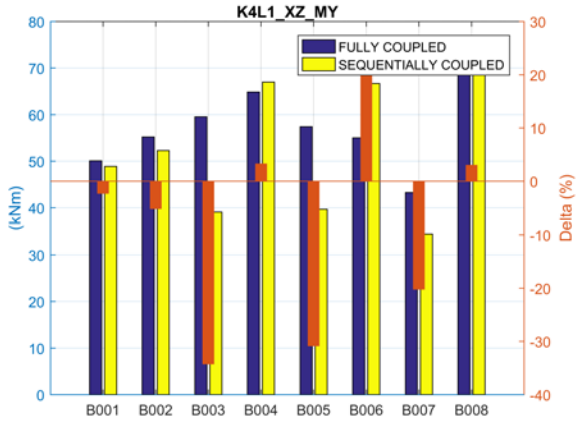

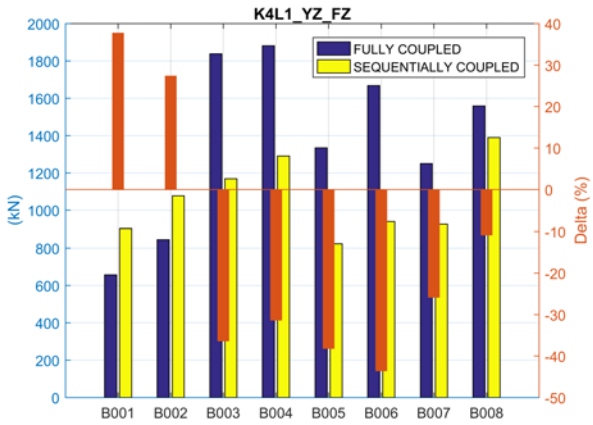

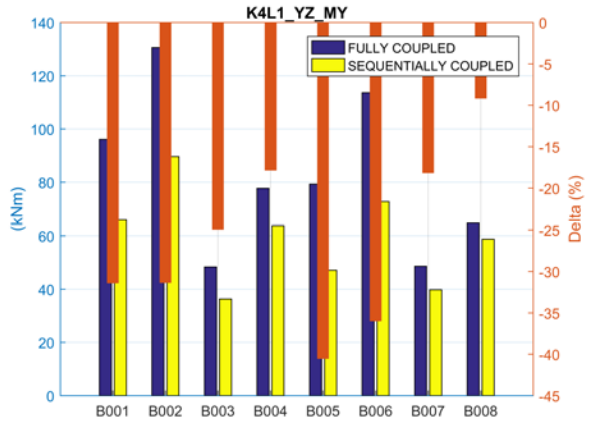

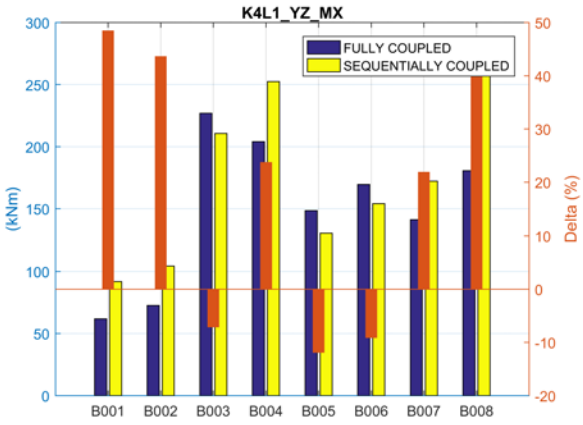

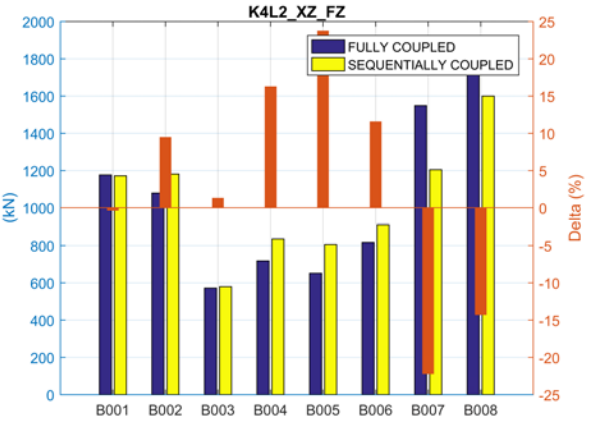

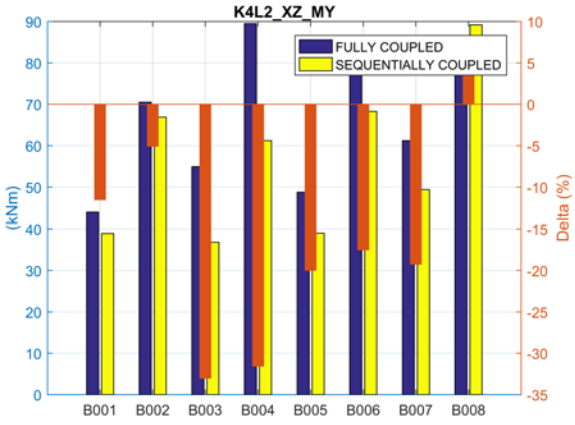

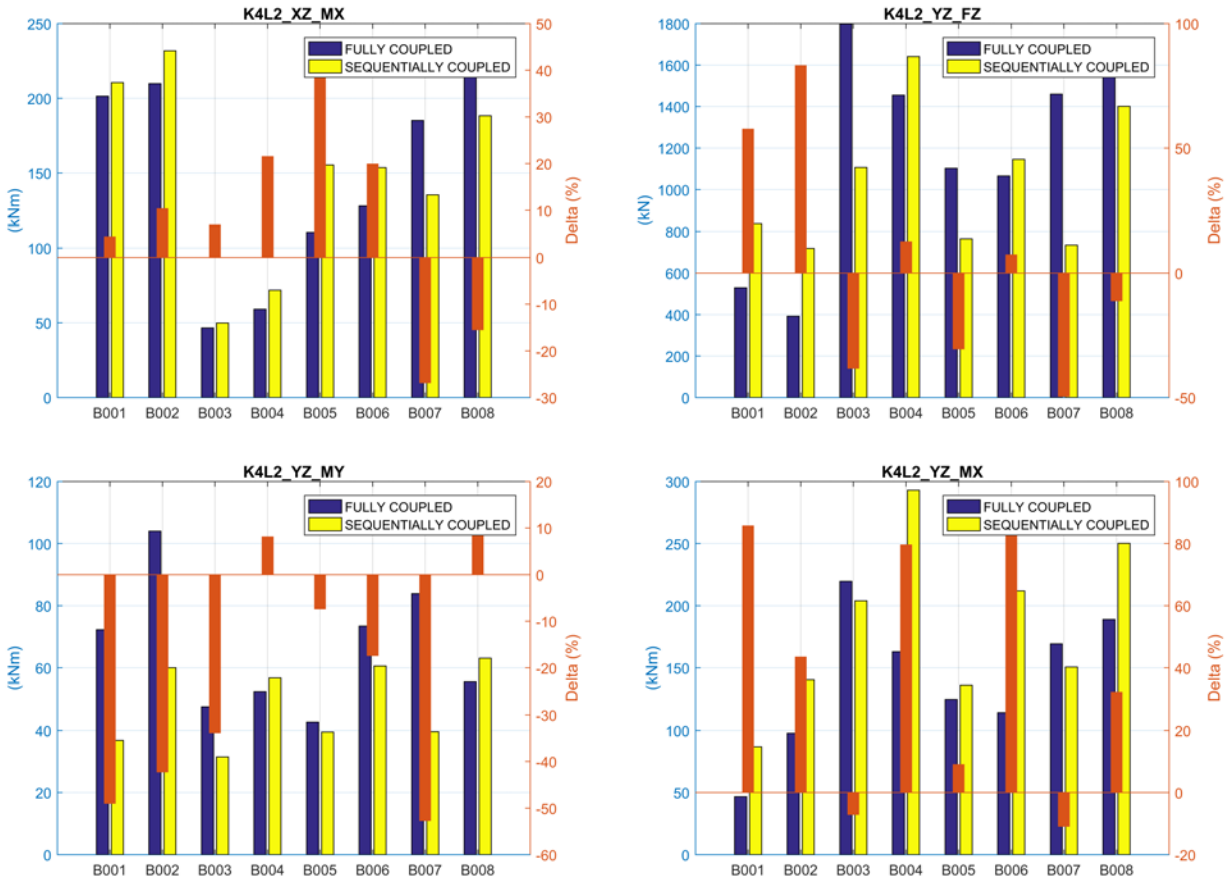

Figure A23. ULS loads of the jacket substructure members during extreme conditions